SEAT DESIGN FOR NECK PROTECTION IN AUTONOMOUS CAR CRASHES

OTONOM ARAÇ ÇARPIŞMALARINDA BOYNUN KORUNMASI İÇİN KOLTUK TASARIMI

SAMET YAVUZ

ASSIST. PROF. DR. SELÇUK HİMMETOĞLU

Supervisor

Submitted to

Graduate School of Science and Engineering of Hacettepe University

as a Partial Fulfillment to the Requirements

for the Award of the Degree of Doctor of Philosophy

in Mechanical Engineering

2024

This thesis is dedicated to my beloved dog, Fox.

ABSTRACT

SEAT DESIGN FOR NECK PROTECTION IN AUTONOMOUS CAR CRASHES

Samet YAVUZ

Doctor of Philosophy, Department of Mechanical Engineering

Supervisor: Assist. Prof. Dr. Selçuk HİMMETOĞLU

June 2024, 101 pages

It is expected that autonomous vehicles will be sold more in the coming years, and this may cause new problems in restrictive protection systems which are called restraint systems. Because uncommon seating positions may put passengers at greater risk. For example, in a frontal crash scenario, a person traveling in a rearward turned seat may suffer more neck injury. When US NCAP crash test conditions are taken into account, statistically, frontal crashes occur at higher intensities than rear-end crashes.

Sudden movement of the head relative to the upper body in rear-end crashes creates a high risk of neck injury. This sudden movement typically causes discomfort and pain in the head and neck system. This neck injury can be prevented in cases where the seat and head restraint work together effectively to absorb the energy of the crash. This is achieved by restricting the neck movement during the crash.

Autonomous vehicles can include swivel, tilt and expandable seating plans. Current restraint protection systems in use are optimized for conventional sitting positions. A change in sitting position requires different restraint systems.

In this thesis, new and effective restraint protection systems are designed for non-conventional sitting positions. Since these restrictive protection systems will be integrated with the passenger seat, the studies are gathered under the title of seat design.

Keywords: safety in autonomous vehicles, neck injury, seat design, restraint systems

ÖZET

OTONOM ARAÇ ÇARPIŞMALARINDA BOYNUN KORUNMASI İÇİN KOLTUK TASARIMI

Samet YAVUZ

Doktora, Makine Mühendisliği Bölümü

Tez Danışmanı: Dr. Öğr. Üyesi Selçuk HİMMETOĞLU

Haziran 2024, 101 sayfa

Otonom araçların gelecek yıllarda daha fazla satışta olması beklenen bir durumdur ve bu durum kısıtlayıcı koruma sistemlerinde yeni sorunlar doğurabilmektedir. Çünkü yaygın olmayan oturma pozisyonları yolcuları daha fazla risk altında bırakabilmektedir. Örneğin bir önden çarpışma senaryosunda geriye doğru döndürülmüş koltukta yolculuk eden birisi daha fazla boyun zedelenmesine maruz kalabilmektedir. US NCAP çarpışma test koşulları da dikkate alındığında istatistiksel olarak önden çarpışma durumları, arkadan çarpışma durumlarına göre daha yüksek şiddetlerde gerçekleşmektedir.

Trafik kazalarında arkadan çarpışma durumlarında başın üst vücuda göre ani hareketi yüksek bir boyun incinmesi riski yaratmaktadır. Bu ani hareketlenme tipik olarak baş-boyun sisteminde rahatsızlık ve ağrı yaratmaktadır. Bu boyun incinmesi durumu koltuk ve koltuk başlığı sistemlerinin birlikte efektif olarak çalışarak çarpışma enerjisini absorbe

ettiği durumlarda engellenebilmektedir. Bu durum boyun hareketinin çarpışma sırasında kısıtlanması ile sağlanmaktadır.

Otonom araçlar dönebilir, eğilebilir ve genişletilebilir oturma planları içerebilmektedirler. Şu an kullanılmakta olan mevcut kısıtlayıcı koruma sistemleri ise konveksiyonel oturma pozisyonları için optimize edilmiştir. Oturma pozisyonunda yapılacak bir değişiklik farklı kısıtlayıcı koruma sistemleri gerektirmektedir.

Gerçekleştirilen bu tez çalışmasında ise, konveksiyonel olmayan oturma pozisyonları için yeni ve etkili kısıtlayıcı koruma sistemleri tasarlanmıştır. Bu kısıtlayıcı koruma sistemleri yolcu koltuğuyla bütünleşik olacağı için yapılan çalışmalar koltuk tasarımı başlığı altında toplanmıştır.

Anahtar Kelimeler: otonom araçlarda güvenlik, boyun incinmesi, koltuk tasarımı, kısıtlayıcı koruma sistemleri

ACKNOWLEDGEMENT

I would like to express my sincere gratitude to my supervisor Assist Prof. Dr. Selçuk Himmetoğlu for his continuous support, patience and motivation during my study. I have benefited greatly from his wealth of knowledge and meticulous editing. I also thank to my committee members Prof. Dr. Çağlar Başlamışlı, Assist Prof. Dr. Kutluk Bilge Arıkan for their continuous support and encouragement. I would also like to say a heartfelt thank to my mother Vasfiye Yavuz for always believing in me and encouraging me to follow my dreams. Also, I want to thank my coworker Assist Prof. Dr. Banu Sarıbay for always giving me courage during my academic works.

TABLE OF CONTENTS

ABSTRACT i

OZET iii

ACKNOWLEDGEMENT v

TABLE OF CONTENTS vi

LIST OF FIGURES viii

LIST OF TABLES xii

LIST OF SYMBOLS AND ABBREVIATIONS xiv

1. INTRODUCTION 1

   1.1. Literature Survey 4

2. PRO ACTIVE SEATBACK DESIGN 17

   2.1. Mechanism Geometry 17
   2.2. Obtaining the Differential Equations 21
   2.3. Head Restraint Mechanism 28
   2.4. Behaviour of the Mechanism and Applied Crash Pulses 30
   2.5. Results 32

3. VEHICLE MODELLING 39

   3.1. Design Parameters of the Vehicles 40
   3.2. Wall Force-Vehicle Deformation Behaviour 46
   3.3. Results 50
   3.4. Nonlinear Suspension Spring Application to Crash Validation Model 59
   3.5. Ride Comfort 63
      3.5.1. Body Bounce Frequency 64
      3.5.2. Wheel Hop Frequency 64
      3.5.3. Pitch Frequency 65
      3.5.4. Suspension Damping Ratio 65

4. TORSO PLATES AND TORSION BAR 67

4.1. Whiplash Mitigating Forward-Facing Seat 67
4.2. Torso Plates 71
4.3. Performance of the Torso Plates 75
4.4. Torsion Bar 85

5. DISCUSSION and CONCLUSION 89

6. REFERENCES..98

APPENDIX 102

AP 1 - Publications Derived from the Thesis 102
AP 2 - Conference Papers Derived from the Thesis....................................103
AP 3 - Thesis Originality Report 104

CIRRICULUM VITAE 105

LIST OF FIGURES

Figure 1.1. Definition of seating orientations (Adapted from [7].). 6
Figure 1.2. Initial positions of the seat model (45^{o} on the lef and 90^{o} on the right) (Adapted from [11].). 11
Figure 1.3. Comparison of contact forces between three different human body models and seatbacks (Adapted from [12].) 13
Figure 2.1. Proposed mechanism.……………….. 18
Figure 2.2. Representative image of the proposed mechanism in simulation environment. ……………………………………………..……………………………….. 17
Figure 2.3. FBD of part 3. 22
Figure 2.4. FBDs of part 2 and part 1...22
Figure 2.5. Behaviour of the mechanism for male models of different height and weight. 28
Figure 2.6. Forward movement of head restraint. 28
Figure 2.7. Behaviour of head restraint. 30
Figure 2.8. Forward movement of the seatback and head restraint................................30
Figure 2.9. SN 9.4 crash pulse.. 31
Figure 2.10. SN 13 crash pulse. 31
Figure 2.11. TR 16 crash pulse. 31
Figure 2.12. IIWPG crash pulse. 31
Figure 2.13. SN 20.4 crash pulse. 31
Figure 2.14. TR 24 crash pulse. 31
Figure 2.15. FMVSSHS crash pulse 32
Figure 2.16. OC and C1 vertebras. 33
Figure 2.17. C7 and T1 vertabras. 33
Figure 2.18. Movements of the head with respect to the neck.......................................33
Figure 2.19. Iiwpg crash..37
Figure 2.20. Tr24 crash 38
Figure 2.21. Fmvsshs crash 38
Figure 3.1. Real crash tests of the Subaru Impreza (top) and Toyota Yaris (bottom). ...39
Figure 3.2. Design parameters of Subaru Impreza model vehicle. 41

Figure 3.3. Calculation of the position of the centre of gravity for Subaru Impreza model vehicle (Adapted from [22].) 43
Figure 3.4. Wheel sizes of Subaru Impreza model vehicle (Adapted from [23].). 43
Figure 3.5. Wheel sizes of Toyota Yaris model vehicle (Adapted from [23].)............... 44
Figure 3.6. Normalized moments of inertia (Adapted from [22].)... 45
Figure 3.7. (a) Frontal impact test, (b) and (c) crushing force and deformation curves. 47
Figure 3.8. Lumped-mass model of a car in FWRB impact test. 48
Figure 3.9. Modelling of the loading phase. 48
Figure 3.10. Modelling of the unloading phase 49
Figure 3.11. Location of accelerometers placed on Subaru Impreza (Adapted from [20].) 49
Figure 3.12. Time dependent variation of barrier force applied to Subaru Impreza model vehicle 50
Figure 3.13. Barrier force-vehicle deformation graph applied to Subaru Impreza model vehicle 51
Figure 3.14. Acceleration-time graph of Subaru Impreza model vehicle in X direction 51
Figure 3.15. Acceleration-time graph of Subaru Impreza model vehicle in Z direction 52
Figure 3.16. Velocity-time graph of Subaru Impreza model vehicle in X direction 52
Figure 3.17. Velocity-time graph of Subaru Impreza model vehicle in Z direction....... 52
Figure 3.18. Position-time graph of Subaru Impreza model vehicle in X direction....... 53
Figure 3.19. Position-time graph of Subaru Impreza model vehicle in Z direction 53
Figure 3.20. Angular acceleration-time graph of Subaru Impreza model vehicle around Y axis 54
Figure 3.21. Angular displacement-time graph of Subaru Impreza model vehicle around Y axis 54
Figure 3.22. Acceleration-time graph of Toyota Yaris model vehicle in X direction.... 55
Figure 3.23. Acceleration-time graph of Toyota Yaris model vehicle in Z direction. ... 55
Figure 3.24. Velocity-time graph of Toyota Yaris model vehicle in X direction........... 55
Figure 3.25. Velocity-time graph of Toyota Yaris model vehicle in Z direction. 56
Figure 3.26. Position-time graph of Toyota Yaris model vehicle in X direction. 56
Figure 3.27. Position-time graph of Toyota Yaris model vehicle in Z direction............ 56
Figure 3.28. Angular acceleration-time graph of Toyota Yaris model vehicle around Y axis. 57

Figure 3.29. Angular displacement-time graph of Toyota Yaris model vehicle around Y axis. 57
Figure 3.30. Screenshots from simulation and real crash test videos (Toyota Yaris).....58
Figure 3.31. Force-displacement graph of the suspension spring of Hyundai Elentra model vehicle (Adapted from [24].). 59
Figure 3.32. Obtaining nonlinear suspension spring behavior…..…………………….. 60
Figure 3.33. Suspension spring behavior obtained in simulation environment 60
Figure 3.34. Acceleration-time graphs in X direction of Subaru Impreza model vehicle with linear (left) and non-linear (right) suspension springs 61
Figure 3.35. Acceleration-time graphs of Subaru Impreza model vehicle in Z direction obtained by using linear (left) and non-linear (right) suspension springs....61
Figure 3.36. X-direction velocity-time graphs of a Subaru Impreza model vehicle using linear (left) and non-linear (right) suspension springs 61
Figure 3.37. X-direction velocity-time graphs of the Subaru Impreza model vehicle using linear (left) and non-linear (right) suspension springs 62
Figure 3.38. X direction position-time plots of Subaru Impreza model vehicle using linear (left) and non-linear (right) suspension springs. 62
Figure 3.39. Z direction position-time plots of Subaru Impreza model vehicle using linear (left) and non-linear (right) suspension springs 62
Figure 3.40. Angular displacement-time plots of the Subaru Impreza model vehicle around the Y-axis obtained by using linear (left) and non-linear (right) suspension springs. 63
Figure 3.41. Accepted axes of motion of a vehicle (Adapted from [25].)....63
Figure 4.1. Forward-facing seat properties: (a) seat-occupant model; (b) recliner stiffness; (c) energy absorber (D)... 68
Figure 4.2. OC and C1 vertebrae and C7 and T1 vertebrae. 69
Figure 4.3. The angular and translational accelerations around the carfloor (from FE simulation)....72
Figure 4.4. The proposed system for rear-facing seats. 74
Figure 4.5. Seatpan forward movement. 75
Figure 4.6 Simulation of a frontal crash with the passenger sitting in the rear-facing seat at a speed of 56 km/h (NC(64))....84

Figure 4.7. Application of rear impact to forward facing seat without (top figure) and with (middle figure) torsion bar and frontal impact to rear facing seat without (bottom figure) torsion bar……………………………………………………………………. ………...85
Figure 4.8. Characteristics of the torsion bar torsion element.. 86
Figure 4.9. Torsion bar torsion element behavior in simulation environment at 56 kph crash severity 86
Figure 5.1. Classification of IIWPG neck force (Adapted from [39].) 90
Figure 5.2. The motion sequence of the seat-occupant system subjected to the pulse NCAP(64) 96

LIST OF TABLES

Table 1.1. Applied crash pulses. 2
Table 1.2. Comparison of injury criteria of flexible and rigid seat hinge. 8
Table 1.3. Injury criteria according to the distance between head and head restraint.......9
Table 1.4. Injury criteria according to seatback angles. 9
Table 1.5. Comparison of active and passive simulations. 12
Table 1.6. Peak displacements of the human body models used. 13
Table 2.1. Dimensions of the different human models used in the simulations. 19
Table 2.2. Sizes of the mechanism parts. 20
Table 2.3. Distances of the centres of mass of the parts composing body 3 to the rotation centre. 24
Table 2.4. Shear force comparison after implementation of several crash pulses. 34
Table 2.5. Tensile force comparison after implementation of several crash pulses........34
Table 2.6. N_{km} comparison after implementation of several crash pulses. 35
Table 2.7. NIC comparison after implementation of several crash pulses......................35
Table 2.8. S shape comparison after implementation of several crash pulses. 36
Table 2.9. Vhead wrt Sled comparison after implementation of several crash pulses....36
Table 2.10. Maximum seatback rear rotation comparison after implementation of several crash pulses. 37
Table 3.1. Design parameters of vehicles. 41
Table 3.2. Tyre and suspension spring-damper coefficients of vehicles. 44
Table 3.3. Moment of inertia values of the vehicles. 46
Table 4.1 Used crash pulses in simulations...68
Table 4.2. Forward-facing seat performance. 70
Table 4.3. Whiplash injury assessment reference values (IARVs) [28]. 77
Table 4.4. IARVs for low speed (LS) speed impacts [28].. 78
Table 4.5. IARVs for high speed (HS) speed impacts [28]..78
Table 4.6 High speed crash pulses properties [38]..80
Table 4.7 Performance of the proposed rear-facing seat...80
Table 4.8 Performance of the rear-facing seat at higher severities (head). 81
Table 4.9 Performance of the rear-facing seat at higher severities (upper neck). 81

Table 4.10 Performance of the rear-facing seat at higher severities (lower neck). 82
Table 4.11 Performance of the rear-facing seat at higher severities (overall neck) 83
Table 4.12 Performance of the rear-facing seat at higher severities (thorax)................ 83
Table 4.13 Performance of the rear-facing seat at higher severities (lumber spine). 83
Table 4.14 Performance of the rear-facing seat at higher severities (hip-femur-tibia)... 84
Table 4.15 Performance values of seat with and without torsion bar at 40 kph and 56 kph crash severities. 87
Table 5.1. Shear force comparison after implementation of several crash pulses.......... 91
Table 5.2. Tensile force comparison after implementation of several crash pulses. 91

LIST OF SYMBOLS AND ABBREVIATIONS

Symbols

Delta-V	The change in speed experienced by a car during a collision (km/h)
a_{mean}	Mean acceleration of the crash pulse (g)
a_{peak}	Peak acceleration of the crash pulse (g)
T	Torque/Moment (Nm) (Chapter 2), Track width (m) (Chapter 3)
J	Mass moment of inertia (kgm^2)
F	Force (N)
m	Mass (kg)
c	Damping coefficient (Ns/m)
k	Spring coefficient (N/m)
r	Radius (m)
b	Width (m)
h	Height (m)
θ	Rotation (degree)
g	Gravitational acceleration (m/s^2)
ω_n	Naturel frequency (Hz)
ζ	Damper ratio (unitless)
M	Vehicle mass (kg)
L	Wheelbase (m)
ω_{bb}	Body bounce frequency (Hz)
ω_{wh}	Wheel hop frequency (Hz)
ω_p	Pitch frequency (Hz)
v_r	Head rebound velocity (m/s)
$F_{sh}^{(+)}$	Maximum upper neck positive shear force (N)

$F_{sh}^{(-)}$	Maximum upper neck negative shear force (N)
F_{tn}	Upper and lower neck tension force (N)
F_{cm}	Upper and lower neck compression force (N)
M_{yU}	Largest upper neck moment (Nm)
F_{shL}	Largest lower neck shear force (N)
M_{yL}	Largest lower neck moment (N)
T_{1a}	Largest acceleration of the first thoracic vertebra (T1) (m/s^2)
H_{rCt}	Head restraint contact time (s)
T_{a3}	Maximum clip thorax acceleration value of 3 ms (g)
L_{tn}	Lumbar tensile force (N)
L_{cm}	Lumbar compression force (N)
N_{ij}	A neck injury criteria which is a combination of upper neck axial forces and extension/flexion moments (unitless)
cd	Maximum chest deflection (mm)
V_C	Viscous criterion (m/s)
H_{cm}	Hip fracture and dislocation force (N)
F_{cm}	Patellar and femur fracture/dislocation force (N)
T_{cm}	Tibia plateau or condyle injury force (N)

Abbreviations

US NCAP	United States New Car Assessment Program
GIDAS	German In-Depth Accident Research
IIHS	Insurance Institute for Highway Safety

IIWPG	International Insurance Whiplash Prevention Working Group
SUV	Sports utility vehicle
ECE	Economic Commission for Europe
M1 vehicles	Vehicles designed and constructed for the carriage of passengers and comprising no more than eight seats in addition to the driver's seat
MAIS 2	Injuries are bone fractures and concussions with brief loss of consciousness
FE	Finite elements
THUMS	Total human model for safety
GHBMC	Global Human Body Models Consortium
M50-OS	50th percentile simplified male FE model
HIC	Head injury criterion
BrIC	Brain injury criterion
ATD	Anthropomorphic testing devices
HBM	Human body model
FBD	Free body diagram
ODE45	Ordinary differential equations (45 means the solver implements the Runge-Kutta (4,5) method.
OC	Occipital condyles
C1	First cervical vertebra
N_{km}	An injury criterion that uses the combination of the shear force and the moment acting on the OC
NIC	Neck injury criteria
C7	Seventh cervical vertebrae
T1	First thorax vertebrae
CG	Center of gravity

HR	Head restraint
SB	Seatback
SP	Seat panel
R	Recliner
D	Shock absorber
NDI	Neck distortion index
CF	Cabin floor
S	Slot
W	Wedge
L	Locking ping
HL	High performance
LL	Low performance
CL	Limit boundaries
IARVs	Injury assessment reference values
TI	Tibia index
HS	High speed
LS	Low speed

1. INTRODUCTION

In autonomous vehicles, users can travel in non-standard seating positions. Examples of these sitting positions seat can be turned 90 degrees or 180 degrees according to the standard sitting position (forward-facing), or with the seatback can be leaned back. In this case, all restrictive protection systems (i.e. restraint systems) have to be redesigned. Because current restraint systems are designed to protect people traveling in standard sitting positions from crashes. Seat belts and airbags are examples of these protection systems. In addition, unconventional seating positions may pose more risks during a collision. In the normal sitting position, rear-end collisions occur with low crash severity, yet neck injuries are very common. In the scenario with 180 degrees we rotated seat, the same neck injuries can be observed when the frontal crash is considered. Statistically, frontal collisions are more severe and therefore higher protection is required. In high-intensity frontal collisions, there is a rise in the rear of the vehicle and such effects will also be considered in this thesis. Restrictive protection systems designed so far have been designed by giving horizontal collision acceleration. While horizontal accelerations are sufficient in low-intensity collisions, they are not sufficient in high-intensity collisions. Vertical and angular accelerations should also be considered in such scenarios.

Whiplash is an injury that occurs in the neck region as a result of sudden forward and backward movements of the head. In the neck region, there are spine, disc, nerves, muscles and other connective tissues. As a result of this sudden whiplash movement, these structures in the neck are damaged. In road traffic accidents, impacts from behind cause a high risk of whiplash. This sudden motion is usually accompanied by complaints and pain in the head and neck region. A common cause of neck trauma is thought to be an S-shaped deformation of the neck with respect to backward motion (retraction) of the head in relation to the torso. Car seats, where the seat and head restraint work together to effectively absorb the energy of impact, can alleviate neck injury. When the internal movement of the neck and neck forces are reduced during the collision, the whiplash is attenuated [1]. The GIDAS (German In-Depth Accident Research) database says that between 2005 and 2016, rear-end collisions mostly occurred at relative speeds between

10 and 45 km/h. Here, the relative speed expresses the difference between the speeds of the colliding vehicles [2]. Another study [3] compared rates of claims for bodily injury insurance in rear-end collisions with corresponding seat/head restraint ratings (by the Insurance Institute for Highway Safety (IIHS)) for cars and SUVs manufactured from 2001 to 2014. Good performing vehicles showed 11.2% fewer injuries compared to poor performing vehicles. The GIDAS database was also examined for accidents between 2000 and 2015 to assess whether emergency braking with maximum deceleration poses a significant risk of neck injury [4]. This study [4] detected 14,070 isolated frontal collisions involving full braking (average deceleration of more than 6 m/s2) in 4,690 cases. In these cases, 597 out of a total of 6,473 passengers had sustained neck injuries. An accident database survey conducted in 2005 on single rear-end collisions offers the following; 77% of cars had a Delta-V of less than 15 km/h, 16% had a Delta-V between 15 and 25 km/h, and 7% had a Delta-V greater than 25 km/h [5]. Delta-V is the change in speed experienced by a car during a collision. It is calculated from the acceleration-time graph crashing car by integrating the curve. The characteristics of all crash pulses used in this PhD thesis study are given in the Table 1.1 below.

Table 1.1. Applied crash pulses.

Pulse	ΔV [km/h]	a_{mean} [g]	a_{peak} [g]		Pulse	ΔV [km/h]	a_{mean} [g]	a_{peak} [g]
SN(9.4)	9.4	3.1	11.7		TR(24)	24	6.5	7.5
SN(13)	13	4.7	10.3		FMVSS	30	4	16
IIWPG	15	3.5	10		HS(35)	35	10.54	16
TR(16)	16	4.5	5		NCAP(43)	43	14	36.6
SN(16)	16	5	10		NCAP(64)	64	15	38
SN(20.5)	20.5	5.2	10.6					

Within the scope of this doctoral thesis, design studies were carried out for both forward and backward facing seats in autonomous vehicles. In particular, it is aimed to design a seat that covers all collision intensities that can be encountered in autonomous vehicles and provides optimum neck protection. This designed seat can be used in autonomous vehicles while looking both forward and backward directions. The main purpose of the realized designs is to restrict the passenger's range of motion just before the collision. In particular, designs based on eliminating the gaps between the dorsal region, neck and head of the passenger and the seatback and head restraint of the seat are presented within the scope of the thesis.

In the plan of the thesis, the applied crash severities were applied in an increasing order. Within the scope of the thesis in chapter 2, a mechanism that will be activated just before the collision is presented. This mechanism will move the seatback to a more upright position. Thus, the distance between the passenger/driver's back and the seatback will be reduced to a minimum. This will have the effect of restricting the freedom of movement of the passenger/driver’s bodies while traveling in the vehicle. The more upright position of the seatback will also contribute to more effective absorption of collision energy. In the relevant part of the thesis (chapter 2), a head restraint that works simultaneously with the seatback is also presented. The head restraint will also move forward before the collision. This forward movement of the head restraint will allow the head to be supported earlier. This will limit the movement of the neck relative to the head. With the aid of the presented mechanism forward crash scenarios on rearward facing seat were simulated up to 30 km/h ΔV values. For more severe crash pulses, mentioned protection system was found insufficient and more effective protection system was proposed in chapter 4.

The next part of the thesis (chapter 3) includes the validation of two different vehicles in the simulation environment. These validations were needed to study higher crash intensities. Because real crash tests include horizontal and vertical acceleration data of vehicles at the time of collision. Angular acceleration data are also needed to apply higher crash intensities to the human-seat model. These estimated high severity crash pulses (at ΔV 40 km/h and ΔV 56 km/h) from validation studies in chapter 3 were used to test the restriction system given in the chapter 4. Crash scenario validations were performed by using the dimensional and mechanical properties of two different vehicles (2007 model Toyota Yaris and 2014 model Subaru Impreza).

The last part of the thesis (chapter 4) includes the application of the horizontal, vertical and angular acceleration data obtained in the previous section to the human-seat model at high crash intensities (at ΔV 35, 40 and 56 km/h respectively). Firstly, a whiplash mitigating forward-facing seat was proposed for rear impact scenarios up to 24 km/h ΔV values crash pulses. Performance of the this seat was good at these crash pulses. When this seat turned 180 degree back (looking rearward orientation), it’s protection performance was decreased espacially at high severeties. These applications have shown that additional protection systems are needed to prevent neck injuries. For this purpose, a design called torso plates, which supports the body during the collision and minimizes the effects of the collision, has been presented (this application was performed on rear facing seat for frontal impacts at higher crash severeties). In addition to the aforementioned design, a torsion element (torsion bar) is proposed to prevent the seat from turning inside the vehicle cabin during the collision and to reduce compressive loading on the spine (for the same seat looking forward this time and was applied the same high crash pulses from rear of the vehicle). This torsion element has yielded efficient results in high-intensity collision intensities. Thus, within the scope of this chapter, the designed seat were tested applying high crash intensities in both forward and rear facing conditions by using torso plates.

1.1. Literature Survey

Himmetoğlu and Kılıç addressed the issue of safety in fully autonomous vehicles from a Turkish perspective [6]. In this study, 21 men and 20 women aged between 11 and 60 were asked 12 questions about the safety of fully autonomous vehicles and only 30 per cent of them answered "I feel safe in fully autonomous vehicles".

It is a well-known fact that ninety percent of traffic accidents are caused by human error. The ideas behind the development of fully automated vehicles are: to take control away from the human driver, to ensure road safety, to improve traffic flow, to save fuel, to enable other tasks other than driving, and to ensure the safe transportation of passengers who are easily prone to injury (such as the physically disabled, children and the elderly).

In their study, the authors cite information from a recent study of autonomous car accidents in California: most common accidents are rear-end collisions in which conventional cars impact autonomous cars. In such accidents, the autonomous vehicle was reported to be mainly to blame in 15% of cases, and these accidents occurred at intersections. In only 3 out of 26 cases, the autonomous technology was able to detect and react before the collision. In mixed traffic flows with conventional and autonomous vehicles, autonomous vehicles are reported to be 10 times more accident prone than conventional vehicles.

In autonomous vehicles, seating arrangements different from the traditional seating arrangements can be used. Seats in different orientations can be used for tasks such as sleeping, eating or reading. Unconventional seating positions can increase the risk of being injured in the event of an accident.

If the vehicle is taken over by hackers, it is a question mark how an inexperienced driver can safely control the vehicle. In addition, drivers may need to take control in bad weather conditions or complex traffic conditions.

Considering these situations, it is seen that people living in Turkey have difficulty in trusting automated vehicles and fear cyber-attacks. One of the most important security issues in autonomous vehicles is the question of how to protect passengers in different seating arrangements. Below this problem is analyzed and solutions are proposed in the literature.

Jin et al. [7] state in their paper that the protection of existing protection systems varies in different seating arrangements and that changing the seat position according to the direction of impact will protect the occupants. Since fully autonomous vehicles detect the unavoidable collision 200 ms in advance, they argue that there is enough additional time for the vehicle seats to take a position to protect the occupants. According to the simulation results, the position where the seatback is completely turned to the front of the vehicle during a frontal collision is safer than other positions. Moreover, the 200 ms time was sufficient to rotate the occupant +- 45 degrees without causing additional injuries.

In addition, the simulation results of Jin et al. showed that in the 180-degree sitting position, the passenger is stopped by the seatback and minimum head rotation is achieved. Again, minimum chest deformation was observed in the 180-degree position. The benefit of receiving the impact from the rear in frontal impacts is due to the distribution of the force over a large area behind the seat. Again, the high number of injuries in 45 and 135 degree collisions is due to the seat belt design (Figure 1.1). In the seat rotation simulations, it was observed that the 45-degree rotation caused less injury than the 90-degree rotation.

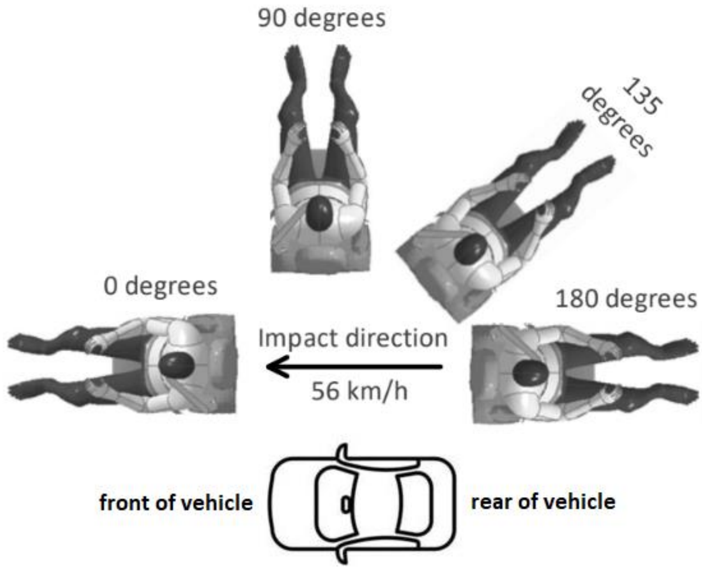

Figure 1.1. Definition of seating orientations (Adapted from [7].).

There mainly three limitations in this study. Firstly, in front-end collision conditions the human-body model has not been quantified against experimental data for chosen four initial seating orientations. Secondly, there are small number of seating positions (four). Finally, the seat structure is modelled as rigid. It is a known fact that deformable seat structures absorb more energy.

Zellmer and Manneck [8] argue in their study that occupant protection in a rear-facing seat should be at the same level as in a forward-facing seat. They conducted, analyzed and discussed the results of sled tests under frontal impact conditions at a speed of 56 km/h on a rearward facing seat.

A limitation of their work is that only the full preload aspects have been studied. They did not focus on the head support. The head is fixed to the head restraint with no gap between them.

The authors say that although several rear-facing seats on car models, there has been almost no publication of accident analyses for these vehicles. The German In-Depth Accident Study (GIDAS) reports only five incidents in ECE M1 vehicles. Only one rear seat passenger reported injured (MAIS 2). In all crashes, however, the speed change Δv of the colliding vehicle was below 25 km/h.

Some studies were also conducted by the authors to determine the risk of getting hurt in rear-ended crash with high Δv up to 40 km/h. As a result, in this study, frontal crash scenarios with rear-facing seats with a rotation of less than 5% were validated.

Hasija et al. [9] used the FE driver seat model of the Toyota Yaris in conjunction with the Total Human Model for Safety (THUMS) FE model to analyze rear-end collisions. Simulations were performed at 15 mph and 35 mph Delta-V which are low and high speeds respectively to understand how seat hinge stiffness affects the THUMS kinematics. The authors also evaluated other design modifications such as integrated seat belts and active head restraint. They then analyzed injury measurements for male occupants of average height and weight with a range of seatback angles and in a variety of seat configurations. In this phase of the study, the authors used the Global Human Body Models Consortium (GHBMC) 50th percentile simplified (M50-OS) male FE model in combination with the Honda Accord FE driver seat model. Head Injury Criterion (HIC) and Brain Injury Criterion (BrIC) were used for head and brain injury criteria, while chest injury was used for maximum chest deformation. Countermeasures to reduce BrIC were examined for various seat orientations on with the potential highest BrIC value. It was observed that a rigid seat hinge, an integrated seat belt and an active head restraint helped to reduce the injury matrix. In frontal and rear crashes, high BrIC values were found at high seatback angles. Chest deformation was high for frontal crashes at higher seatback recline angles but showed an opposite trend for rear crashes. According to the authors, existing test methods and procedures and Anthropomorphic Testing Devices (ATD) would not sufficient for the assessment of the risk of getting injured in all of these scenarios.

Human FE models for designing new car interiors with flexible seating orientations and arrangements play key role in assessing occupant protection. Currently, most high-speed vehicle crash tests are carried out for front-end crash scenarios with all occupants located in the forward-facing seats. Low-speed rear crash scenarios for vehicles with autonomous driving systems are currently being carried out for occupant protection, but high-speed rear impact tests should also be performed to evaluate seats and seat belts and to understand occupant kinematics. The following tables summarize the work done by Hasija et al.

Table 1.2. Comparison of injury criteria of flexible and rigid seat hinge (Adapted from [9].).

	Delta-V=15 mph			Delta-V=35 mph		
Seat Hinge	BrIC	HIC_{15}	Chest Deformation (mm)	BrIC	HIC_{15}	Chest Deformation (mm)
Flexible	0.58	92	28	1.85	3466	85
Rigid	0.28	78	15	0.93	490	36

Table 1.3. Injury criteria according to the distance between head and head restraint (Adapted from [9].).

Distance Between Head and Head Restraint (mm)	BrIC	HIC_{15}	Chest Deformation (mm)
45	0.93	490	36
1	0.90	357	31

Table 1.4. Injury criteria according to seatback angles (Adapted from [9].).

	Forward Collision			Rear Collision		
Seatback Angle	BrIC	HIC_{15}	Chest Deformation (mm)	BrIC	HIC_{15}	Chest Deformation (mm)
20^0	0.81	1106	38	0.22	145	21
45^0	0.88	236	44	0.42	166	18

As can be seen from the above tables, when the flexible seat hinge was used, the rotation of the seat back results in an elevation of the occupant along the seat back. This ramped motion leaded backward rotation of head and made hade to hit the head restraint and jolt. This can cause severe injuries on neck and head. In the study, the seat hinge was replaced with a rigid hinge to reduce the potential risk of injury. The rigid seat hinge raised the capacity of energy absorbing seat frame, and the occupant protected from accumulation of excessive speed. The integrated seat belt used in combination with the rigid seat hinge was a factor in preventing from injury risk. A head restraint that minimizes head and head restraint clearance is also a factor that reduces injuries. Lower seatback angles (positions where the seat is close to the vertical) resulted in fewer injuries.

One of the expectations of users from future vehicles is to be able to travel in a horizontal position (i.e. reclined seating posture) in the vehicle. This poses new challenges in frontal crashes. Current vehicles are designed for upright seating positions and are not suitable for travelling in a horizontal position. In their study, Östh et al. [10] investigated the upright positioning of the occupant prior to a frontal collision. When the seatback was moved to the upright position during the collision, similar head kinematics were obtained as in the initial upright position.

This study investigated how moving the driver from a horizontal position to a more upright position prior to the crash would affect the kinematics and the constraint interaction during the crash.

Initial simulations were run both actively and passively to examine the effect of moving the seatback to a more upright position on injury prediction and passenger kinematics.

In the scenario of repositioning the passenger by lifting the seatback prior to the crash, the occupant's position and spinal curvature were observed to be quite similar in the upright and horizontal position, with the orientation of the pelvis not fully preserved.

Different strategies to move the occupants from a horizontal position to a more upright position resulted in less stress on the head and chest. This is because the protection systems used in this study (airbag and seat belt) were designed for travelling in an upright position. The reason for the higher impact velocity in the horizontal position is the increased distance to the airbag and seat belt.

Becker et al. [11] also investigated the principles of accident protection for passengers travelling at different seating angles in highly or fully autonomous vehicles. In this study, the main focus of the safety concept was to rearrange to position of the occupant to a safer seating arrangement just before an accident. In the event of an unavoidable accident, the seat is turned in the direction of collision to provide adequate restraint of the airbag and seat belt. Two principals were analyzed in the study: the first one is based on active rotation, while the second one is based on inertia of the seat and the occupant. As a result of the analyses, the authors found that occupant moved to a near standard position just before the accident by both adjustment mechanisms.

In their study, the authors note that rotating the seat at a high speed in the pre-crash phase leads to a high risk of injury. A rotation of 45 degrees in a 200 ms period is considered appropriate. A 90-degree rotation in a 200 ms period showed some bone connective tissue strains and this movement was considered above the injury threshold.

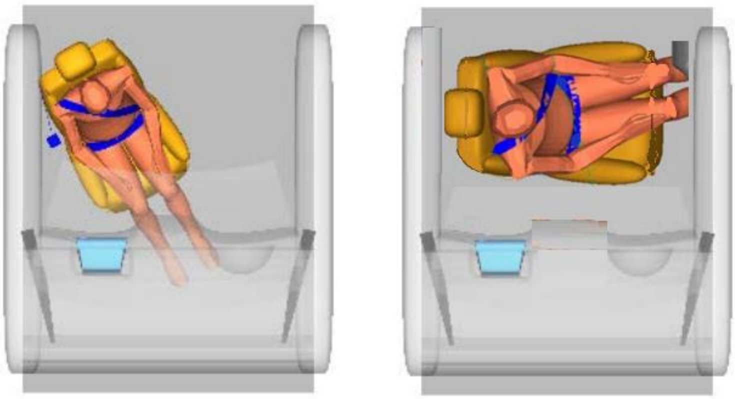

Figure 1.2. Initial positions of the seat model (45^o on the left and 90^o on the right) (Adapted from [11].).

In the first protection principle, the authors aimed to position the seat close to the standard travelling position (i.e. forward facing). In this scenario, the person is sitting in the passenger seat. The study aimed to rotate the seat up to 30 degrees. A number of measures were also taken to measure the longitudinal pressure of the seat belt during rotation. The second protection principle is a special case of the first one and the seat-passenger rotation is achieved by the system's own mass inertia. This rotation is provided by the relative acceleration caused by the automatic emergency braking and is considered as a passive protection since it only works when this braking occurs. The system, which works by releasing a rotary joint before the accident occurs, is locked when the rotation angle changes from 30 degrees to 0 degrees. A comparison of the two principles can be seen in the table below.

Table 1.5. Comparison of active and passive simulations (Adapted from [11].).

Simulation Number	X Coordinate Rotation Axis(m)	Y Coordinate Rotation Axis(m)	Average Rotation Speed (^{0}/s)
PP1 run_071	0.18	0.00	60
PP1 run_091	0.09	0.25	200
PP2 run_071	0.18	0.00	43
PP2 run_091	0.09	0.25	76

In the study, four different angles were defined to see the effectiveness of rotating the seat before the accident. These angles are between the seat angle and the passenger's head, shoulders, hips and knees. The purpose of using these angles is to determine how well the different parts of the body follow the rotation of the seat. These angle values were higher at higher rotation speeds.

The relative repositioning of PP1 is higher than that of PP2. This results in a smaller relative difference in the angle between the seatback-seatpan and the various parts of the occupant (head, shoulder, hip and knee relative angles). PP1 is also characterized by an earlier start time for the turn and a not too high turn speed. In both sets of simulations, after the seat stopped turning, the passenger continued to turn until contact with the airbag.

Soni et al. [12] state that in future autonomous vehicles, the front seats may be positioned rear facing which may put the passengers at risk in frontal collisions. Despite this risk, they also state that there are not many high-speed setups that can test such crash scenarios today. Only Ohio State University is working on a test rig. From the perspective of accident data analysis, rear-facing seats are only available on a few car models. Furthermore, analyses focusing on adult car occupants in rear-facing seats are scarce. In their study, the authors report that when the seat is rear facing, the occupant's head moves upwards along the seatback and the loading on the neck is at its highest value. The authors studied frontal crashes with different simulation dummies. They analyzed the kinematics, acceleration, forces and moments of the dummies used and tried to understand the similarities and differences between them. The table below shows a comparison of the peak displacements of the human body models used.

Table 1.6. Peak displacements of the human body models used (Adapted from [12].).

Peak Displacements													
Rotating Seatback							Fixed Seatback						
	THOR		H350		SAFER-HBM			THOR		H350		SAFER-HBM	
	x	z	x	z	x	z		x	z	x	z	x	z
Head	330	-86	300	-51	318	-95	Head	23	-30	32	5	30	-22
Chest	265	-50	198	-36	310	-70	Chest	65	11	31	9	75	12
Hip	168	18	108	8	163	33	Hip	66	15	43	-7	70	-6

Of the three, the H350 model has the least displacement in all conditions. The head and chest trajectories between THOR and SAFER-HBM were close to each other, while the pelvis displacement differed. The figure below gives a comparison of the contact forces between the three different human body models and the seatback.

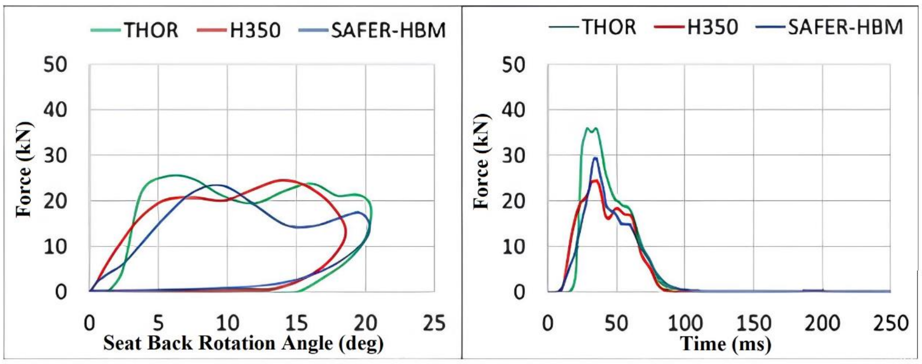

Figure 1.3. Comparison of contact forces between three different human body models and seatbacks (Adapted from [12].).

The peak force values in the rotating seatback simulations were similar between the passenger models. Compared to the rotating seatback, the peak force values were higher in the fixed seatback. When the neck deformations were analyzed, SAFER-HBM and THOR showed high deformations, while the neck was almost undeformed in the H350 model.

The authors point out that the main limitation of this study is that the models used in this study have not been validated for frontal crashes with a rear-facing seat. Nevertheless, they say that the SAFER-HBM model gives more accurate results than the others due to its closeness to human anatomy.

In another study, Luttenberger et al. [13] mention that existing protection systems will be insufficient in different sitting positions in autonomous vehicles. For this purpose, seat-mounted airbags, inflatable seat belts, seat design similar to racing cars and child seats, life-cell airbags and side-impact airbags are suggested from the literature.

The authors first exposed the passenger model to severe rear and frontal crash pulses. Then they equipped the vehicle with comprehensive new seat-mounted protection principles (three-point seat belt, comprehensive safety vest and head restraint system).

As a result of the simulations, the protection systems used showed deficiencies in both frontal and rear impacts. Although the comprehensive safety vest showed potential, it still has limitations in reclined seating positions in frontal and rear impacts.

In addition, rear crashes were categorized as less critical in the study. This is because the contact surfaces of the backrest, headrest and tibia function as a restraint system. In a car crash from rear-end, the neck and head were displaced upwards over the head restraint, resulting in high loads on the neck.

Considering the kinematics and kinematics of the occupants, comprehensive restraint systems provided advantages over conventional restraint systems.

In their study, according to Wu et al. [14] existing protective systems can vary in effectiveness depending from one seating position to another and better occupant protection with seat adjusted to the direction of impact. In their simulation results, they found that during a frontal collision, the rearward seat is more protective than the other seats. This is because the forces in a collision are distributed over a large area of the back of the seat. They also say that 200 milliseconds is enough for a 45 degree or 90 degree rotation of the seat without the risk of additional injury. Here, 200 ms is the time required to detect unavoidable collisions and take precautions. In the study, firstly, the injury risks of passengers in different seating positions were investigated and compared. Then, the crash pulse was applied after the seat was returned to a safer position. As a result, the authors reached similar results with [11].

Rawska et al. [15] investigated how occupant size affects, seat backrest and knee support position on injury in frontal crashes for a reclining seat. The authors concluded that submarining is likely to increase with autonomous vehicles and will pose major challenges for reclining seats. In this case, passengers will move more forwards during an accident, there is an increased risk of the lower limbs being injured, and an increased load on the lower part of the chest, abdomen and vertebrae.

McMurry et al. [16] analyzed the frequency, demographics and injury outcomes of passengers sitting in non-traditional seating positions in automobiles. The authors also compared the outcomes of minor accidents occurring in conventional seating positions with the outcomes of accidents occurring in non-traditional seating positions. The study concluded that the number of unusual sitting positions was insufficient to reach a definitive conclusion about injury outcome.

Finally, Moon et al. [17] have previously proposed the idea of turning the seatback upwards before an inevitable collision but did not mention how this turning process would be realized.

The literature survey has shown that crash safety in autonomous vehicles is a new and intriguing topic. The literature review has also shown that the number of existing studies and the data obtained are insufficient. The general opinion in the reviewed studies is that the existing protection systems will not be sufficient in different seating arrangements in autonomous vehicles. The proposed solution is either to bring the seating arrangement to the usual seating arrangement before the accident or to develop new restraint systems.

As mentioned at the end of the introduction, studies have been carried out both to adjust the seating position to minimize neck damage and to develop new restraint systems. In addition, real crash tests were validated in computer environment in order to simulate high speed crashes in computer environment. High speed collisions were simulated with the data obtained as a result of these validations. According to these simulation results, new restraint systems were proposed, tested and proved to be effective.

2. PRO ACTIVE SEATBACK DESIGN

In this part of the thesis, a mechanism has been designed to provide energy absorption by moving the vehicle seatback to a more upright position before a crash in autonomous vehicles. This design was tested for rearward seats by applying forward crashes up to pulses that have 30 km/h ΔV values. This upright position of the seatback will ensure that the crash energy is absorbed by a larger surface of seatback. This will increase the crash energy absorption of the seat. Again, the upright position of the seatback will reduce the distance between the passenger and the seatback. This will have the positive effect of reducing the volume in which the occupants can move, or rather be thrown, in the event of a crash. This mechanism will provide additional protection by activating just before an inevitable crash scenario. With this mechanism, the head restraint has also been provided to move slightly forward. This forward movement of the head restraint will ensure that the head is supported at an early stage during the crash. Thus, the movement of the neck relative to the head will be restricted and will have a preventive effect on neck injury. The main purpose of designing this mechanism is to ensure that the head restraint and the seatback work together effectively. This co-operation of the seatback and head restraint will ensure that the crash energy is absorbed to a great extent.

In the following sections, the geometry of the proposed mechanism is introduced, the differential equations are obtained, the behavior of the head restraint is explained, the behavior of the mechanism, the applied crash severities and the results are presented.

2.1. Mechanism Geometry

In this section, firstly the geometry of the specified mechanism is analyzed. The details of the mechanism and its constituent parts are given below (Figure 2.1, Figure 2.2).

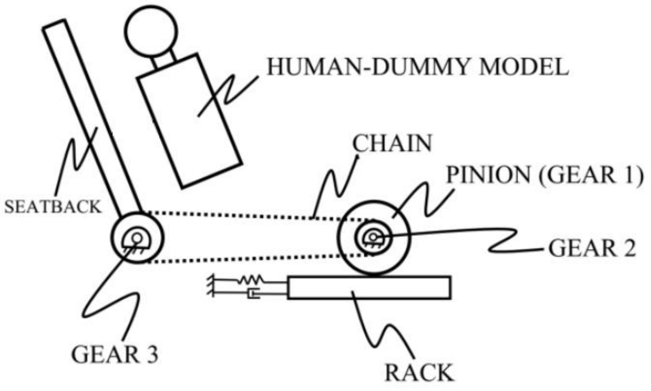

Figure 2.1. Proposed mechanism.

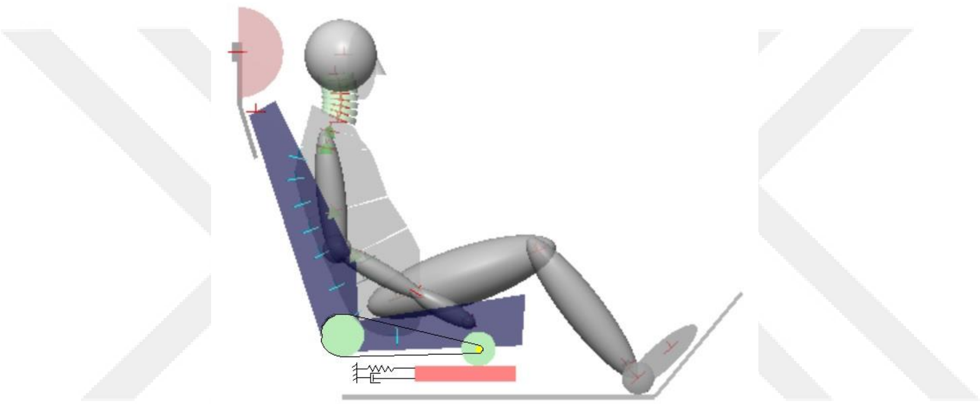

Figure 2.2. Representative image of the mechanism proposed in this study.

The proposed mechanism consists of a spring, a damper, a rack and pinion duo, a gear pair connected by a chain, a driver's seat backrest and a human model. The connection between the rack and the ground plane is made by means of a spring with pre-tension and a damper. The release of the spring with pre-tension will force the rack element to move to the left. The leftward movement of the rack will rotate the pinion gear clockwise. In order to provide the desired rotation angle for the driver's seat backrest, a gear ratio is determined between the second and third gear. The third gear will rotate in the same direction as the second gear with the help of the chain link. This movement of the third gear connected to the driver's seatback will bring the driver's seatback to a more upright position. The human model will rotate with the driver's seatback. When the predetermined driver's seatback rotation is achieved, a locking mechanism will lock the third gear.

The physical quantities of the human model [18] and the components of the mechanism presented on Figure 2.1 are given in Table 2.1 and Table 2.2 below. The mechanism was tested using a male model with three different masses. The purpose of performing these different simulations is to test whether the mechanism works well with people of different sizes and masses.

Table 2.1. Dimensions of the different human models used in the simulations.

Model	Part	Mass	Size
Average Man	Head	4.6 kg	0.1 m (radius)
	Neck	1.63 kg	0.05 m (radius) 0.11 m (height)
	Torso	43.925 kg	0.23 m (width) 0.67 m (height)
	Total	50.155 kg	-
Plumb Man	Head	4.481 kg	0.1 m (radius)
	Neck	1.71 kg	0.067 m (radius) 0.15 m (height)
	Torso	53.22 kg	0.32 m (width) 0.62 m (height)
	Total	59.411 kg	-
Thin Man	Head	4.105 kg	0.1 m (radius)
	Neck	1.46 kg	0.05 m (radius) 0.1 m (height)
	Torso	32.62 kg	0.2 m (width) 0.57 m (height)
	Total	38.185 kg	-

Table 2.2. Sizes of the mechanism parts.

Part	Mass	Size
Seatback	10 kg	0.1 m (width) 0.7 m (height)
Gear 3	1.37 kg	0.12 m (radius)
Gear 2	0.96 kg (together)	0.01 m (raduis)
Gear 1		Approximately 0.1 m (raduis – calculated)
Rack	0.942 kg	0.2 m (desired rack displacement)

Before the crash, the proposed mechanism is required to rotate the seatback forward by 10 degrees. In order to realize this request, a gear ratio has been determined between the seatback and the mechanism. Looking at Table 2, it can be seen that there is a gear ratio of 12 between gear 3 and gear 2. Again, as stated in table 2, a displacement of 0.2 m of the rack is required. This value is also the amount of compression of the pre-tensioned spring. In the light of the values given here, the radius of the gear 1 can be calculated by the following formula.

$$r_1 = \frac{rd*180}{gr*sr*\pi} \quad (1)$$

In this formula r1, rd, gr and sr are given as follow;

r_1: Radius of Gear 1 (meter)

rd: Displacement of Rack (meter)

gr: Gear ratio

sr: Rotation amount of Seatback

After this stage, the Newton-Euler method was used for the dynamic analysis of the mechanism to obtain the differential equation of the presented mechanism. After obtaining the differential equation, the differential equation was solved for the rotation angle of the seatback and the coefficients of damper and spring were selected for the mechanism. With the selected spring and damper coefficients, it was tested whether the mechanism could rotate the seatback to a more upright position in the desired amount of time.

2.2. Obtaining the Differential Equations

Newton-Euler method was used to investigate the dynamic behavior of the mechanism. Newton-Euler method is one of the methods of expressing the behavior of physical systems in time domain. It is used to analyze the translational and rotational movements of objects. To use this method, one must be necessary to analyze each moving part of the system separately. Again, to understand the overall behavior of the system, one must be necessary to define the motion relationships between these moving parts. To perform mechanism dynamic analysis, the mechanism is divided into three parts. These parts are the rack, the pinion (second) gear and the third gear-driver seat backrest-human model trio. The third gear, which is expressed as the third part, provides the movement of the driver's seatback and the human model at the same time. This movement is the rotation movement around the geometric center of the third gear. For this reason, the third gear, the driver's seatback and the human model were considered as a single part and included in the dynamic analysis. The second gear’s connection was made by a chain to the third gear, and the first pinion gear, which is concentric with it, are considered as a single part.

The rack in contact with the pinion is the first part in the dynamic analysis. Here, a contact force is generated between the rack and pinion. This contact force is also shown in the FBDs of the parts. In the same way, the forces arising from the pre-tension spring and damper to which the rack is connected must also be taken into account. With the release of the pre-tension spring, the force due to the mass of the rack, which starts to accelerate, will also be included in the equations. When the second part is examined, there is a contact force on it due to its contact with the rack. Again, there is a moment coming from the third gear to which it is connected with the chain. This moment relationship is defined by considering the gear ratio between the third gear and the second gear. Finally, a moment arising from the inertia of the second part will also occur. When the third part is examined, it can be seen that the center of gravity is not on the rotation axis. Therefore, the moment effect of the weight of the third part around the rotation center must also be considered. In addition, a moment coming from the second gear to which the third gear is connected with the chain and the moment of inertia of the third part are also included in the calculations. The dynamic equations of the mechanism were derived from seatback to the rack. The FBDs of the mechanism parts are given below (Figure 2.3, Figure 2.4).

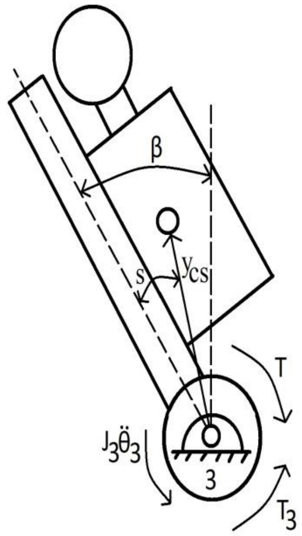

Figure 2.3. FBD of part 3.

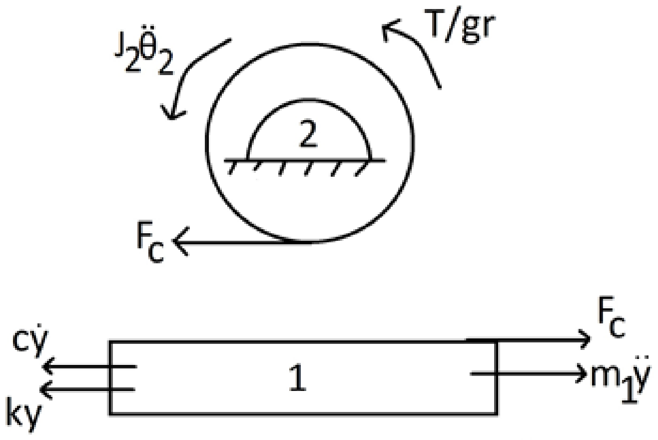

Figure 2.4. FBDs of part 2 and part 1.

Since the movement of the mechanism is planar (two dimensional), there is no need to use coordinate transformation matrices between the parts.

When Figure 2.3 is analyzed, the following explanations can be made.

β: angle between the vertical axis of the ground coordinate and the vertical axis of the driver's seat seatback (degree)

y_{cs}: magnitude of the center of gravity vector of the human model-driver seatback system (meter)

s: the angle between the vertical axis of the driver's seatback and the center of gravity vector of the human-driver seat system (degree)

T: moment transmitted between the second and third gear (Nm)

T_3: the moment created at the third gear center by the force generated by the mass of the human model - driver's seatback system (Nm)

J_3: mass moment of inertia of the third part (kg m^2)

When Figure 2.4 is analyzed, the following explanations can be made.

F_c: contact force between the first and second masses (Newton)

gr: gear ratio between Gear 2 and Gear 3

J_2: mass moment of inertia of the second part (kg m2)

m_1: mass of Part 1 (kg)

c: coefficient of damper (Ns/m)

k: coefficient of spring (N/m)

As mentioned above, the human model (head, neck and torso), seatback and gear 3 are considered as a single part. Here, this single part performs a rotation around geometric center of gear 3 (not center of gravity around the gear 3). Therefore, the moment of mass inertia of this part must be calculated around the specified center. The distance of the centers of mass of the seatback, neck, head and torso parts respectively to the geometric center of the gear 3 is given in Table 2.3.

Table 2.3. Distances of the centers of mass of the parts composing body 3 to the rotation center.

Part	Distance		
	Average Man	Plumb Man	Thin Man
Seatback	0.35 m	0.35 m	0.35 m
Head	0.87 m	0.87 m	0.75 m
Neck	0.74 m	0.72 m	0.65 m
Torso	0.37 m	0.38 m	0.32 m

When the seatback is considered as a rectangular prism, the head as a sphere, the neck as a cylinder and the body as a rectangular prism, the mass moments of inertia of these parts can be calculated by the following formulae.

$J_{3gear} = 0.5 * m_{3gear} * r_{3gear}^2$ (2)

$J_{seat} = (1/12) * m_{seat} * (b_{seat}^2 + h_{seat}^2) + m_{seat} * r_{3seat}^2$ (3)

$J_{head} = (2/5) * m_{head} * r_{head}^2 + m_{head} * r_{3head}^2$ (4)

$J_{neck} = (1/12) * m_{neck} * (h_{neck}^2 + 3 * r_{neck}^2) + m_{neck} * r_{3neck}^2$ (5)
$J_{body} = (1/12) * m_{body} * (h_{body}^2 + r_{body}^2) + m_{body} * r_{3body}^2$ (6)

$J_3 = J_{3gear} + J_{seat} + J_{head} + J_{neck} + J_{body}$ (7)

In the light of this information, Euler equation of the third part can be written as follows;

$T_3 - T = J_3\ddot{\theta}_3$ (8)

It has already been mentioned above that the term T3 here is the moment created at the third gear center by the force resulting from the mass of the human model-driver seat-back system. We can express this moment as follows;

$T_3 = m_3 g y_{cs} Cos(\theta_3 + \alpha - s)$ (9)

The expression ycs in Equation (9) is the distance of the gravity center of the system mentioned above to the geometric center of the third gear. In the same way, α gives the initial position of the seatback relative to the ground in radians. We can write the Euler equation of the second part through Figure 2.4. Here, the gear ratio is taken into account when specifying the moment transmitted by the chain. It is also necessary to mention the moment created by the contact force between the rack and the pinion at the center of the second gear.

$\frac{T}{gr} - r_2 F_c = J_2 \ddot{\theta}_2$ (10)

Again through Figure 4, we can write the Newton equation of the first part as follows.

$m_1 \ddot{y} + c\dot{y} + ky = F_c$ (11)

Equation (9) is inserted into equation (8) and the moment T is obtained.

$T = m_3 g y_{r3} Cos(\theta_3 + \alpha - s) - J_3 \ddot{\theta}_3$ (12)

Equation (10) is solved for the contact force.

$F_c = \frac{T}{r_2 gr} - \frac{J_2 \ddot{\theta}_2}{r_2}$ (13)

Equation (12) is then inserted into equation (13).

$$F_c = \frac{m_3 g y_{r3}}{r_2 gr} Cos(\theta_3 + \alpha - s) - \frac{J_3}{r_2 gr}\ddot{\theta}_3 - \frac{J_2}{gr}\ddot{\theta}_2 \ (14)$$

Finally, if equation (14) is inserted into equation (11), the following expression is obtained.

$$m_1\ddot{y} + c\dot{y} + ky = \frac{m_3 g y_{r3}}{r_2 gr} Cos(\theta_3 + \alpha - s) - \frac{J_3}{r_2 gr}\ddot{\theta}_3 - \frac{J_2}{gr}\ddot{\theta}_2 \ (15)$$

The following transformations are made on equation (15).

$$\theta_2 = \frac{y-b}{r_2}, \theta_3 = \frac{y-b}{r_2 gr}, \ddot{\theta}_2 = \frac{\ddot{y}}{r_2}, \ddot{\theta}_3 = \frac{\ddot{y}}{r_2 gr} \ (16)$$

Here, the expression b gives the amount of pre-tension of the spring. Equation (16) is inserted into equation (15) and the following equation is obtained.

$$\left(m_1 + \frac{J_2}{r_2^2} + \frac{J_3}{r_2^2 gr^2}\right)\ddot{y} + c\dot{y} + ky - \frac{m_3 g y_{r3}}{r_2 gr} Cos\left(\frac{y-b}{r_2 gr} + \alpha - s\right) = 0 \ (17)$$

In equation (17), Let's $M = m_1 + \frac{J_2}{r_2^2} + \frac{J_3}{r_2^2 gr^2}$ ve $K = -\frac{m_3 g y_{r3}}{r_2 gr}$;

$$M\ddot{y} + c\dot{y} + ky + K\ Cos\left(\frac{y-b}{r_2 gr} + \alpha - s\right) = 0 \ (18)$$

The whole equation is divided into the expression M.

$$\ddot{y} + \frac{c}{M}\dot{y} + \frac{k}{M}y + \frac{K}{M}\ Cos\left(\frac{y-b}{r_2 gr} + \alpha - s\right) = 0 \ (19)$$

Finally $A_1 = \frac{c}{M}, A_2 = \frac{k}{M}, A_3 = \frac{K}{M}$ transformations were made to obtain final differantial equation.

$$\ddot{y} + A_1\dot{y} + A_2 y + A_3\ Cos\left(\frac{y-b}{r_2 gr} + \alpha - s\right) = 0 \ (20)$$

When Equation (20) is analyzed, it can be seen that the differential equation depends on the displacement of the rack element. In order to solve the second order equation (20) with ODE45 in MATLAB environment, two first order equations are needed. These equations are obtained by the variable substitution method.

$$\dot{y}_1 = y_2 \ (21)$$

$$\dot{y}_2 = -A_1 y_2 - A_2 y_1 - A_3 Cos\left(\frac{y_1-b}{r_2 gr} + \alpha - s\right) \ (22)$$

The mechanism was requested to rotate the driver's seat backrest and the human model to a more upright position by approximately 10 degrees in 0.3 seconds. For this purpose, a gear ratio of 12 was selected and it was planned to move the rack element 0.2 meters to the left with the release of the pre-tension spring. In order to achieve this movement, a large number of spring and damper constants were tried and as a result, spring and damper constants of 25000 N/m and 2000 N s/m were determined respectively. In addition to the mass and length measurements of an average male body (50th), thin and plumb male models were also used as models in the study. Thus, it was tested whether the mechanism gives the same response to people of different sizes and weights. Equation (21) and equation (22) were solved with the ODE45 function of MATLAB software and the result was obtained as the amount of displacement of the rack element. Then, by applying the following relation in MATLAB environment, the rotation graph of the driver's seat backrest (Figure 2.5) was obtained.

$$\theta_3 = \frac{180(y_1 - b)}{\pi\ gr\ r_2} \ (23)$$

Since the rotation of the driver's seat backrest is given in radians in Equation (23), a conversion to degrees is made.

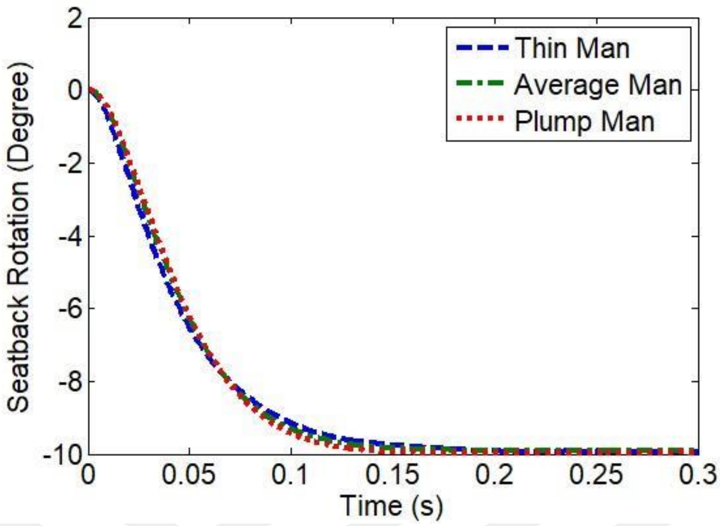

Figure 2.5. Behavior of the mechanism for male models of different height and weight.

2.3. Head Restraint Mechanism

In addition to this mechanism, a spring-damper element with pre-compression is used in the headrest. As already mentioned, the absorption of crash energy is only possible if the head restraint and seatback work effectively together. The head restraint will move forwards by means of an electrically activated switch. Head restraint’s forward movement will restrict the head retraction as the seatback rotates forwards just before impact. The head restraint will move forward relative to the backrest by 2 cm within 30 ms (Figure 2.6).

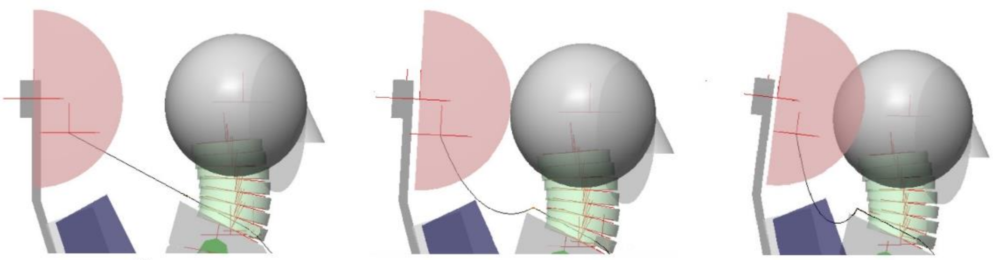

Figure 2.6. Forward movement of head restraint.

The classical mass-spring-damper system is used here.

$m\ddot{y} + c\dot{y} + ky = 0$ (24)

When this equation is solved as a function of time, the displacement equation is obtained as follows.

$y(t) = e^{-\zeta\omega_n t}\left(a_1 e^{-\sqrt{\zeta^2-1}\omega_n t} + a_2 e^{\sqrt{\zeta^2-1}\omega_n t}\right)$ (25)

$a_1 = \frac{-v_0+\left(-\zeta+\sqrt{\zeta^2-1}\right)\omega_n y_0}{2\omega_n\sqrt{\zeta^2-1}}$ (26)

$a_2 = \frac{v_0+\left(\zeta+\sqrt{\zeta^2-1}\right)\omega_n y_0}{2\omega_n\sqrt{\zeta^2-1}}$ (27)

$\omega_n = \sqrt{\frac{k}{m}}\ ve\ \zeta = \frac{c}{2m\omega_n}$ (28)

In the above equations v_0, $_y0$, w_n and ζ can be described as follow.

v_0: initial velocity (m/s, there is no initial velocity)

y_0: initial position (compression rate of spring, 0.02 m)

ω_n: naturel frequency

ζ: damper ratio.

The values of mass, spring constant and damper constant in equation (24) are chosen as 1 kg, 43500 N/m and 390 Ns/m respectively. The damper ratio is approximately 0.93. This makes the system almost a critically damped system (Figure 2.7).

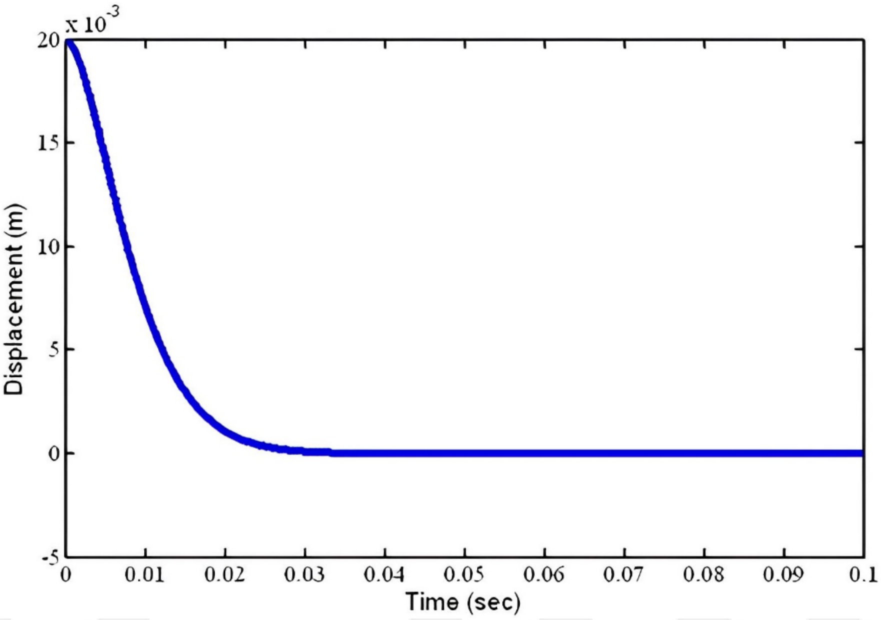

Figure 2.7. Behavior of head restraint.

2.4. Behavior of the Mechanism and Applied Crash Pulses

The forward movement of the seatback with the head restraint in the simulation environment just before crash pulse applied is shown in Figure 2.8. The movement of the seatback is given into the simulation environment as the rotation angle of the seatback (in degree) with respect to time. The following figures show the crash pulses applied to this seat-human model system.

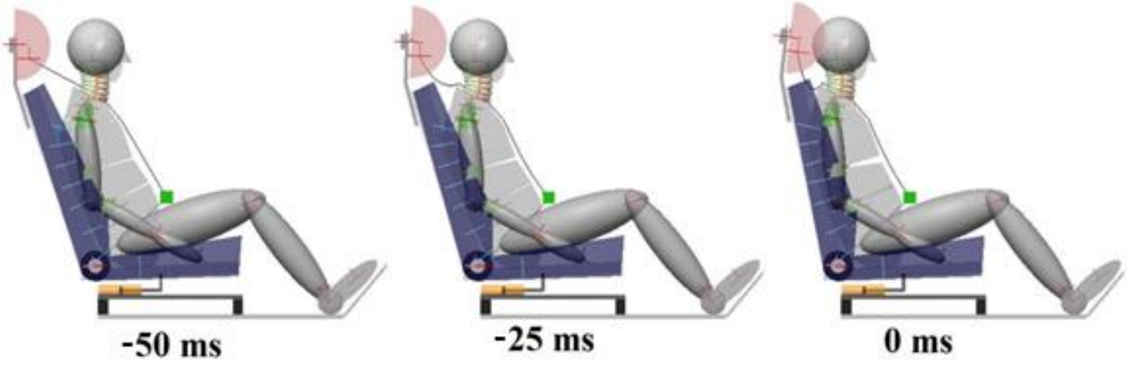

Figure 2.8. Forward movement of the seatback and head restraint.

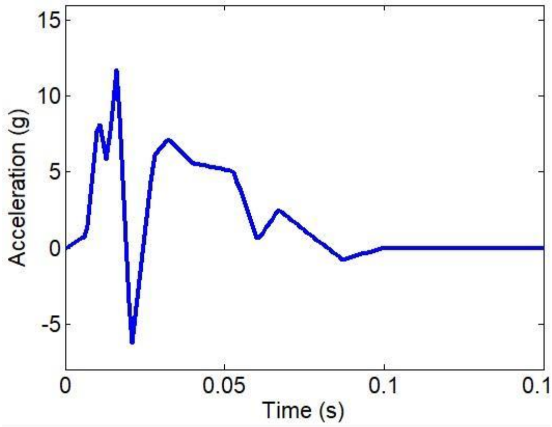

Figure 2.9. SN 9.4 crash pulse.

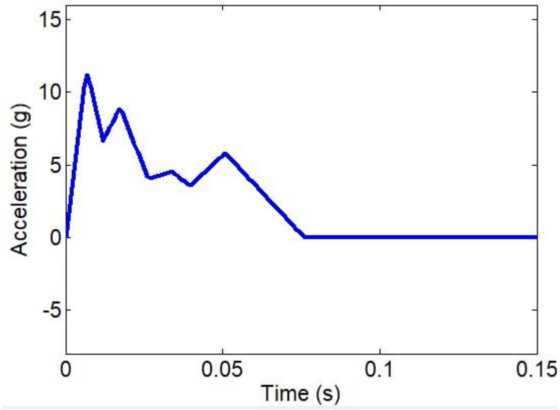

Figure 2.10. SN 13 crash pulse.

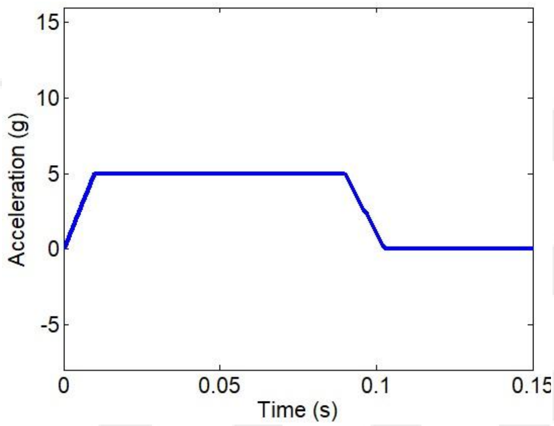

Figure 2.11. TR 16 crash pulse.

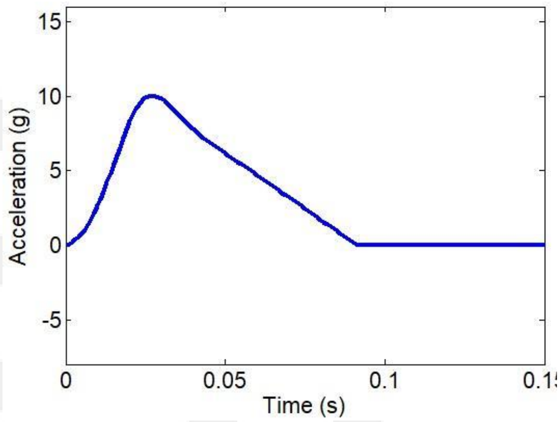

Figure 2.12. IIWPG crash pulse.

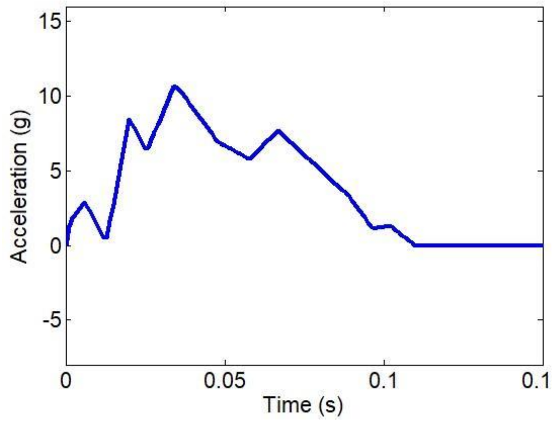

Figure 2.13. SN 20.4 crash pulse.

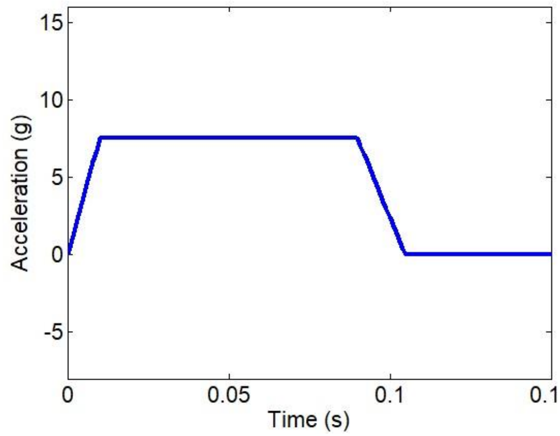

Figure 2.14. TR 24 crash pulse.

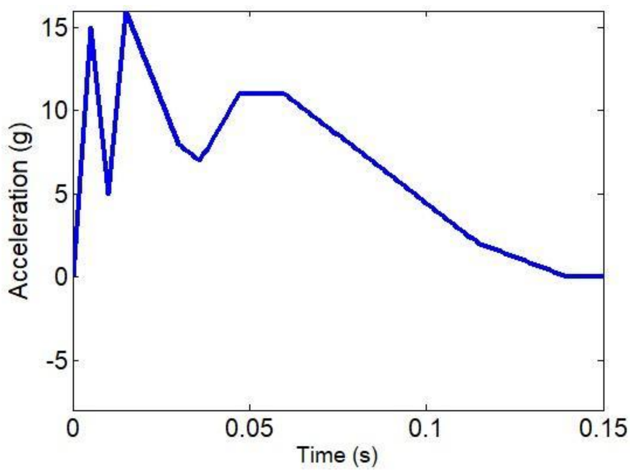

Figure 2.15. FMVSSHS crash pulse.

2.5. Results

The results obtained after the application of the crash pulses can be seen in tables below (Tables 2.4, 2.5, 2.6, 2.7, 2.8, 2.9 and 2.10). The shear force applied to the joint between the occipital condyles (OC) and the first vertebra (C1) (Figure 2.16) during the application of the crash pulses was measured. The maximum value of the shear force was taken for comparison. Similarly, tensile forces were measured at the same joint and their maximum values can be seen in Table 2.5. Nkm is an injury criterion (threshold value is 1) that uses the combination of the shear force and the moment acting on the occipital condyles (OC). The variation of Nkm values is shown in Table 2.6. NIC is measured from the relative velocity and acceleration between occipital condyles (OC) and first vertebra (C1). The threshold value is 15. The comparison of NIC values before and after the mechanism can be seen in Table 2.7 below. S shape [19] is the changes in the rotation of the intervertebral discs of the upper and lower cervical vertebrae and is measured from the formulation $-\theta_{OC/C1} + \theta_{C7/T1}$ ($\theta_{OC/C1}$: intervertebral rotation between occipital condyles (OC) and first vertebra (C1), $\theta_{C7/T1}$: intervertebral rotation between seventh cervical vertebra (C7) and first thoracic vertebra (T1), (Figure 2.17)). In Table 2.8, negative values represent extension and positive values represent retraction (Figure 2.18). Table 2.9 and Table 2.10 show the head velocity relative to the sled and the maximum seatback backward rotation values, respectively.

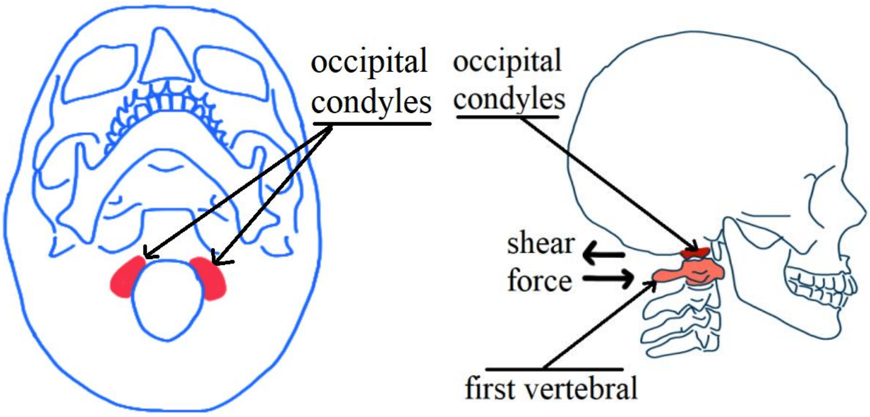

Figure 2.16. OC and C1 vertebras.

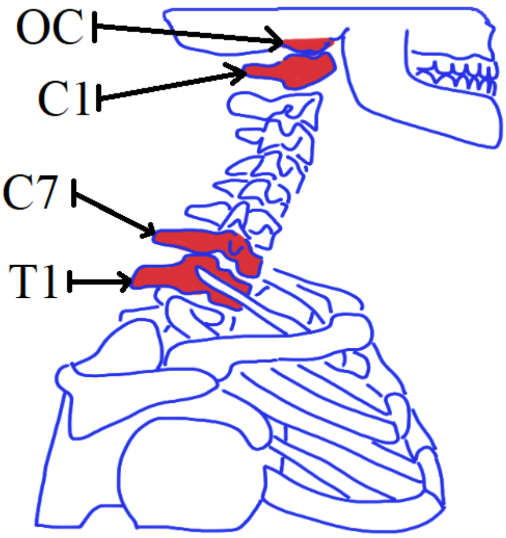

Figure 2.17. C7 and T1 vertebras.

A: flexion
B: extension
C: protraction
D: retraction

Figure 2.18. Head movements with respect to neck.

When forces that occurred when the seat was turned upward position just before the accident were examined, it was seen that there were very small forces. The resulting shear maximum force is 21 N, maximum tensile force is 5 N and the maximum NIC value is 3.5 m^2/s^2.

Table 2.4. Shear force comparison after implementation of several crash pulses.

Crash pulse	Maximum shear force (N)		% shear force reduction
	Without mechanism	With mechanism	
SN 9.4	80.418	61.668	23.3
SN 13	107.29	76.39	28.8
TR 16	122.49	81.182	33.7
IIWPG	113.72	82.165	27.7
SN 20.4	162.15	90.927	43.9
TR 24	167.17	109.15	34.7
FMVSSHS	237.18	166.72	29.7

Table 2.5. Tensile force comparison after implementation of several crash pulses.

Crash pulse	Maximum tensile force (N)		% tensile force reduction
	Without mechanism	With mechanism	
SN 9.4	164.95	33.65	79.5
SN 13	167.32	42.248	74.7
TR 16	110.33	120.82	-9.5
IIWPG	207.51	101.21	51.2
SN 20.4	151.48	103.79	31.5
TR 24	87.485	168.69	-92.8
FMVSSHS	573.13	190.81	66.7

Table 2.6. N_{km} comparison after implementation of several crash pulses.

Crash pulse	Maximum N_{km}		% N_{km} reduction
	Without mechanism	With mechanism	
SN 9.4	0.17278	0.16458	4.7
SN 13	0.24309	0.20182	16.9
TR 16	0.29655	0.16587	44.1
IIWPG	0.22808	0.18758	17.8
SN 20.4	0.43313	0.186	57.1
TR 24	0.43271	0.17621	59.3
FMVSSHS	0.63044	0.35375	43.9

Table 2.7. NIC comparison after implementation of several crash pulses.

Crash pulse	Maximum NIC (m^2/s^2)		% NIC reduction
	Without mechanism	With mechanism	
SN 9.4	7.4899	6.7131	10.4
SN 13	8.7595	6.1837	29.4
TR 16	6.7023	10.634	-58.7
IIWPG	8.7754	9.8636	-12.4
SN 20.4	9.4351	10.035	-6.4
TR 24	7.9824	6.4762	18.9
FMVSSHS	19.939	10.121	49.2

Table 2.8. S shape comparison after implementation of several crash pulses.

Crash pulse	Minimum/Maximum S shape		% S shape reduction
	Without mechanism	With mechanism	
SN 9.4	-1.8141/1.0672	0/2.5579	100/-139.68
SN 13	-1.0917/1.2259	-0.59536/2.5378	45.46/-107.02
TR 16	-0.59729/0.28564	-1.1512/2.539	-92.74/-788.88
IIWPG	-0.74791/0.44764	-0.71738/2.5755	4.08/-475.35
SN 20.4	-1.8691/0.27397	0/2.5073	100/-815.17
TR 24	-5.1993/1.7082	-0.20338/2.5071	96.09/-46.77
FMVSSHS	-7.7783/0.20483	-3.2157/2.508	58.66/-1124.43

Table 2.9. Vhead wrt Sled comparison after implementation of several crash pulses.

Crash pulse	Vhead wrt Sled (m/s)		% velocity reduction
	Without mechanism	With mechanism	
SN 9.4	1.4012	1.2682	9.49
SN 13	1.2579	1.1363	9.67
TR 16	1.4247	1.3238	7.08
IIWPG	1.3501	1.3819	-2.36
SN 20.4	1.3351	1.3423	-0.54
TR 24	1.0963	1.0283	6.2
FMVSSHS	1.6452	1.2306	25.2

Table 2.10. Maximum seatback rear rotation comparison after implementation of several crash pulses.

Crash pulse	Maximum seatback rear rotation (°)		% rotation reduction
	Without mechanism	With mechanism	
SN 9.4	23.181	13.0934	43.52
SN 13	24.7231	13.5233	45.3
TR 16	27.859	15.7088	43.61
IIWPG	28.9471	17.6939	38.88
SN 20.4	35.781	23.52	34.27
TR 24	45.376	32.872	27.56
FMVSSHS	49.452	35.88	27.44

The following figures (Figures 2.19, 2.20 and 2.21) show the behavior of the seat under the action of the mechanism at different crash severities. Moments (a), (b), (c) and (d) in the figures show the time zero moment, the moment of maximum body entry into the seatback, the moment of maximum rotation of the seatback and the moment when the head ceases to be in contact with the head restraint, respectively.

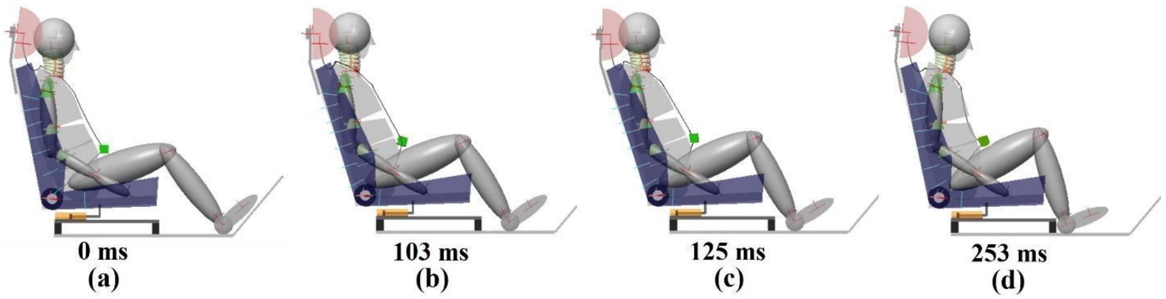

Figure 2.19. Iiwpg crash.

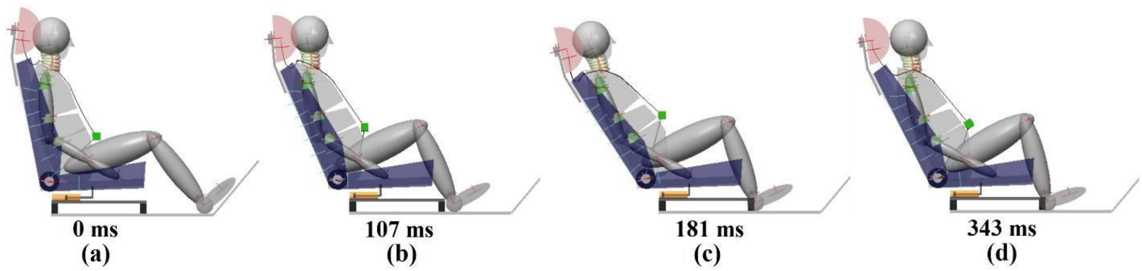

Figure 2.20. Tr24 crash.

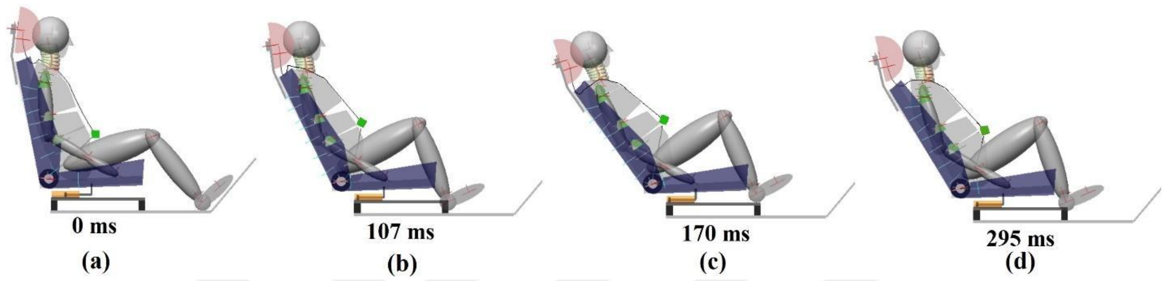

Figure 2.21. Fmvsshs crash.

3. VEHICLE MODELLING

In this section, the modelling and validation of real crash scenarios in a computer environment were carried out. Subaru Impreza and Toyota Yaris model vehicles were used in the crash simulations (Figure 3.1).

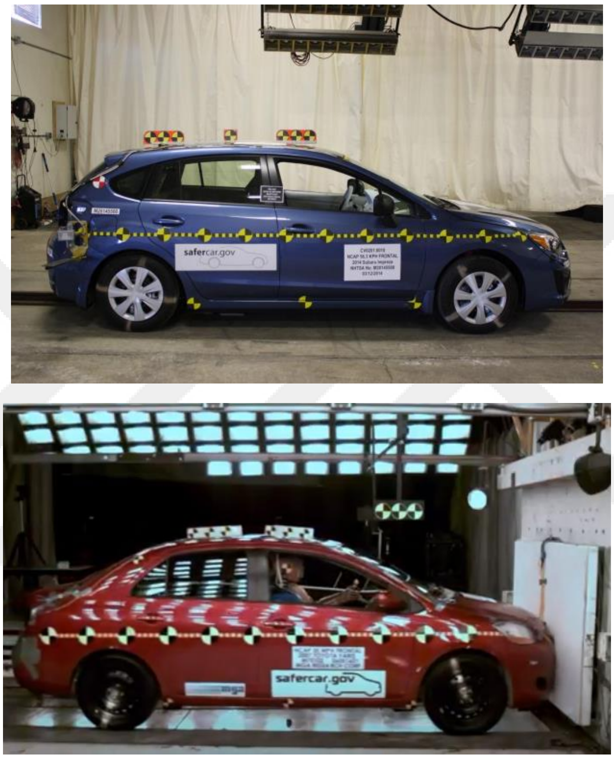

Figure 3.1. Real crash tests of the Subaru Impreza (top) and Toyota Yaris (bottom).

In severe crashes, in addition to horizontal accelerations, vertical and angular accelerations also occur. In actual crash test reports, horizontal and vertical acceleration data are presented. However, no information is given about angular acceleration data. In high-speed frontal impact situations, horizontal and vertical accelerations occur on the vehicle. In addition to these, angular accelerations also occur due to the lifting of the rear of the vehicle into the air with the moment created by the collision.

These angular acceleration data are needed in order to apply higher crash severities to the existing human-seat model. Because it is desired to develop protection systems that will protect the passengers at high crash severities. In this context, the aforementioned two vehicles were modelled in VNastran environment and the environment under real crash conditions was simulated. Horizontal and vertical displacement, velocity and acceleration data obtained from the simulations were compared with the actual crash data to verify the simulations. Afterwards, the horizontal, vertical and angular acceleration data obtained from the simulation were applied to the human-seat model and the effectiveness of the protective systems to be discussed in the following sections were tested.

3.1. Design Parameters of the Vehicles

In order to set up the simulation environment, firstly, the physical dimensions of these vehicles are needed. This information was taken from NCAP-CAL-14-013 report dated 15 April 2014 for Subaru Impreza model vehicle and NCAP-MGA-2006-011 report dated 21 June 2006 for Toyota Yaris model vehicle (Figure 3.2 and Table 3.1).

A 2014 Subaru Impreza five-door station wagon vehicle was used in the actual crash test performed on the Subaru Impreza. A 56.30 km/h (35 mph), NCAP Frontal Impact Test was performed on the vehicle in accordance with the Office of Crashworthiness Standards Frontal NCAP Laboratory Test Procedure specifications. The barrier impact speed of the vehicle was 56.5 km/h. The maximum static crush of the subject vehicle after the test was 549 mm at C3 to the left of the vehicle center line [20].

The actual crash test on the Toyota Yaris model vehicle was conducted on 16 May 2006 using the 2007 Toyota Yaris model vehicle. This crash test was also conducted as a front barrier impact. The impact speed was 56.3 km/h. A maximum static crush of 546 mm occurred at the center line of the vehicle. The test vehicle was equipped with a 3-point continuous belt system and airbags in both front outer seating positions [21].

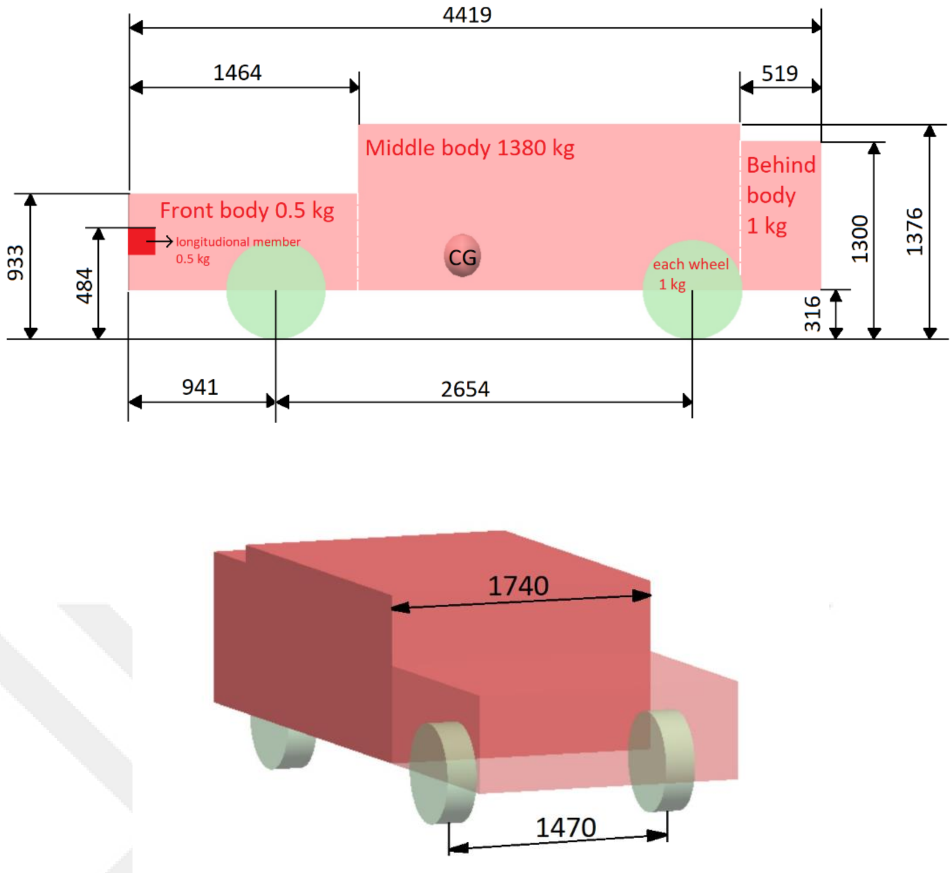

Figure 3.2. Design parameters of Subaru Impreza model vehicle.

Table 3.1. Design parameters of vehicles.

Vehicle	Subaru Impreza	Toyota Yaris
Design Parameter	Value (mm)	Value (mm)
Vehicle Length	4419	4428,9
Vehicle Width	1740	1689
Vertical Distance Between Vehicle Ceiling and Ground	1376	1456,6
Wheelbase	2654	2640
Track Width	1470	1505,8
Wheel Diameter	635	590

Wheel Tread Width	195	187,2
Rim Diameter	15 inch	20 inch
Horizontal Distance Between Front Wheel Center and Front Bumper	941	850,7
Horizontal Distance Between Rear Wheel Center - Rear Bumper	824	937,7
Vertical Distance Between the Front Suspension’s Top Point and Front Wheel Center	597	432
Vertical Distance Between the Rear Suspension’s Top Point and Rear Wheel Center	597	428,8
Center of Gravity (X – Component)	-1189	-1836
Center of Gravity (Y – Component)	0	-11
Center of Gravity (Z – Component)	537	330,7

While determining the center of gravity of the vehicles, it was observed that only the horizontal center of gravity position from the front axle backwards was given in the reports. While calculating center of gravity height from the ground, the study of Heydinger et al. [22] was used. In order to use the graph in this study, the total mass of the vehicles is needed. The horizontal axis shows the total mass of the vehicles and the vertical axis shows the center of gravity/ceiling height ratio. In the graph, passenger cars are expressed with a diamond-shaped indicator (Figure 3.3).

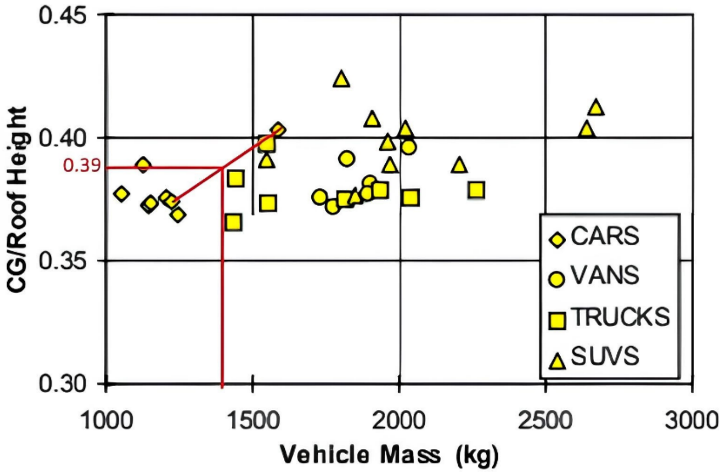

Figure 3.3. Calculation of the position of the center of gravity for Subaru Impreza model vehicle (Adapted from [22].).

Accurate wheel sizes are needed both to indicate the ground clearance of the vehicles and to place their suspensions in the correct position. Looking at the crash test reports, the wheel size used for Subaru Impreza is P195/65R15 and the wheel size used for Toyota Yaris is P185/60R15. Here, the value after the letter P is the wheel width. The value in front of the letter R is the ratio of the wheel height to the wheel width. Both values have the unit mm. The value after the letter R is the wheel diameter and is expressed in inches. A web page for wheel size calculation [23] was used to determine the dimensions needed for the wheels (Figure 3.4 and Figure 3.5). The spring and damper coefficients of the suspension and tyre are given in Table 3.2. [24].

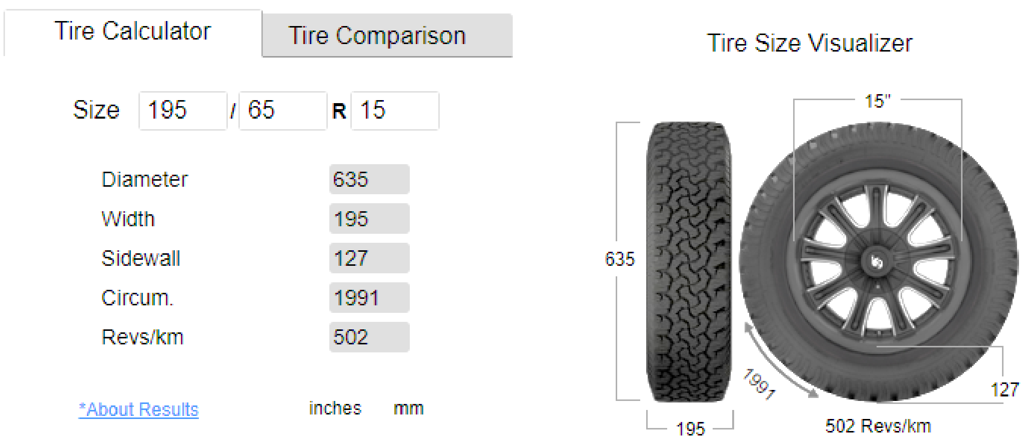

Figure 3.4. Wheel sizes of Subaru Impreza model vehicle (Adapted from [23].).

Figure 3.5. Wheel sizes of Toyota Yaris model vehicle (Adapted from [23].).

Table 3.2. Tire and suspension spring-damper coefficients of vehicles (Adapted from [24].).

	Spring Coefficient			Damping Coefficient	
	Tire	Front Suspension	Rear Suspension	Front Suspension	Rear Suspension
Value	225000 N/m	20000 N/m	19000 N/m	1350 Ns/m	1450 Ns/m

The work of Heydinger et al. [22] was also used to calculate the moments of inertia of the vehicles. The graphs below show the normalized driver only moments of inertia for the vehicles (Figure 3.6).

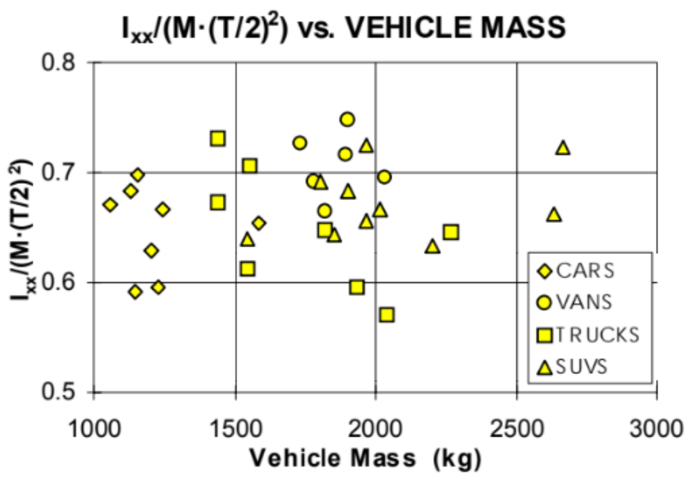

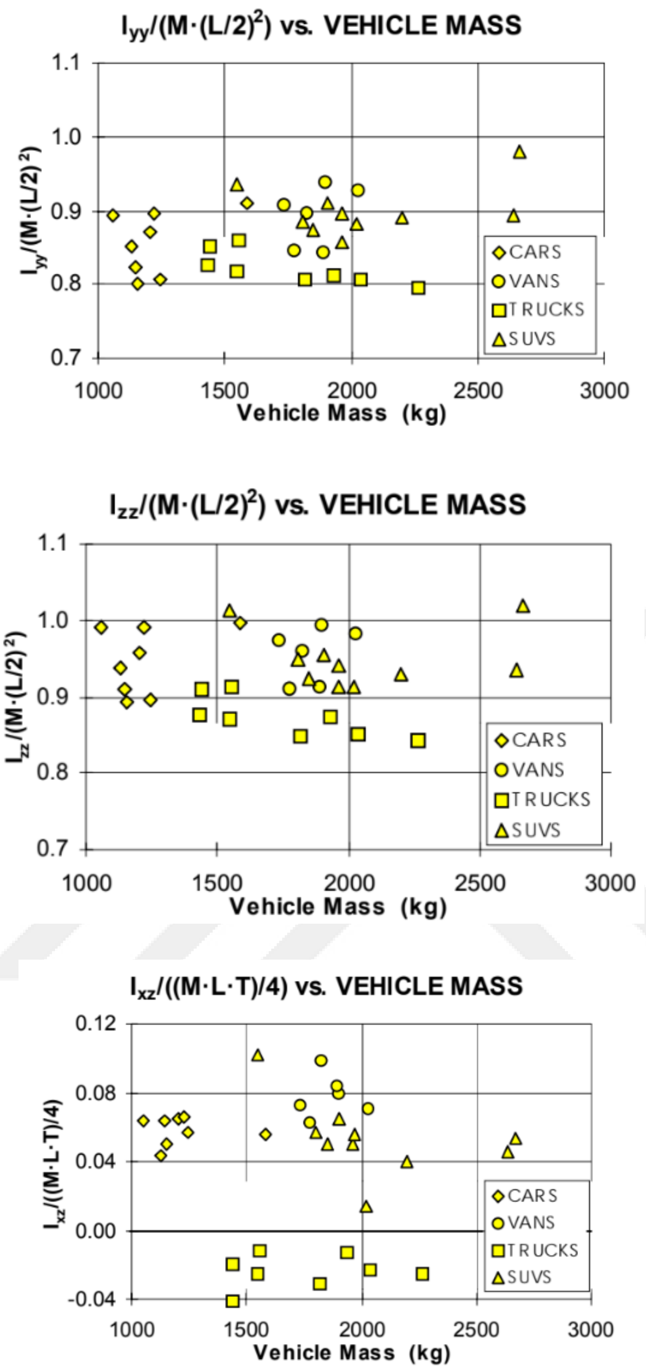

Figure 3.6. Normalized moments of inertia (Adapted from [22].).

From the graphs above, the normalized moments of inertia corresponding to the mass of the vehicles should be drawn. In the graphs, passenger cars are again indicated with diamond symbols. In the formulae in the graphs M, T and L were indicated as following expressions;

M: Vehicle mass

T: Track width

L: Wheelbase

Within this information, in Table 3.3 the moments of inertia of both vehicles are approximately given.

Table 3.3. Moment of inertia values of the vehicles.

Moment of Inertia (kgm^2)	Vehicle	
	Subaru Impreza	Toyota Yaris
I_{xx}	529	395
I_{yy}	2218	1498
I_{zz}	2456	1739
I_{xz}	81.9	72.7

3.2. Wall Force-Vehicle Deformation Behavior

In some frontal impact tests, cars hit a fixed rigid surface at full width (Figure 3.7(a)). These tests provide information on the performance of the restraint systems and the crashworthiness of the vehicle. The rigid wall contains load cells that measure the crushing forces and moments acting on the vehicle cabin. The displacement and deformation of the vehicle are also calculated by means of accelerometers mounted on the vehicle. In these tests, the deformation behavior against the total wall force (or crushing force) is similar to the curve given in Figure 3.7(b). The loading and unloading behavior of the vehicle structure can also be approximated by the black and grey solid lines, respectively, as shown in Figure 3.7(c). In the loading phase, the relationship between the crushing force and the deformation of the vehicle can be described by the formula F=k x. Here k is the stiffness. As long as there is no very stiff passenger compartment behind the firewall, a linear spring constant can be used as a reasonable approximation.

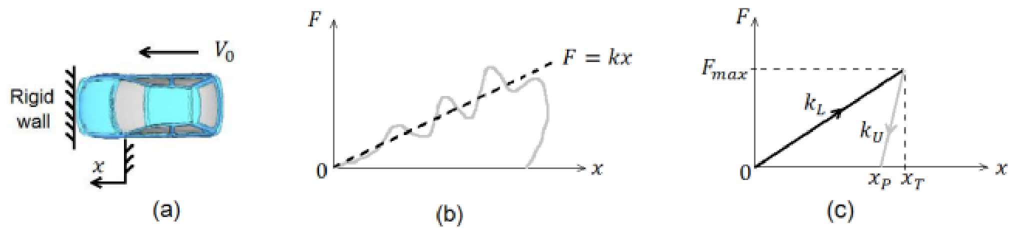

Figure 3.7. (a) Frontal impact test, (b) and (c) crushing force and deformation curves.

The following notation is used to physically describe the system.

x: deformation/displacement of the vehicle

x_T: total (maximum) deformation, dynamic crush

x_P: permanent deformation

x_e: elastic rebound displacement ($x_e=x_T-x_P$)

V_0: collision velocity

k_L: loading stiffness

k_U: unloading stiffness

$F_{max}=k_L\, x_T= k_U\, x_E \rightarrow x_E/x_T=k_L/k_U$ (1)

W_T: total crash energy absorbed by the vehicle structure

$W_T=mV_0^2/2=F_{max}x_T/2=F_{max}^2/(2k_L)$ (2)

m: vehicle mass

W_R: elastic energy returned by the vehicle structure ($W_R=m(V')^2=F_{max}x_E/2=k_Vx_E^2/2$) (3)

e: coefficient of restitution ($e=V_W'-V')(V_0-V_W)=-V'/V_0$) (4)

$W_R/W_T=(V'/V_0)^2=k_Vx_E^2/(k_Lx_T^2)=e^2$ (5)

Using Equations (1) and (5),

$e^2=k_L/k_V$, $e=(x_E/x_T)^{1/2}$ (6)

V': vehicle rebound velocity

V_W: wall velocity at collision onset

V'_W: wall velocity at end of collision

In lumped-mass modelling of a vehicle, the energy absorbing structure of the vehicle can be modelled as a spring element as shown in Figure 3.8. Referring back to Figure 3.7, Figure 3.7(c) also indicates the deformation behavior of this spring element against force. The area under the black line in Figure 3.7(c) represents the collision energy absorbed by the vehicle in the loading phase (Figure 3.10). Again, the area under the grey line is the energy released by the vehicle immediately after the collision. The area under the grey line is considerably smaller than the area under the black line. Therefore, the vehicle structure deformation is predominantly plastic. The slope of the black line is loading stiffness whereas the slope of the grey line is the unloading stiffness of the vehicle.

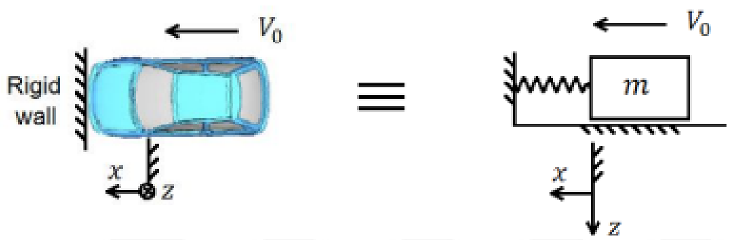

Figure 3.8. Lumped-mass model of a car in FWRB impact test.

The time and deformation dependent graphs of the barrier force applied to the Subaru Impreza model vehicle in the simulation environment are given in Figure 3.12 and Figure 3.13.

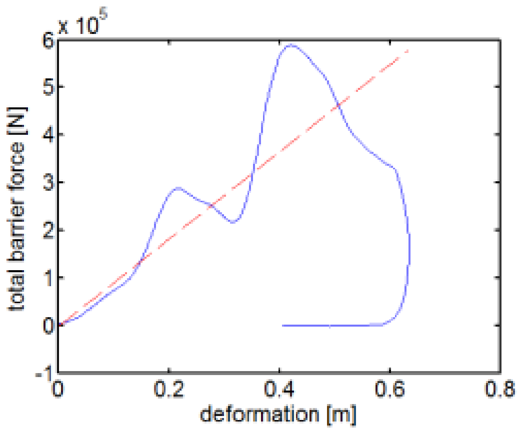

Figure 3.9. Modelling of the loading phase

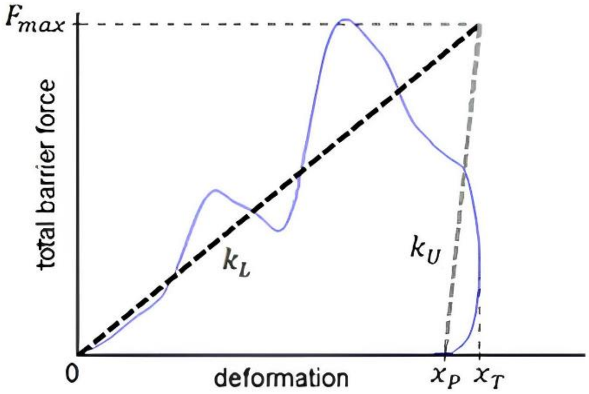

Figure 3.10. Modelling of the unloading phase

Finally, accelerometers, whose locations are specified in the crash test report, were placed on the vehicle modelled in the simulation environment in order to perform the verification (Figure 3.11).

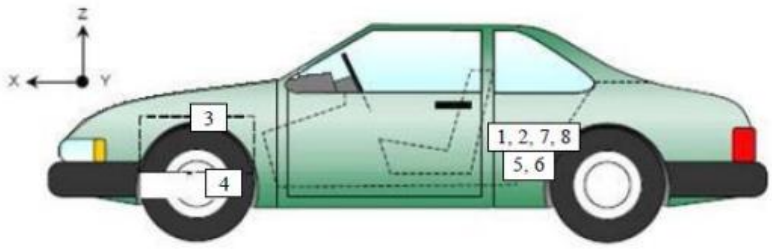

VEHICLE ACCELEROMETER PRE-TEST LOCATIONS

No.	Accelerometer Location	Measurements (mm)		
		X	Y	Z
1	Left Rear Accelerometer – X Direction	1629	-528	232
2	Right Rear Accelerometer – X Direction	1624	513	226
3	Engine Top X	3695	-78	-276
4	Engine Bottom X	3571	162	298
5	Left Rear Accelerometer – Z Direction	1623	-532	220
6	Right Rear Accelerometer – Z Direction	1629	-504	234
7	Left Rear Accelerometer – X Direction Redundant	1629	-528	232
8	Right Rear Accelerometer – X Direction Redundant	1624	513	226

Reference Points: *X – Rear Surface of Vehicle (+ forward)*
Y – Vehicle Centerline (+ to right)
Z – Ground Plane (+ down)

Figure 3.11. Location of accelerometers placed on Subaru Impreza (Adapted from [20].).

The data obtained from the accelerometer in the simulation are listed below. The graphs of these data in the actual crash tests and the graphs in the verification simulations and also screenshots from real crash test video and crash simulation video are presented in the figures below (Figures 3.14, 3.15, 3.16, 3.17, 3.18, 3.19, 3.20, 3.21, 3.22, 3.23, 3.24, 3.25, 3.26, 3.27, 3.28, 3.29 and 3.30). These data are;

- X direction vehicle acceleration
- Z direction vehicle acceleration
- X direction vehicle velocity
- Z direction vehicle velocity
- X direction vehicle displacement
- Z direction vehicle displacement
- Vehicle angular acceleration about y-axis
- Vehicle angular displacement about the y-axis

3.3. Results

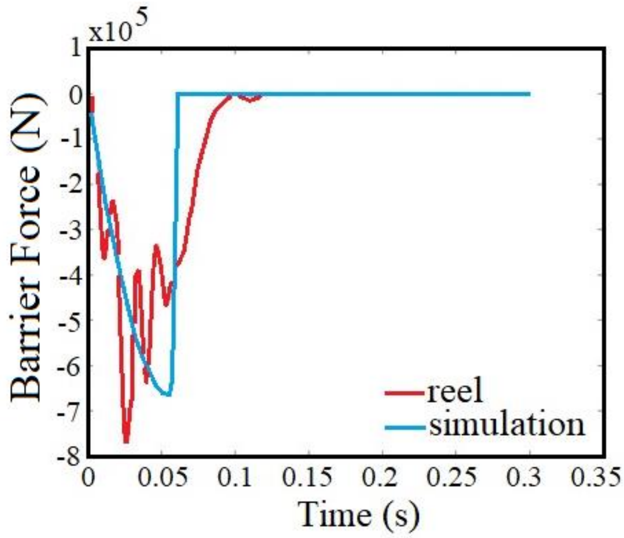

Figure 3.12. Time dependent variation of barrier force applied to Subaru Impreza model vehicle.

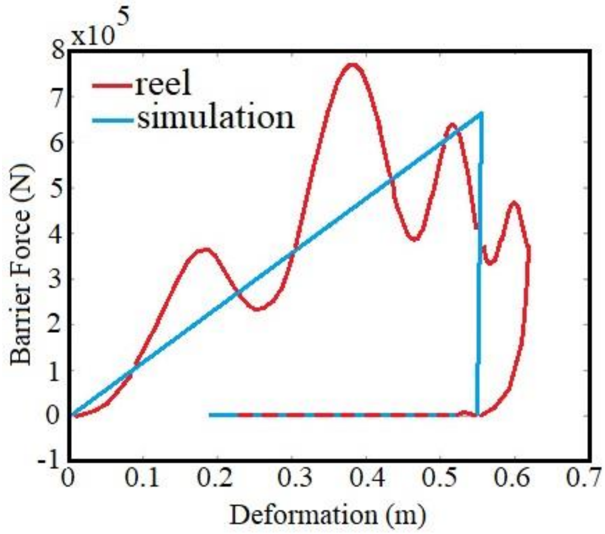

Figure 3.13. Barrier force-vehicle deformation graph applied to Subaru Impreza model vehicle.

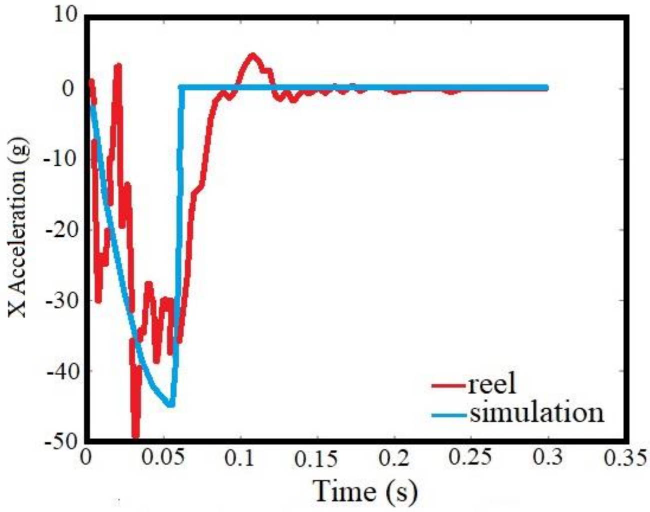

Figure 3.14. Acceleration-time graph of Subaru Impreza model vehicle in X direction.

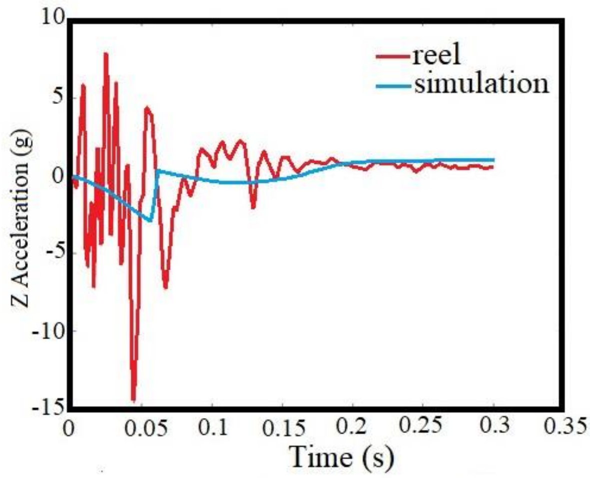

Figure 3.15. Acceleration-time graph of Subaru Impreza model vehicle in Z direction.

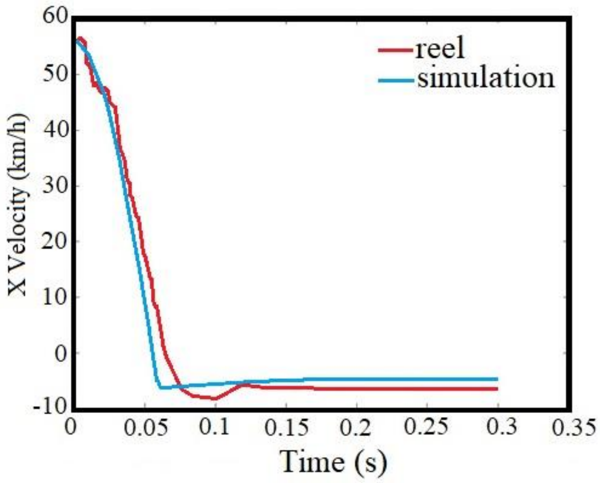

Figure 3.16. Velocity-time graph of Subaru Impreza model vehicle in X direction.

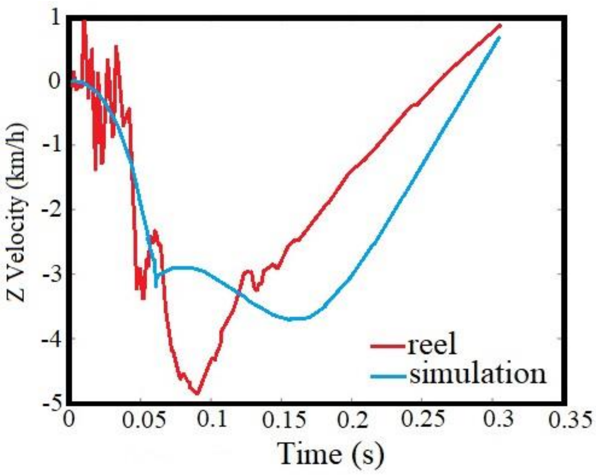

Figure 3.17. Velocity-time graph of Subaru Impreza model vehicle in Z direction.

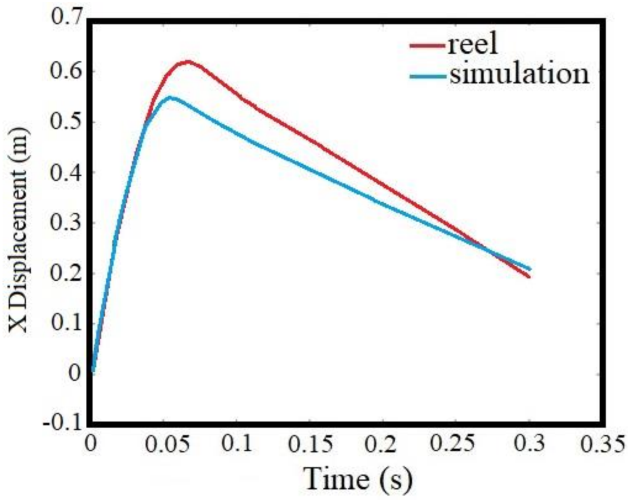

Figure 3.18. Position-time graph of Subaru Impreza model vehicle in X direction.

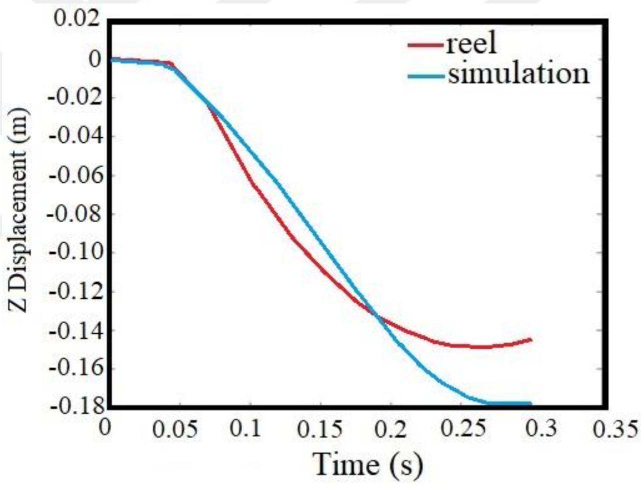

Figure 3.19. Position-time graph of Subaru Impreza model vehicle in Z direction.

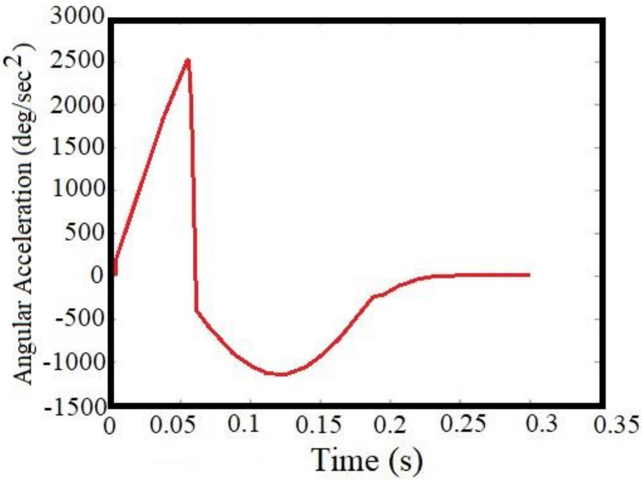

Figure 3.20. Angular acceleration-time graph of Subaru Impreza model vehicle around Y axis.

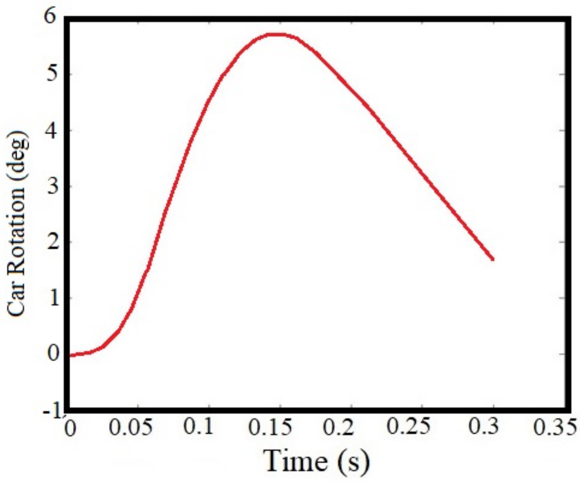

Figure 3.21. Angular displacement-time graph of Subaru Impreza model vehicle around Y axis.

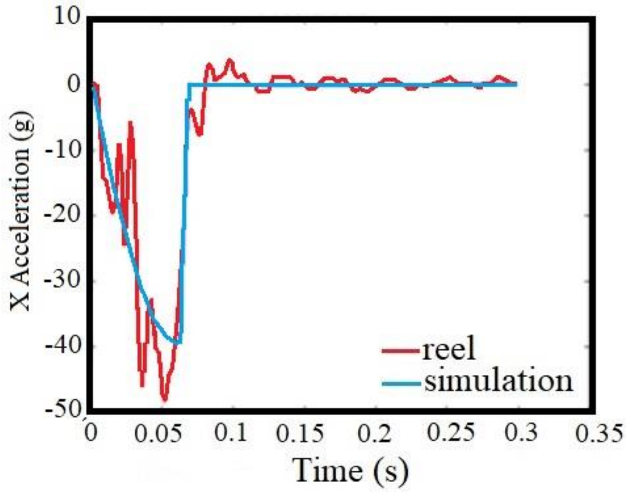

Figure 3.22. Acceleration-time graph of Toyota Yaris model vehicle in X direction.

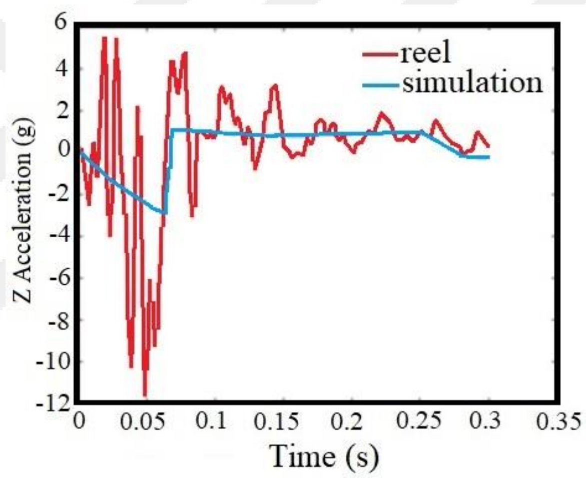

Figure 3.23. Acceleration-time graph of Toyota Yaris model vehicle in Z direction.

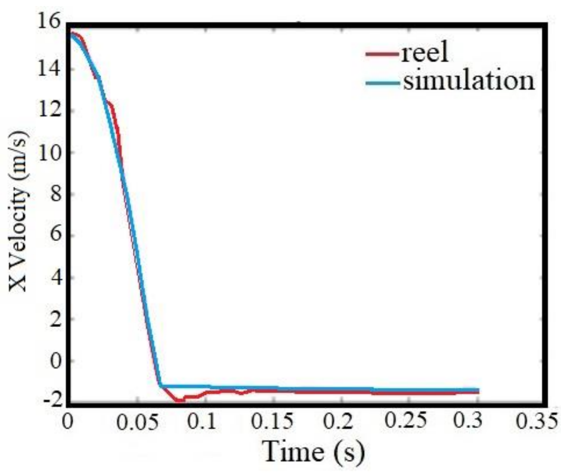

Figure 3.24. Velocity-time graph of Toyota Yaris model vehicle in X direction.

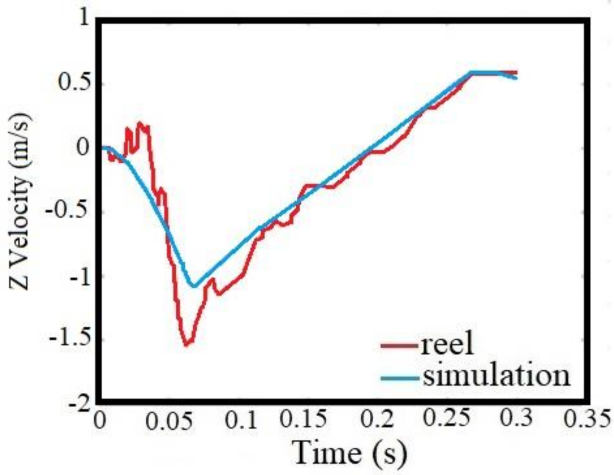

Figure 3.25. Velocity-time graph of Toyota Yaris model vehicle in Z direction.

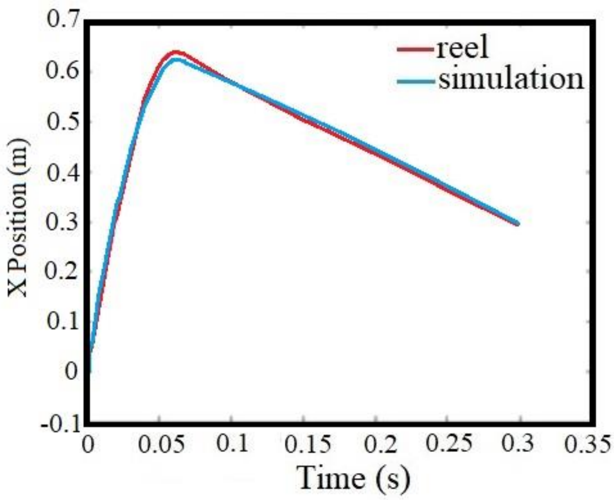

Figure 3.26. Position-time graph of Toyota Yaris model vehicle in X direction.

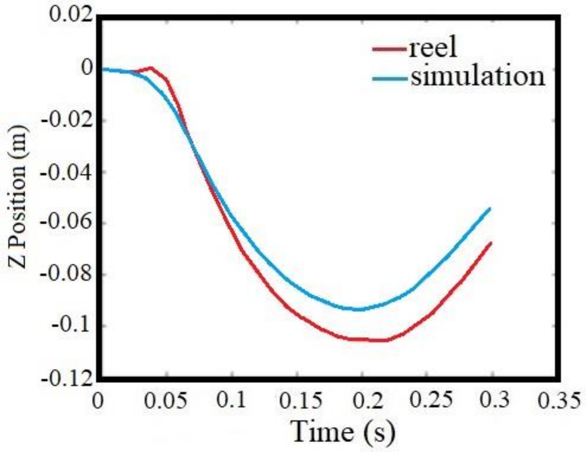

Figure 3.27. Position-time graph of Toyota Yaris model vehicle in Z direction.

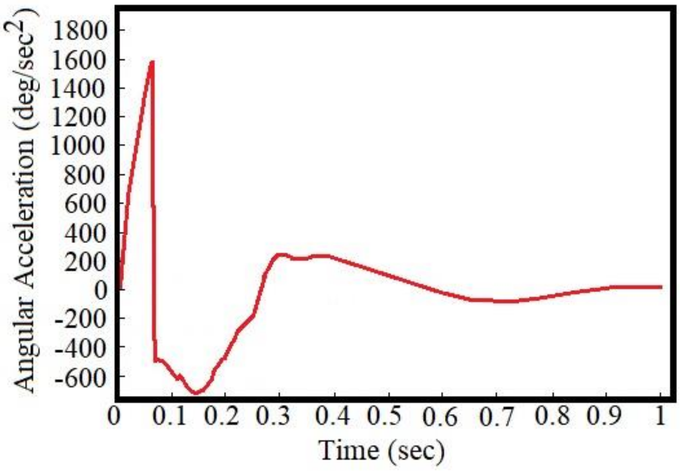

Figure 3.28. Angular acceleration-time graph of Toyota Yaris model vehicle around Y axis.

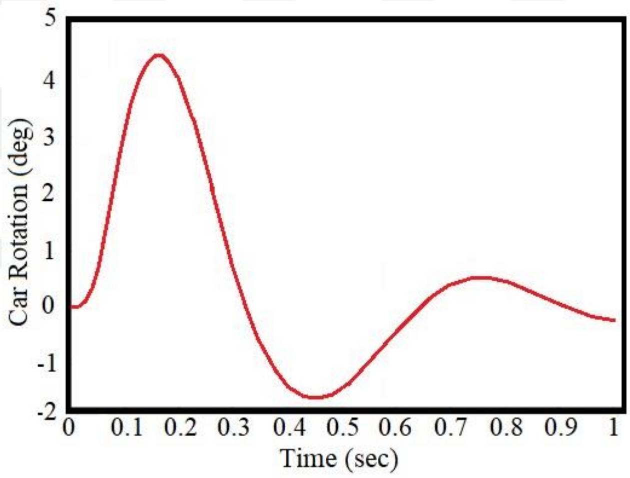

Figure 3.29. Angular displacement-time graph of Toyota Yaris model vehicle around Y axis.

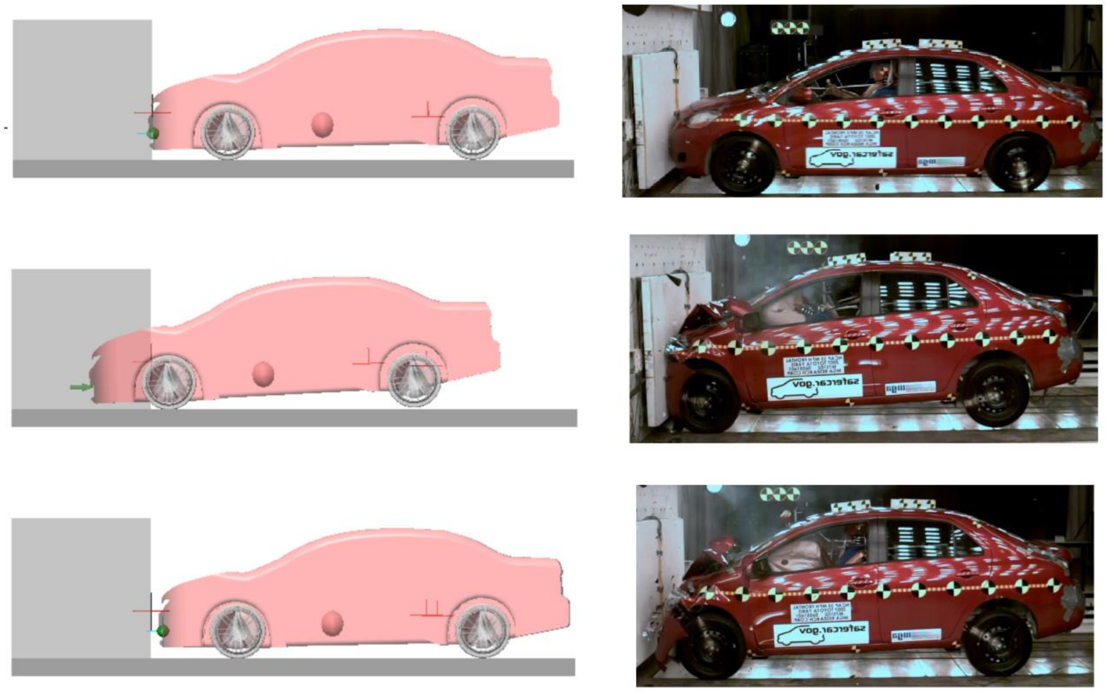

Figure 3.30. Screenshots from simulation and real crash test videos (Toyota Yaris).

The moving average acceleration of the collision impact appears to better represent the collision severity. The calculation of the moving average acceleration involves the average value of the acceleration over a given travelling time interval. This travelling time interval can be selected as 25 ms or 50 ms. For example, the maximum (or peak) value of the moving average accelerations for the entire duration of the impact pulse covering a time interval of 50 ms is reported. Moving average acceleration values were calculated based on data from actual crash test and crash validation simulations of Subaru Impreza model car.

- for acceleration in the x direction;

- Actual Crash Test: -29.40 g
- Crash Validation Simulation: -33.72 g

- for acceleration in the z direction;

- Actual Crash Test: -2.72 g
- Crash Validation Simulation: -1.58 g

3.4. Nonlinear Suspension Spring Application to Crash Validation Model

In real applications, the spring element of the suspension does not give a linear force-displacement behavior. Therefore, this should be taken into account when modelling the actual crash scenario. In their study, Patil and Sawant [24] presented the force and displacement graphs of the suspension spring of a Hyundai Elentra model vehicle (Figure 3.31).

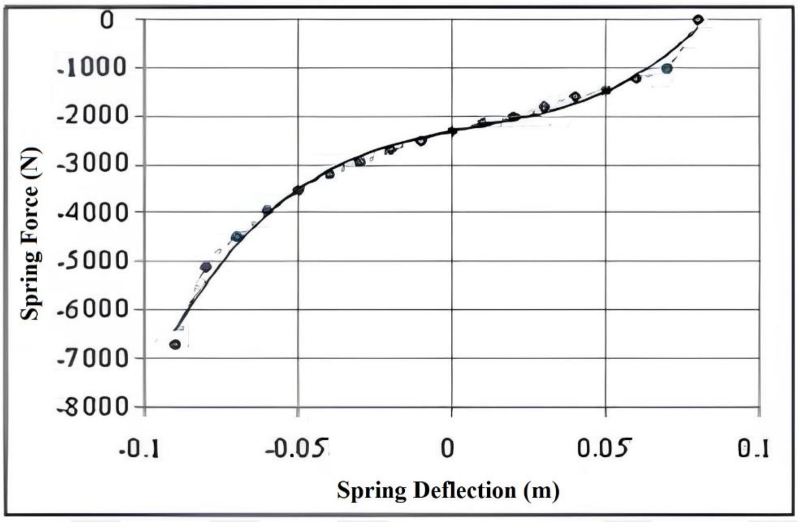

Figure 3.31. Force-displacement graph of the suspension spring of Hyundai Elentra model vehicle (Adapted from [24].).

In the modelling studies of the crash scenario, a constant value was taken for the spring coefficient. The spring force and displacement graph obtained with this constant value was compared with the graph in Patil and Sawant's study [24] and a non-linear force - displacement graph was obtained. The suspension spring coefficient value taken primarily for the front wheels is given above as 20000 N/m and the suspension spring coefficient value taken primarily for the rear wheels is given above as 19000 N/m. A non-linear force-displacement plot was fitted to the data sets obtained from the simulation environment (Figure 3.32) and tested in the simulation environment (Figure 3.33). In the below graphs, one was indicated that 0.3-meter displacement value is limit for suspensions which means suspensions cannot compress any further.

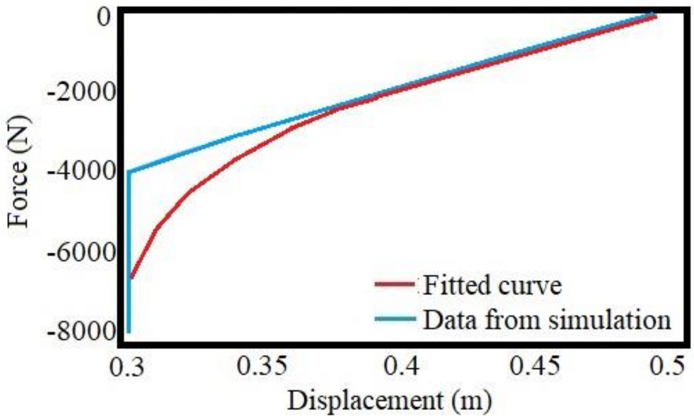

Figure 3.32. Obtaining nonlinear suspension spring behavior.

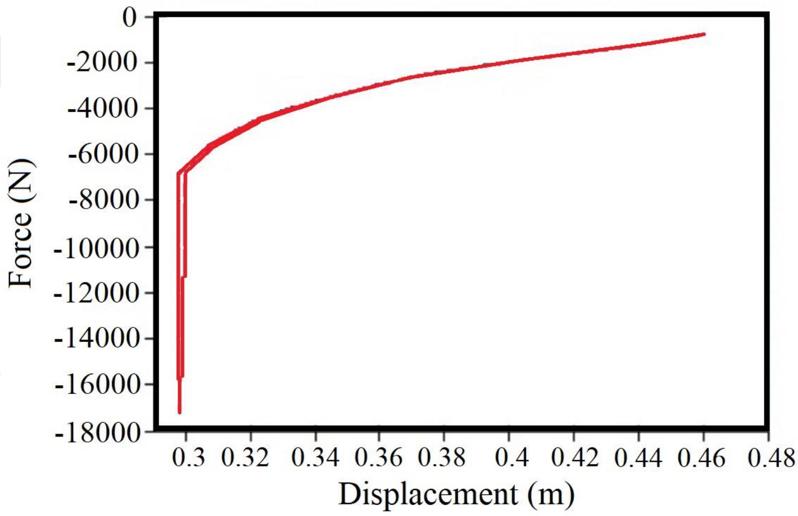

Figure 3.33. Suspension spring behavior obtained in simulation environment

The displacement, velocity and acceleration graphs obtained as a result of the simulation gave similar results in the case of using linear and non-linear suspension springs.

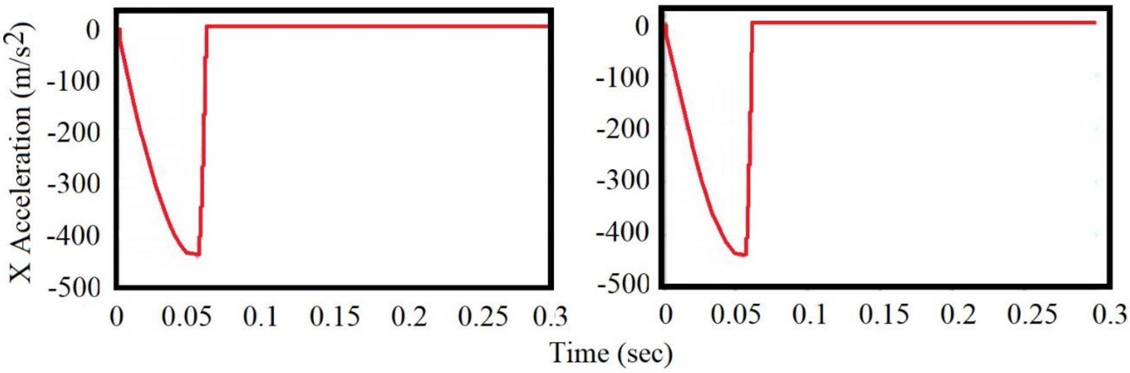

Figure 3.34. Acceleration-time graphs in X direction of Subaru Impreza model vehicle with linear (left) and non-linear (right) suspension springs.

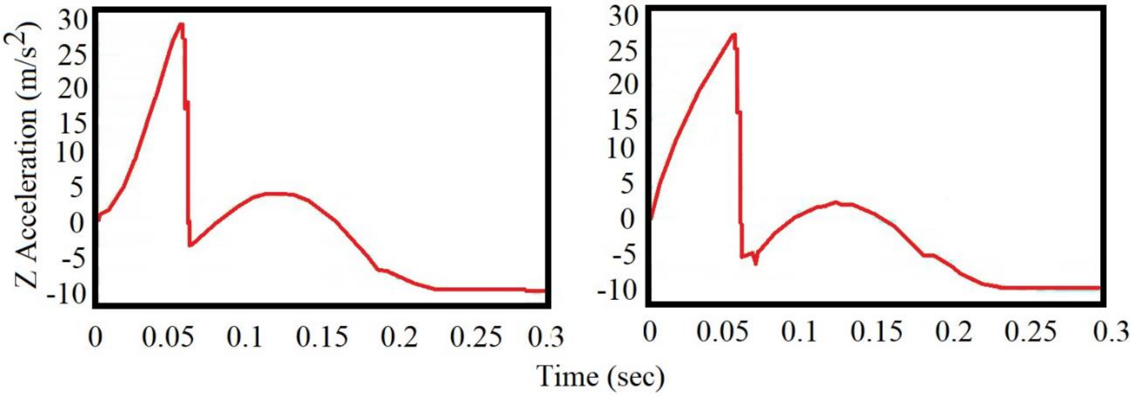

Figure 3.35. Acceleration-time graphs of Subaru Impreza model vehicle in Z direction obtained by using linear (left) and non-linear (right) suspension springs.

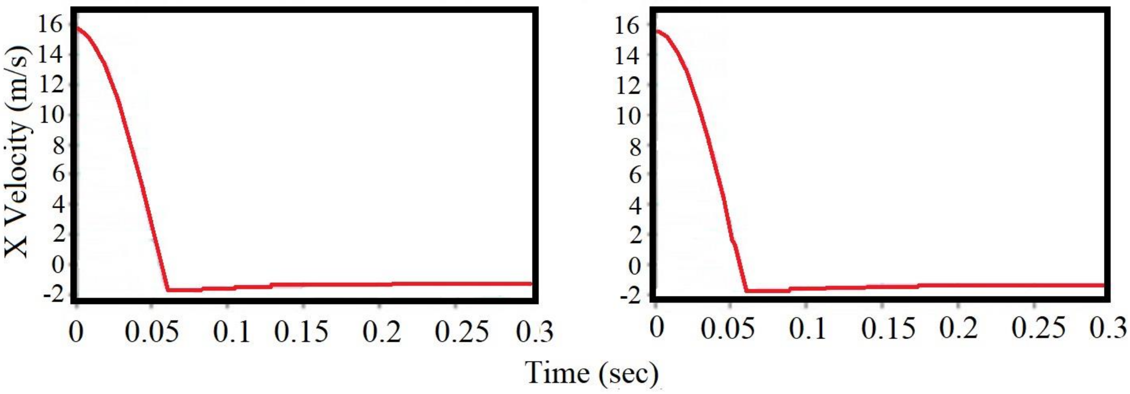

Figure 3.36. X-direction velocity-time graphs of a Subaru Impreza model vehicle using linear (left) and non-linear (right) suspension springs.

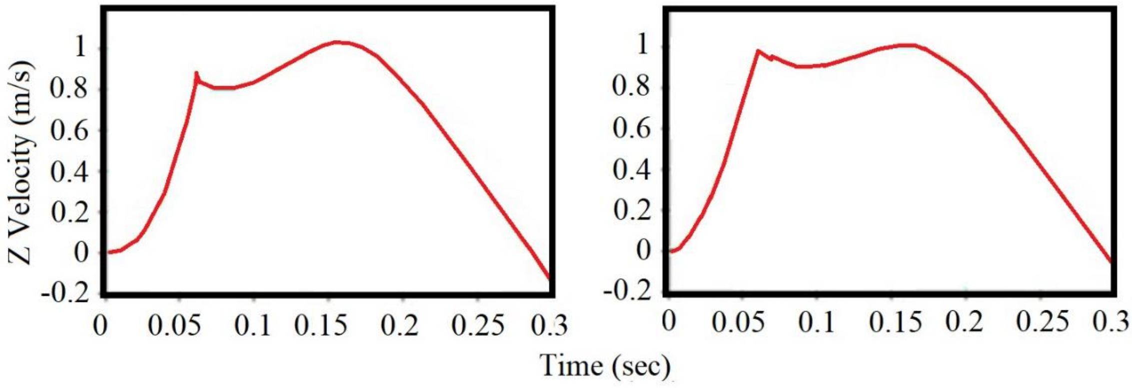

Figure 3.37. X-direction velocity-time graphs of the Subaru Impreza model vehicle using linear (left) and non-linear (right) suspension springs.

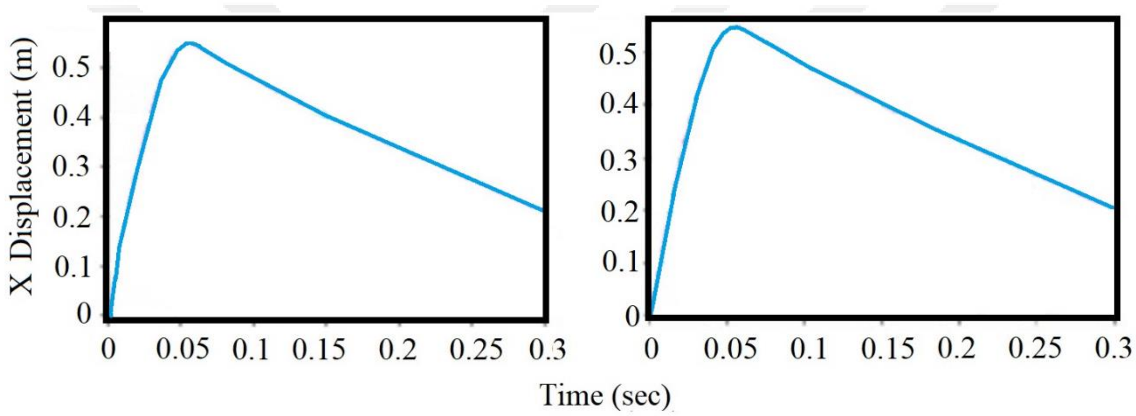

Figure 3.38. X direction position-time plots of Subaru Impreza model vehicle using linear (left) and non-linear (right) suspension springs.

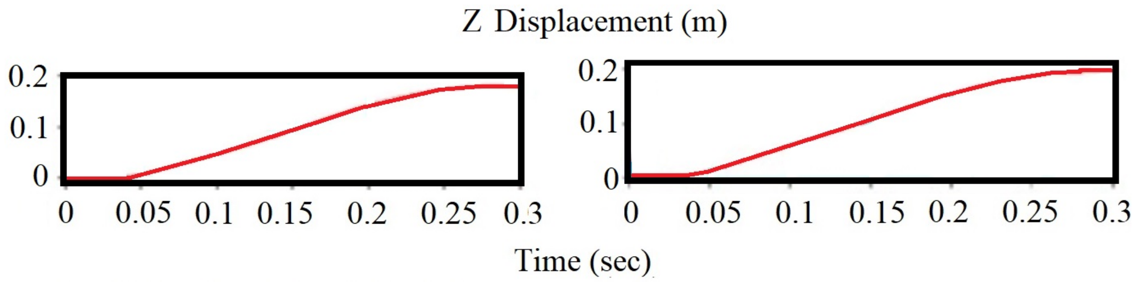

Figure 3.39. Z direction position-time plots of Subaru Impreza model vehicle using linear (left) and non-linear (right) suspension springs.

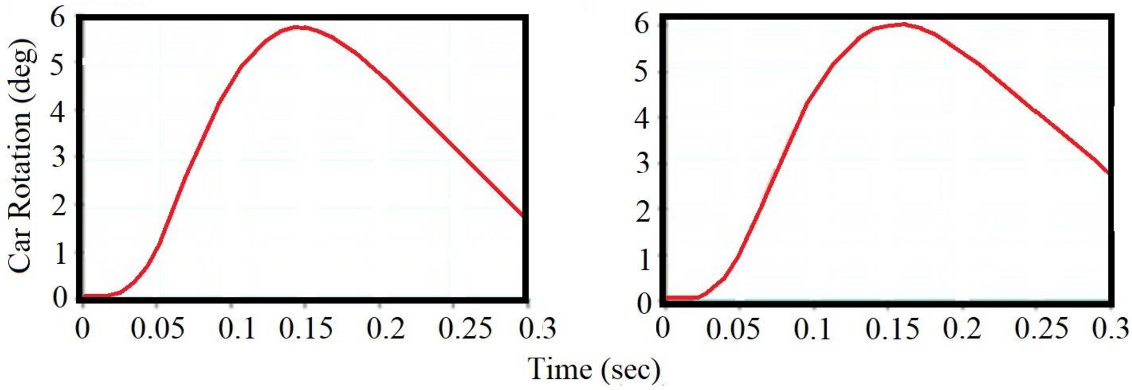

Figure 3.40. Angular displacement-time plots of the Subaru Impreza model vehicle around the Y-axis obtained by using linear (left) and non-linear (right) suspension springs.

3.5. Ride Comfort

Vibrations that adversely affect the passengers or the load carried in a vehicle impair ride comfort. These vibrations may be generated by different types of sources. Vibrations caused by engine imbalance, torsional fluctuations at the engine output, tires, uneven road surface profile, etc. can have a detrimental effect on ride comfort. In real applications, while a vehicle has many degrees of freedom, it is accepted that it has 6 degrees of freedom for its analyses to be performed ([25], Figure 3.41). Three of these degrees of freedom are linear motion and three are angular motion. In this section, based on the Subaru Impreza model vehicle, some ride comfort values are provided for the simulation environment.

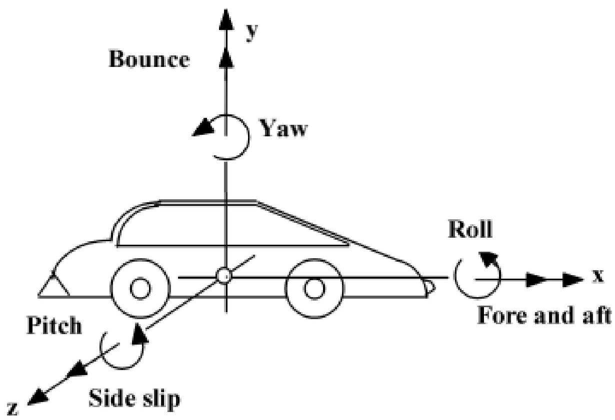

Figure 3.41. Accepted axes of motion of a vehicle (Adapted from [25].).

3.5.1. Body Bounce Frequency

Body bounce motion is the name given to the up-down, i.e. vertical movement of the sprung mass on the suspension spring [25]. Here the sprung mass is considered to be point-like and the suspension system consists of a viscous damper and a parallel linear spring. The unsprung mass and tire elasticity are not taken into account. This model is used to predict the body bounce frequency of the vehicle when the values of sprung mass and suspension spring stiffness are available. For quarter vehicle model, body bounce frequency should be around 1.2 Hz for light vehicles [25].

$$\omega_{bb} = \sqrt{\frac{k}{m}} \quad (1)$$

$$\omega_{bb} = \frac{\sqrt{\frac{20000}{345}}}{2\pi} = 1.2\ Hz$$

- sprung mass for quarter car: 345 kg

3.5.2. Wheel Hop Frequency

In this mode, the wheel hub assembly, i.e. the unsprung mass, bounces on the tire and suspension spring and the movement is damped by the shock absorber [25]. For quarter vehicle model Wheel hop frequency can be up to 16 Hz in light vehicles [26].

$$\omega_{wh} = \sqrt{\frac{k_s+k_t}{m}} \quad (2)$$

$$\omega_{wh} = \frac{\sqrt{\frac{225000+20000}{40}}}{2\pi} = 12.46\ Hz$$

Here;

- tyre stiffness=225000 N/m,
- suspension stiffness=20000 N/m
- unsprung mass=40 kg

3.5.3. Pitch Frequency

Pitch can be defined as the weight transfer from front to rear or from rear to front during acceleration or braking. The frequency value is expected to be between 1 Hz and 1.5 Hz [27].

$$\omega_p = \sqrt{\frac{a^2 k_{sf} + b^2 k_{sr}}{m\ a\ b}} \ (3)$$

$$\omega_p = \frac{\sqrt{\frac{1.189^2 40000 + 1.465^2 38000}{1382\ 1.189\ 1.465}}}{2\pi} = 1.2\ Hz$$

- a: distance between center of gravity-front wheel=1.189 m
- b: distance between center of gravity-rear wheel =1.465 m
- m: sprung mass=1382 kg
- k_{sf}=40000 N/m (Front suspension stiffness)
- k_{sr}=38000 N/m (Rear suspension stiffness)

3.5.4. Suspension Damping Ratio

The dampers in the suspensions are expected to provide a damping ratio of approximately 0.2 to 0.4 for each quarter car model.

$$\zeta = \frac{c}{2\sqrt{m\ k}} \ (4)$$

In the Subaru Impreza model vehicle,

- the quarter vehicle model mass: 345 kg.
- spring coefficient for the front wheels: 20000 N/m
- damper coefficient for the front wheels: 2000 kg/s
- the damping ratio value for the front wheels: $\zeta = \frac{c}{2\sqrt{m\,k}} = \frac{2000}{2\sqrt{345\ 20000}}$ =0.37.
- spring coefficient for the rear wheels: 19000 N/m
- damper coefficient for the rear wheels: 2000 kg/s
- the damping ratio value for the rear wheels: $\zeta = \frac{c}{2\sqrt{m\,k}} = \frac{2000}{2\sqrt{345\ 19000}}$ =0.38.

4. TORSO PLATES AND TORSION BAR

In this part of the thesis, a forward-facing passive seat and a rearward facing seat optimized for rear impact conditions are investigated. Forward-facing conventional seat was tested with the low crash severities and the rearward-facing seat was tested with the high crash severities. In order to ensure that the rearward-facing seat performs protection to the passengers at high crash severities, this seat is equipped with so-called torso plates.

4.1. Whiplash Mitigating Forward-Facing Seat

This seat has a typical head restraint (HR), seatback (SB), seat panel (SP), 3-point seat belt, recliner (R) and a shock absorber (D) under the seat panel (Figure 4.1). The reclining mechanism is designed to undergo plastic deformation to absorb the crash energy. This design is similar to the load limiters used in seat belt retractors. The quasi-static stiffness characteristics of the tilt mechanism can be seen in Figure 4.1b. The curvature shape in Figure 4.1b is similar to that of some commercially available mass-produced car seats. However, Figure 4.1b shows that the recliner has an additional rupture element that produces a high torque at the initial deformation.

This breakaway element is similar to the pretensioners in seat belts. One of the functions of this breakaway torque is to limit the tipping of the seatback at the onset of a collision. A viscous damping coefficient of 1 Nms/degree was applied to the reclining seat to simulate the structural damping that occurs during the backward rotation of the seatback in a rear impact. Again, a viscous damping coefficient of 15 Nms/degree was applied to simulate the unloading behavior of the reclining mechanism during the rebound movement of the seatback. The rigidity of the reclining mechanism increases considerably after the seatback is rotated by 21 degrees. A shock absorber equipped with a non-linear spring and a parallel viscous shock absorber is located under the seat pan. The mechanical properties of this shock absorber are given below (Figure 4.1c). The energy absorber (D) has a high damping (30 kNs/m). This is a value to reduce the back and forth rebound movement of the seat pan. This device also includes a brake element that prevents activation in everyday use and at low impact intensities (smaller than 10 km/h Delta-V value). In the proposed seat, the load on the body is limited by the sharing of the crash energy by the shock absorber (D) and the reclining mechanism (R). This seat provides balanced protection at all crash intensities up to 24 km/h Delta-V (Table 4.1 and Table 4.2).

The head restraint foam is 8 cm in thickness. The dynamic force versus deformation behavior of the head restraint is such that head restraint foam produces 800 N of force at 8 cm deformation. The seatback foam and seat suspension of the seat allows the passenger to be embedded maximum 5 centimeter in the seatback structure. The deformation of the seatpan foam is a maximum of 4 cm. The seatback foam is soft enough to ensure early contact between the head restraint and the head. The seatback and head restraint are adjusted to limit the internal movements of the neck when the body is recessed into the seat. The initial position of the seatback is set at 20 degrees. The horizontal distance between the head restraint and the head before impact was 6 centimeter (Figure 4.1).

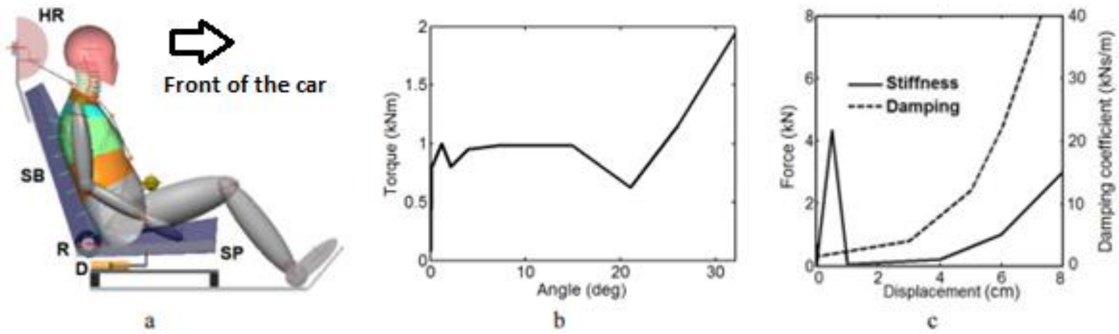

Figure 4.1. Forward-facing seat properties: (a) seat-occupant model; (b) recliner stiffness; (c) energy absorber (D).

Table 4.1 Used crash pulses in simulations.

Pulse	ΔV [km/h]	a_{mean} [g]	a_{peak} [g]		Pulse	ΔV [km/h]	a_{mean} [g]	a_{peak} [g]
SN(9.4)	9.4	3.1	11.7		TR(24)	24	6.5	7.5
SN(13)	13	4.7	10.3		HS(35)	35	7	16
SN(16)	16	5	10		NCAP(43)	43	14	36.6
SN(20.5)	20.5	5.2	10.6		NCAP(64)	64	15	38

The forward-facing seat's performance is shown in Table 4.2. In this table;

F_{sh} ve F_{tn}: maximum shear and tensile forces acting on the top of the neck, respectively

N_{km}: an injury criterion derived from the combination of shear forces and moments acting on the neck

NIC: an injury criterion due to S-shaped deformation of the neck

v_r: maximum forward speed of the head with respect to the vehicle floor from the moment the occupant head starts to retract from the head restraint

NDI: neck distortion index based on rotations between the upper and lower cervical vertebrae

NDI = $-\theta_{OC/C1} + \theta_{C7/T1}$ (1)

(Note: Here $\theta_{OC/C1}$ is given as the intervertebral rotation between the occipital condyles and the first cervical vertebra and similarly θC7/T1 is given as the intervertebral rotation between the seventh cervical and first thoracic vertebra (Figure 4.2).)

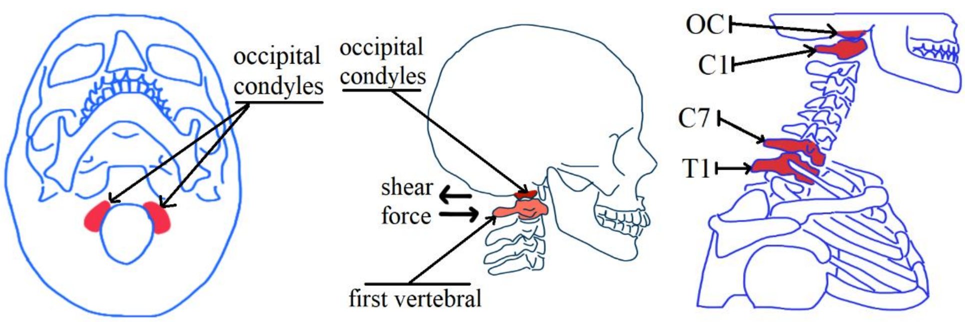

Figure 4.2. OC and C1 vertebrae and C7 and T1 vertebrae.

These expressions refer to flexion (negative angle) and extension (positive angle) indicators of the upper neck and lower neck, respectively. The NDI can be used to quantify the amount of protraction and retraction-type deformations that occur in rear impact situations. Volunteer experiments have shown that in an S-shaped deformation of the neck, the head is retracted relative to the upper body with a positive NDI value. Negative NDI is observed in protraction type deformations in the neck [19].

According to the EuroNCAP neck response assessment protocol, the limit values of upper neck tensile forces are 360 N for SN(16) pulse and 470 N for TR(24) pulse. These values are higher seat performance limits and the values of the proposed seat are well below these limit values. Again, forces occur on the upper neck is in the low neck force region according to the neck force classification of IIWPG. Positive upper neck shear forces $F_{sh}(+)$ (associated with head backward movement with respect to the body) are below the force value of 30 N (upper limit value for high performance seats). The negative upper neck shear forces $F_{sh}(-)$ values associated with the backward movement of the body relative to the head are also well below the values determined according to the EuroNCAP whiplash evaluation protocol (290 N for SN(16) pulse and 360 N for TR(24) pulse). N_{km} values were also obtained well below threshold value that indicated for this injury criteria. The NIC values are much lower than the EuroNCAP limit value (27 m/s^2). v_r values show that injury risk in the rebound phase of rear-end collisions is low. When a limit value for an injury parameter is exceeded, the tested seat fails the test in the EuroNCAP neck response assessment protocol.

In this study, an NDI value of +4.5 degrees was observed in S-shape-like deformation. This NDI value was obtained from male volunteer simulations by using the 50th percentile human body model. In these tests, the volunteers were subjected to a impact with 9.3 km/h Delta-V value on a rigid seat without head support. This value of 4.5 degrees should not be taken as the injury threshold. This is because vertebral configurations may differ from those in other rear-end crash volunteer tests. However, the NDI can be used as a seat design parameter to compare different seat performances.

Table 4.2. Forward-facing seat performance.

Pulse	$F_{sh}^{(+)}$ [N]	$F_{sh}^{(-)}$ [N]	F_{tn} [N]	N_{km}	NIC [m^2/s^2]	v_r [m/s]	NDI [deg]
SN(9.4)	16	49	121	0.11	8.14	1.35	-1.41 / 1.80
SN(13)	33	97	112	0.26	8.89	1.23	-0.63 / 2.18
SN(16)	24	94	192	0.195	11.4	1.28	-1.22 / 1.44

SN(20.5)	14	134	178	0.32	11.9	1.34	-1.13 / 0.31
TR(24)	20	151	102	0.43	11.3	1.17	-3.37 / 1.69

4.2. Torso Plates

The front-facing seat, which was analyzed in detail in the previous section, is placed facing the rear in this section. In this scenario, the rearward-facing seat will be exposed to an impact from the front of the vehicle. In this context, crash impacts with higher crash severity such as HS(35), NCAP(43) and NCAP(64) were applied to the rearward-facing seat. The HS(35) crash severity was derived from the FMVSS301 moving barrier tests aimed at checking fuel integrity. NCAP(43) and NCAP(64) crash severities were obtained from crash simulations performed in VisualNastran multi-body simulation software. The simulations were carried out using a 2010 Toyota Yaris sedan vehicle. The vehicle was modelled with its suspension and crashed into a rigid wall. Acceleration data along the X and Z axes were obtained, as well as data on the rotational acceleration experienced by the vehicle during the collision. Using this acceleration data, NCAP(43) and NCAP(64) crash severity ratings were determined. The impact speed of these crash severities are 40 km/h and 56 km/h, respectively.

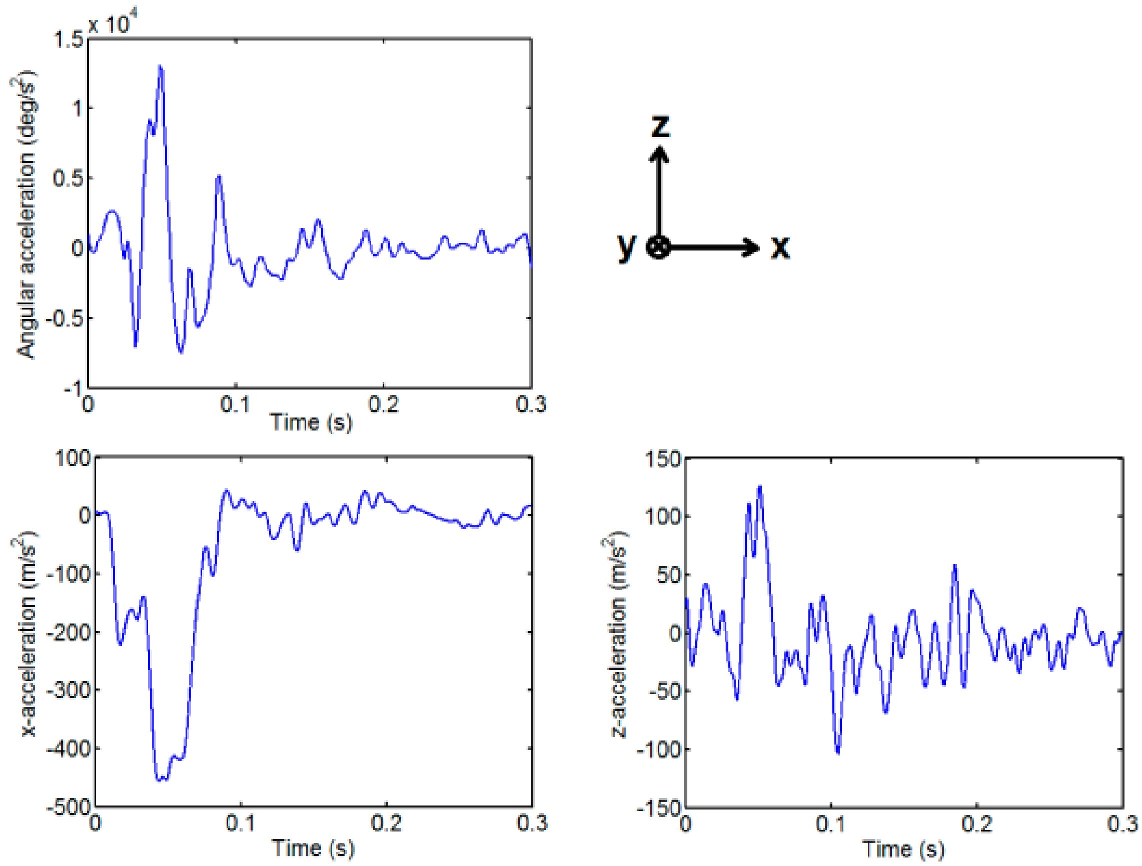

Figure 4.3. The angular and translational accelerations around the carfloor (from FE simulation).

Simulations have shown that the shear forces in the neck area in an NCAP(64) impact exceed the threshold value of 600 N. This is likely to lead to a high neck injury risk in the neck area. This is due to the softness of the recliner, the shock absorber (D), the seatback foam material and the head restraint foam material. Due to these characteristics of these parts, the seat could not carry the human body early enough and could not provide sufficient restraint force intensity. As a result, this significantly increases the human body speed with respect to the vehicle cabin. In the process of the seatback tilting backwards during a collision, the upper part of the occupant torso and the occupant head interact violently with seatback and head restraint. This interaction has a high effect of increasing the risk of head, neck and torso injuries.

The situation described above requires a new approach in vehicle seat design to protect the occupants of the vehicle against frontal and rear impacts in both forward-facing and rearward-facing seat arrangements. The rearward-facing seat design mentioned here is based on the principle of restricting the movement of the occupant head and the occupant torso relative to the head restraint and seatback. For this reason, the gaps between the human body and the seat surfaces are kept to a minimum, except for the extremities. The proposed seat design, which is also equipped with an integrated seat belt, can also be used in autonomous vehicles where the seats can be relocated in different positions (Figure 4.4).

The developed seat system consists of two rigid body plates extending from the seatback to the passenger body. These body plates extend to the chest and waist areas of the passenger and provide movement restriction in the current positions. These body plates can be removed and replaced and their dimensions can be adjusted according to the body size of the passenger. The body plate supporting the back is called thorax body plate and the body plate supporting the lumbar region is called lumbar body plate. When adjusting according to the person, the body plates are loosened from the P point and rotated around this point. Then, the fixing process is performed again from the P points. Thus, the movement of the upper and lower body can be restricted according to the seatback in the event of a collision.

The thorax plate, which limits the speed of the occupant upper torso relative to the upper region of the seatback, increases head and neck protection. The front surface of the seatback has rigid plates covered with a thin foam 1.5 cm thick. Foam and suspension were placed between rear surface of seat surface and seat structure. Seatback maximum penetration to the seat structure is 3.2 centimeter (the allowance limit of foam). The head restraint allows the head to penetrate a maximum of 3 cm with 2250 N force magnitude. The head restraint used in this seat, together with the thorax plate, minimizes head and neck movement relative to the upper part of the body. The lumbar body plate prevents the body from rotating clockwise when the body is embedded in the seat structure. Thus, the head does not become distant from the head restraint. With an active head restraint or manual adjustment, the clearance between the head restraint and the head should be reduced to almost zero. This is necessary to provide the necessary protection at the onset of a collision. The integrated seat belt and thorax plate eliminate the possibility of the seatback lifting up.

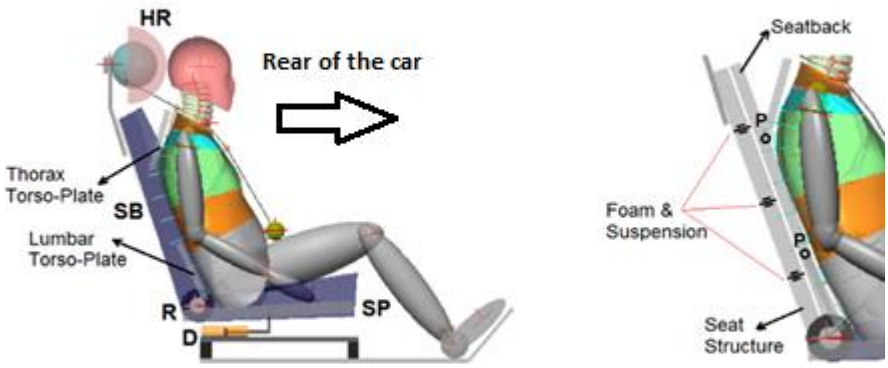

Figure 4.4. The proposed system for rearward-facing seats.

The rearward-facing seat described in this section does not use the reclining mechanism (R) and shock absorber (D) recommended for the forward-facing seat. The reclining mechanism (R) for rearward-facing seats is also fixed. In addition, the seat is moved forwards by about 10 cm at low acceleration values just before the collision. After the seat has been moved forwards, the collision occurs, and the seat is allowed to move backwards due to the impact. At high crash severity, the seat moves backwards for a considerable distance. Moving the seat forwards just before the collision will reduce the distance the seat moves backwards.

Before an unavoidable collision, the seat base is moved forwards by an electric motor by about 10 centimeter in a time interval of 2 seconds relative to the cabin floor (CF) (Figure 4.5). A shock absorber (C) is located under the seat panel (SP). The shock absorber contains a damper and a constant force deformation element. The viscous damping coefficient of the absorber is 1500 kg/s and the constant resistance force of the deformation element is 4250 N. In the literature, it is recommended to use constant force deformation elements for energy absorbing devices in impact applications. At the moment of impact, the seat moves backwards by a maximum of 30 cm. As a result, seat's maximum net rearward displacement only 20 centimeters. During daily use, the seat panel is fixed to the vehicle floor (CF) by means of a locking pin (L). After the inevitable collision is detected (approximately 2 seconds ago, i.e. at -2 seconds), the signal sent through the sensors (lidar, radar) will release the locking pin (L) electromechanically. In this way, an electric motor will be activated. During normal travel, the function of the locking pin (L) is make the fix connection between the energy-absorbing device (C) and the car floor (CF). Between the car floor (CF) and the energy-absorbing device (C) a spiring-loaded rectangular wedge (W) was placed. The electric motor just mentioned operates the energy absorbing device on the floor and the seat base of the car until wedge (W) is placed in the slot (S). When this wedge is plugged in its slot, the seat pan movement towards the car rear-end finishes and the electric motor turns off. WShen time becomes zero a frontal crash begins.

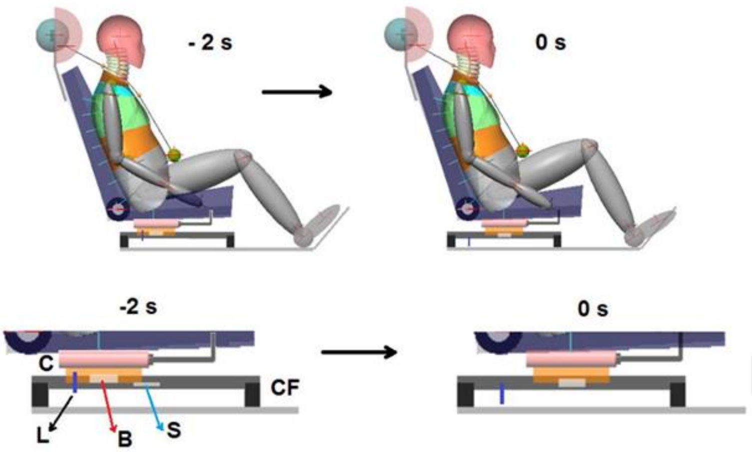

Figure 4.5. Seatpan forward movement.

4.3. Performance of the Torso Plates

The fixed recliner energy absorbing seat whose performance was evaluated was subjected to medium, high and very high impact crashes (SN(16), TR(24) and HS(35) respectively). The EuroNCAP neck response assessment criteria recommended for forward-facing seats were used to obtain the performance evaluation of the recommended seat. The injury assessment reference values corresponding to these criteria are shown in Table 4.3. These criteria’s are;

- NIC (Neck Injury Criteria),
- N_{km},
- v_r (velocity of head rebound),

- $F_{sh}^{(+)}$ (maximum positive shear force of upper neck),
- $F_{sh}^{(-)}$ (maximum negative shear force of upper neck),
- F_{tn} (maximum tension force of upper neck),
- M_{yU} (maximum moment of upper neck),
- F_{shL} (maximum shear force of lower neck),
- M_{yL} (maximum moment of lower neck),
- T_{1a} (largest acceleration value for the first thoracic vertebra (T1)),
- H_{rCt} (contact time between head restraint and head).

High performance (HL) and low performance (LL) limits for some criteria are given in Table 4.4. The N_{km} injury criterion is calculated by combining the upper neck shear force and moment. S-shape-like deformation of the neck is used for NIC calculation and v_r is measured from the moment just the head starts to bounce back from the head restraint and move forwards. Its value is the maximum speed of the head relative to the cabin floor from this moment onwards. The limit boundaries (CL) for the other criteria are defined in Table 4.4. In general, if any limit value obtained in the tests/simulations for an evaluation criterion is exceeded, the suggested seat is considered a failure according to the EuroNCAP protocol.

The EuroNCAP protocol does not include injury assessment reference values for HS(35) impact severity, as most rear-end impacts have Delta-V values below 25 km/h. High-speed frontal impact injury criteria and low- and high-speed rear impact injury criteria were used to evaluate the performance of the aforementioned rearward-facing seat. The rearward-facing seat will be subjected to high-speed frontal impacts. Therefore, injury assessment reference values (IARVs) corresponding to these intensities were also considered. These values represent injury threshold values. These thresholds are [19];

- BrIC: brain injury criteria
- F_{tn}: upper and lower neck tensile force
- F_{cm}: upper and lower neck compression force
- T_{a3}: maximum clip thorax acceleration value of 3 ms

- L_{tn}: lombar tensile force
- L_{cm}: lombar compression force
- N_{ij}: a neck injury criteria which is obtained by combining the upper neck axial forces and extension/flexion moments
- cd: maximum chest deflection
- V_C: viscous criterion (considers the velocity-dependent mechanism of injury in the thorax and can predict serious chest injuries)
- H_{cm}: hip fracture and dislocation force
- F_{cm}: patellar and femur fracture/dislocation force
- T_{cm}: tibial plateau or condyle injury force
- T_I: (tibia index) prediction for tibia shaft fracture

As indicated in Table 4.4 and Table 4.5, these are the criteria for a high intensity frontal impact injury.

Table 4.3. Whiplash injury assessment reference values (IARVs) [28].

Pulse		SN(16)			TR(24)		
	Unit	HL	LL	CL	HL	LL	CL
NIC	m2/s2	11	24	27	13	23	25.5
N_{km}	-	-	-	0.69	-	-	0.78
v_r	m/s	-	-	5.2	-	-	6
$F_{sh}^{(+)}$	N	30	190	290	30	210	364
$F_{sh}^{(-)}$	N	-	-	360	-	-	360

F_{tn}	N	360	750	900	470	770	1024
M_{yU}	Nm	-	-	30	-	-	30
F_{shL}	N	-	-	360	-	-	360
M_{yL}	Nm	-	-	30	-	-	30
T_{1a}	g	-	-	15.55	-	-	17.8
H_{rCt}	ms	-	-	92	-	-	92

Table 4.4. IARVs for low speed (LS) speed impacts [28].

Criterion	HIC_{15}	BrIC	$Fsh^{(+)}$	$Fsh^{(-)}$	F_{tn}	F_{cm}	N_{km}	NIC	v_r	Ta_3	L_{tn}	L_{cm}
Unit	-	-	N	N	N	N	-	m^2/s^2	m/s	g	N	N
IARV-LS	-	-	200	360	760	-	0.74	24	5.6	-	-	-

Table 4.5. IARVs for high speed (HS) speed impacts [28].

Region	Criterion	IARV-HS	Reference
Head	HIC_{15} *BrIC*	700 -	[29] [30]
Upper Neck	$FshU^{(+)}$*(+ shear)* $FshU^{(-)}$*(- shear)* $F_{tn}U$ *(tension)* $F_{cm}U$ *(compr.)* M_yUE *(extension)* M_yUF *(flexsion)* N_{ij}	3100 N 3100 N 3300 N 4000 N 57 Nm 190 Nm 1	[8], [32] [8], [32] [32], [29] [32], [29] [32], [29] [32], [29] [32], [29]

Lower Neck	*$FshL^{(+)}$ (+ shear)* *$FshL^{(-)}$ (- shear)* *$F_{tn}L$ (tension)* *$F_{cm}L$ (compr.)* *M_yLE (extension)* *M_yLF (flexion)*	3100 N 3100 N 3300 N 4000 N 194 Nm 380 Nm	[8], [32] [8], [32] [32], [29] [32], [29] [8] [8]
Thorax	*T_{a3} (thorax acc.)* *cd (chest defl.)* *VC*	60 g 42 mm 1 m/s	[32], [29] [28], [32] [32], [33], [34]
Lumbar Spine	*L_{tn} (tension)* *L_{cm} (compr.)*	12.2 kN 6400 N	[8] [8], [32]
Hip Femur (thigh) Tibia Tibia	*H_{cm} (axial compr.)* *F_{cm} (axial compr.)* *T_{cm} (axial compr.)* *TI*	10 kN 10 kN 8 kN 1.3	[32], [35] [28], [35], [36] [28], [32], [36] [28], [32], [36], [37]

Impact severities of 9.4 km/h Delta-V and 24 km/h Delta-V are low-speed impacts. Impacts greater than 24 km/h Delta-V are defined as high-speed impacts. Low-speed rear-end injury thresholds derived from the EuroNCAP protocol are shown in Table 4.4 as IARV-LS. For medium intensity EuroNCAP SN(16) and high intensity EuroNCAP TR(24) crash impacts, either the limit values or the average of the lower seat performance limits were taken as reference.

The injury thresholds indicated as IARV-HS in Table 4.5 are for high-speed frontal crashes. A single IARV criterion is not specified for the brain injury criterion BrIC. Instead, the available values for slight injury (P1) type AIS1 and moderate injury type AIS2 (P2) are given in Table 4.6. The calculated BrIC values and the corresponding injury probabilities are based on the maximum principal stress. Table 4.6 shows the properties of the high-speed crash pulses and Table 4.7, Table 4.8, Table 4.9, Table 4.10, Table 4.11, Table 4.12, Table 4.13 and Table 4.14 and Figure 4.6 show proposed rearward-facing seat performance in all crash impacts.

Table 4.6 High speed crash pulses properties [38].

Crash Pulse	a_{peak}	Delta-V	a_{m50}
HS(35)	16 g (x)	35 km/h (x)	10.54 g (x)
NC(47)	−27.3 g (x)	−47.5 km/h (x)	−20.7 g (x)
	8.61 g (z)	−1.93 km/h (z)	−1.68 g (z)
	3.72 deg/s^2 (y)	−2.36 deg/s (y)	−570 deg/s^2 (y)
NC(64)	−46.56 g (x)	−64.2 km/h (x)	−31.92 g (x)
	12.89 g (z)	−4.98 km/h (z)	3.26 g (z)
	13,096 deg/s^2 (y)	−12.87 deg/s (y)	2963 deg/s^2 (y)

Table 4.7 Proposed rearward-facing seat performance.

Pulse	SN(9.4)	SN(13)	IIWPG	SN(20.5)	TR(24)	FMVSSHS
HIC_{15}	2.156	4.560	4.244	4.051	5.135	6.859
BrIC	0.044	0.043	0.031	0.028	0.033	0.033
BrIC-P1	0.057	0.054	0.021	0.016	0.026	0.027
BrIC-P2	0	0	0	0	0	0
$Fsh^{(+)}$ [N]	17.59	17.71	15.67	12.82	9.378	15.46
$Fsh^{(-)}$ [N]	87.961	135.33	130.25	115.11	128.39	157.19
F_{tn} [N]	49.356	81.692	97.356	16.734	85.409	76.219
F_{cm} [N]	209.99	365.86	359.05	300.33	311.73	445.75
N_{km}	0.170	0.263	0.253	0.208	0.232	0.294
NIC [m^2/s^2]	7.789	11.35	13.35	9.196	15.24	16.86
NDI$^{(+)}$ [deg]	0.281	0.171	0.291	0.218	0.215	0.145

NDI$^{(-)}$ [deg]	2.292	1.208	2.571	2.791	2.135	3.483
v_r [m/s]	0.49	0.47	0.46	0.41	0.42	0.43
Ta_3 [g]	7.392	8.378	11.39	9.976	11.15	11.97
L_{tn} [N]	0	0	0	0	0	0
L_{cm} [N]	1350	1455.5	1701.9	1720.4	1629.7	2172.4
Myu [Nm]	2.57	3.28	6.08	3.56	3.42	4.74
Myl [Nm]	4.01	3.64	3.55	3.70	3.64	4.41
FshL [N]	83.66	129.29	124.45	105.83	114.37	144.90
T1 x-acc [g]	7.87	12.02	8.87	7.74	8.25	13.43
HrCt [ms]	14	8	16	11	11	7

Table 4.8 Rearward-facing seat performance at higher severities (head).

Pulse	HIC_{15}	BrIC
HS(35)	6.86 (1% IARV) (0% AIS2+)	0.03 (3% AIS1, 0% AIS2)
NC(43)	39.3 (6% IARV) (0% AIS2+)	0.04 (4% AIS1, 0% AIS2)
NC(64)	89.6 (13% IARV) (0% AIS2+)	0.042 (5% AIS1, 0% AIS2)

Table 4.9 Rearward-facing seat performance at higher severities (upper neck).

Pulse	HS(35)	NC(43)	NC(64)
N_{km}	0.29 (29% IARV)	0.42 (42% IARV)	0.67 (67% IARV)
$F_{shU}^{(+)}$	15.5 (0.5% IARV)	13.1 (0.4% IARV)	11.6 (0.4% IARV)

$F_{shU}^{(-)}$	157 (5% IARV)	219 (7% IARV)	350 (11% IARV)
F_{tnU}	76.2 (2% IARV)	223 (7% IARV)	445 (13% IARV)
F_{cmU}	445 (11% IARV)	634 (16% IARV)	729 (18% IARV)
M_{yUE}	4.74 (8% IARV)	7.37 (13% IARV)	10.7 (19% IARV)
M_{yUF}	0.66 (0.3% IARV)	2.54 (0.8% IARV)	5.52 (3% IARV)
N_{ij}	0.12 (13% AIS2+) (12% IARV)	0.15 (13% AIS2+) (15% IARV)	0.19 (14% AIS2+) (19% IARV)

Table 4.10 Rearward-facing seat performance at higher severities (lower neck).

Pulse	HS(35)	NC(43)	NC(64)
$F_{shL}^{(+)}$	75 (2.4% IARV)	124 (4% IARV)	309 (10% IARV)
$F_{shL}^{(-)}$	145 (5% IARV)	133 (4.3% IARV)	149 (4.8% IARV)
F_{tnL}	99 (3% IARV)	125 (4% IARV)	179 (5.4% IARV)
F_{cmL}	420 (11% IARV)	721 (18% IARV)	837 (21% IARV)
M_{yLE}	3.09 (1.6% IARV)	5.02 (2.6% IARV)	14.0 (7.2% IARV)
M_{yLF}	4.41 (1% IARV)	5.09 (1.3% IARV)	5.92 (1.6% IARV)

Table 4.11 Rearward-facing seat performance at higher severities (overall neck).

Pulse	HS(35)	NC(47)	NC(64)
v_r	0.43 (7% IARV)	0.54 (14% IARV)	0.87 (14% IARV)
NIC	16.8 (62% IARV)	10.6 (39% IARV)	19.7 (73% IARV)
$NDI^{(-)}$	3.48	3.49	2.74
$NDI^{(+)}$	0.14	0.29	0.96

Table 4.12 Rearward-facing seat performance at higher severities (thorax).

Pulse	HS(35)	NC(43)	NC(64)
Ta_3	11.9 (20% IARV) (36% AIS2+)	25.2 (42% IARV) (55% AIS2+)	32.6 (54% IARV) (65% AIS2+)
cd	2.3 (5.5% IARV) (14% AIS2+)	2.6 (6.2% IARV) (14% AIS2+)	3.2 (7.6% IARV) (15% AIS2+)
VC	0.0072 (0.72% IARV) (0% AIS2+)	0.005 (0.5% IARV) (0% AIS2+)	0.006 (0.6% IARV) (0% AIS2+)

Table 4.13 Rearward-facing seat performance at higher severities (lumber spine).

Pulse	HS(35)	NC(43)	NC(64)
L_{tn}	0	0	0
L_{cm}	2172 (34% IARV)	2826 (44% IARV)	3512 (55% IARV)

Table 4.14 Rearward-facing seat performance at higher severities (hip-femur-tibia).

Pulse	HS(35)	NC(43)	NC(64)
H_{cm}	1.3 (13% IARV) (0% AIS2+)	2.18 (21.8% IARV) (0% AIS2+)	3.2 (32% IARV) (0% AIS2+)
F_{cm}	0.21 (2.1% IARV) (0% AIS2+)	0.42 (4.2% IARV) (0% AIS2+)	0.50 (5% IARV) (0% AIS2+)
T_{cm}	43 (0.54% IARV) (0% AIS2+)	45 (0.56% IARV) (0% AIS2+)	44 (0.55% IARV) (0% AIS2+)
TI	0.063 (4.8% IARV) (0% AIS2+)	0.11 (8.5% IARV) (0% AIS2+)	0.13 (10% IARV) (0% AIS2+)

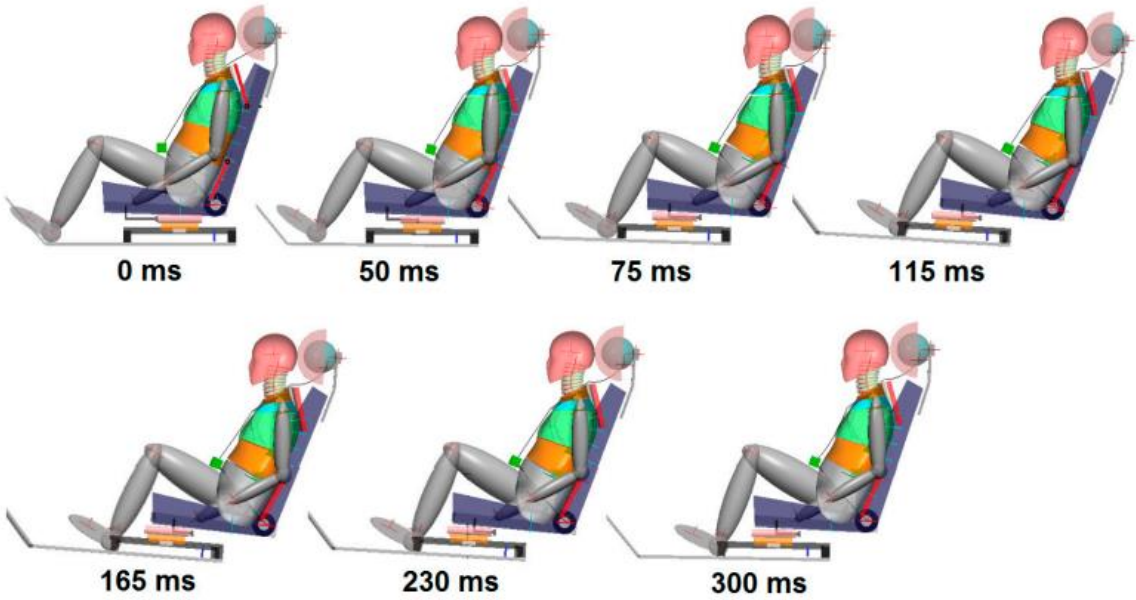

Figure 4.6 Simulation of a frontal crash with the passenger sitting in the rearward-facing seat at a speed of 56 km/h (NC(64)).

Note: Further details are available in the journal paper which can be freely accessed at https://www.mdpi.com/2075-1702/11/12/1076

4.4. Torsion Bar

A crash scenario was realized by applying the horizontal, vertical and rotational acceleration data obtained from the crash simulation of the Toyota Yaris model vehicle at a crash severity of 56 kph to the human-seat model. In order to prevent high compression forces on lumbar region due to uprise movement of the seat with rear impact crash severities (on forward facing seats), a torsion bar was proposed and used to prevent the driver's seat from rotating and uprising (Figure 4.7).

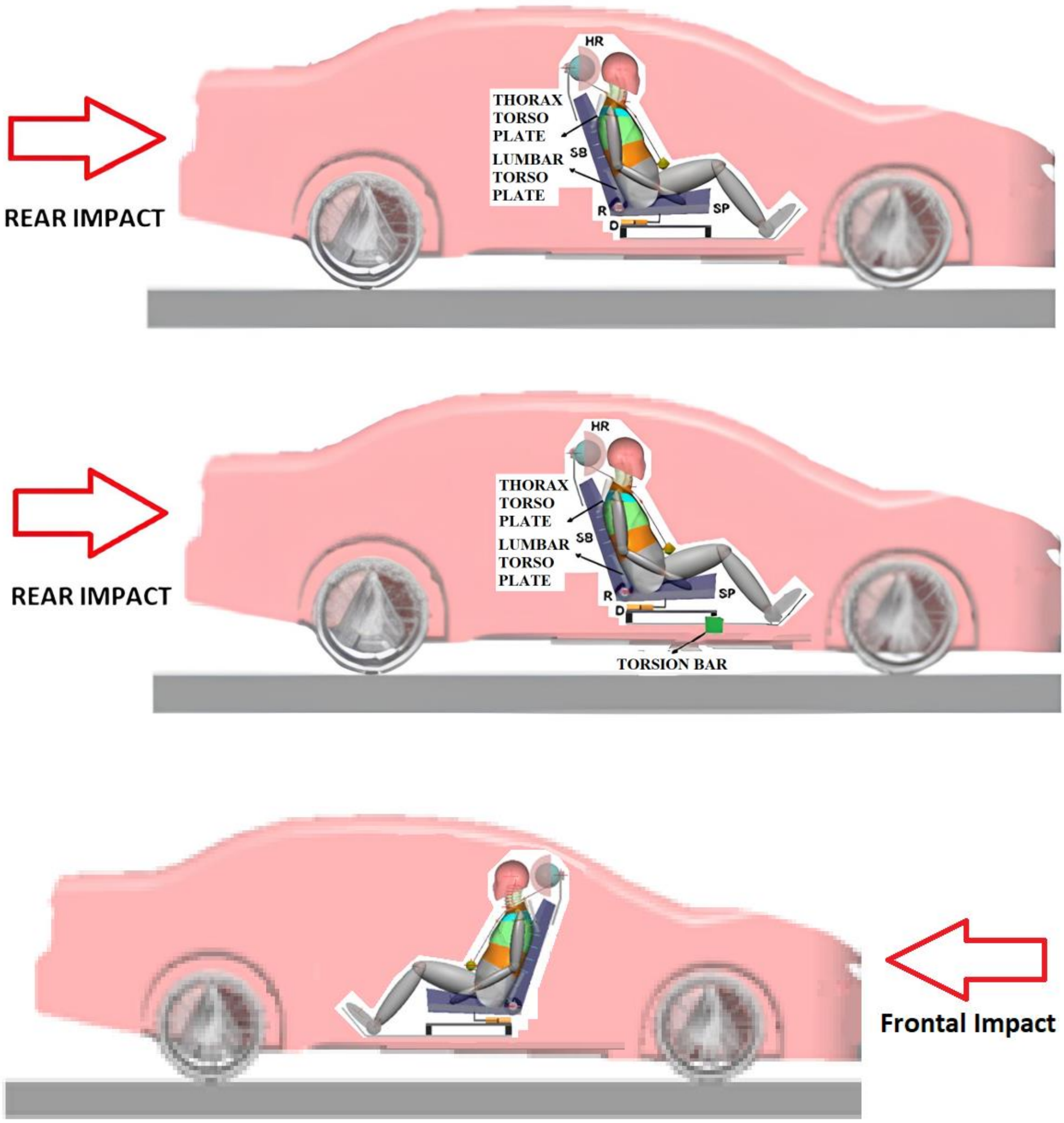

Figure 4.7. Application of rear impact to forward facing seat without (top figure) and with (middle figure) torsion bar and frontal impact to rear facing seat without (bottom figure) torsion bar

The moment values of the torsion bar torsion element depending on the amount of rotation are given below (Figure 4.8). Figure 4.9 shows the behavior of the torsion bar torsion member in the simulation environment at 56 kph crash severity. Finally, Table 4.15 shows the forward-facing seat performance values with and without torsion bar applied at 40 kph and 56 kph rear impact crash severities.

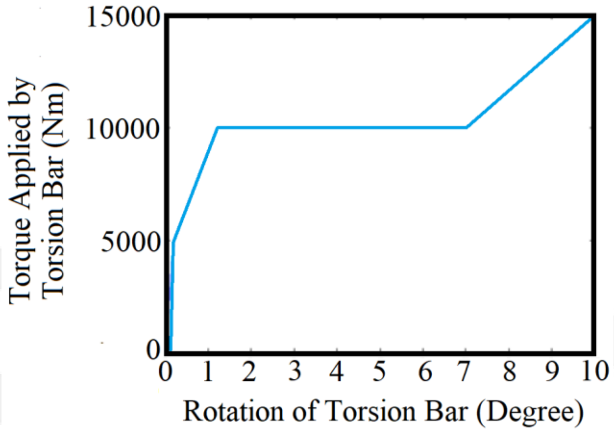

Figure 4.8. Characteristics of the torsion bar torsion element.

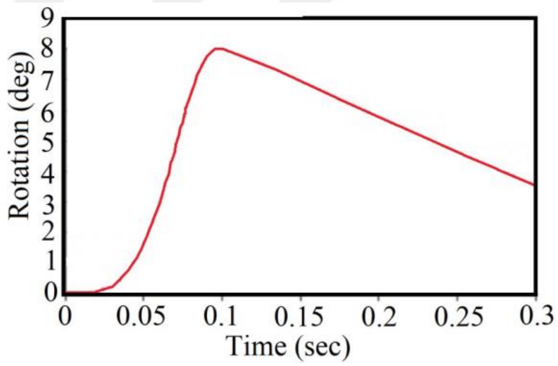

Figure 4.9. Torsion bar torsion element behavior in simulation environment at 56 kph crash severity.

Table 4.15 Performance values of seat with and without torsion bar at 40 kph and 56 kph crash severities.

Pulse	NCAP(43) without torsion bar	NCAP(64) without torsion bar	NCAP(43) with torsion bar	NCAP(64) with torsion bar
$NDI^{(+)}$ [deg]	0.29343	5.9567	0.24298	0.33968
$NDI^{(-)}$ [deg]	-3.495	-0.82108	-3.3961	-3.8622
NIC [m^2/s^2]	10.62500	22.34200	13.09100	10.94200
N_{km}	0.42256	0.81825	0.50768	0.53404
v_r [m/s]	0.53617	1.29300	1.24090	1.38730
$Fsh^{(+)}$ [N]	13.07000	7.53390	14.56600	59.93900
$Fsh^{(-)}$ [N]	219.51000	429.1700	252.06000	319.99000
F_{tn} [N]	223.78000	284.91000	192.45000	457.83000
F_{cm} [N]	634.34000	1193.3000	784.23000	810.83000
Myu [Nm]	7.37660	12.66300	8.95310	16.42000
FshL [N]	133.50000	393.44000	262.81000	344.31000
Myl [Nm]	5.09320	15.87700	11.06200	13.06800
T1 x-acc [g]	25.35700	50.69011	35.93500	39.46600
HrCt [ms]	12.00000	10.00000	12.00000	11.00000
HIC_{15}	39.31960	117.1022	51.70540	78.07030
BrIC	0.04000	0.0887	0.11170	0.09600
BrIC-P1	0.04310	0.34546	0.55790	0.41130
BrIC-P2	4.52*10^-4	0.00433	0.00830	0.00540
Ta_3 [g]	25.18970	35.47960	24.41740	29.61210

L_{tn} [N]	0.00000	0.00000	0.00000	0.00000
L_{cm} [N]	2.826.50000	4671.50000	3.415.30000	3.053.10000
maximum seat-pan displacement(m)	0.18177	0.29259	0.19180	0.28820
maximum seat-pan rotation(deg)	-	-	2.39680	8.01120
Neck Joint Rotations$^{(+)}$[deg]	1.9813	3.1215	1.6938	2.1335
Neck Joint Rotations$^{(-)}$[deg]	-1.9784	-5.0054	-4.938	-4.2415

5. DISCUSSION AND CONCLUSION

In the first part of the thesis, a seatback rotation mechanism based on a rack and pinion driven by a pre-tensioned spring is proposed. When a crash is unavoidable, the seatback is rotated towards a more upright position before the crash. This rotation of the seatback is set to be about 10 degrees in a period of about 100 ms. This mechanism can be activated by a sensor that triggers a mechanical switch that releases the mechanism. The rack is connected to the car floor by a pre-tensioned spring and damper. When the pre-tensioned spring is released, it will pull the rack to the left. The rack will rotate the pinion gear it is in contact with clockwise direction. In order to reach the angle value that will obtain the desired vertical position, a gear ratio between gear-2 and gear-3 was determined. Gear-3 will rotate in the same direction as gear-2, thanks to the chain connection established between it and gear-2. This rotation movement will force the seatback to return to a more upright position with gear-3. The human-dummy model will also come to an upright sitting position with the seatback at the same time as the seatback turns to an upright angle. There is a mechanical connection between the seatback and gear-3. Just before impact, gear-3 suddenly rotates with the seat back. Gear-3 will be locked when the seatback rotates by the predetermined angle value. This locking process can be presented as a locking mechanism that can be designed in various ways. When gear-3 is locked and the crash impact begins, the mechanical connection between the seatback and gear-3 will plastically deform and absorb the crash energy. The forward rotation of the seatback has the side effect that the head is pulled back as the upper body is loaded by the seatback. This head retraction can cause head trauma if there is nothing to support the head. For this reason, the head restraint is moved forward to face the head by 2 cm at 30 ms to support the head early and to limit the head retraction when the seatback is rotated forwards before impact.

Once the forward rotation of the seatback was complete, the seat was subjected to the impact of different severities of the EuroNCAP neck response test. High severity crashes may become more common in autonomous vehicles in the future, especially if passengers start using rear-facing seats. As frontal collisions generally occur at a higher severity than rear collisions, sitting in rear-face oriented seats may result in increasing neck injury risk when a frontal collision occurs.

For assessing the effectiveness of the proposed mechanism (including the forward opening of the head restraint), a neck response mitigating seat was subjected to a high severity crash impact with or without the proposed mechanism. The neck response mitigating seat without the proposed mechanism shows low neck loading at many crash severities already applied, as shown in Table 5.1, Table 5.2 and Figure 5.1. The neck response mitigating seat with the proposed mechanism achieved an average reduction of 31.56% in the neck shear force. With the proposed mechanism, the upper neck tensile force increased when the TR24 crash severity was applied. However, this tensile force is still low as shown in Figure 5.1. There is an average decrease of 39.11% in N_{km} values. At the maximum backward rotation of the backrest (counterclockwise), an average improvement of 37.23% was obtained. The improvement here has two benefits. Firstly, there is less space behind the seat for absorbing the energy caused by crash, so the size of the passenger compartment can be reduced. Secondly, the amount of ramping, which is the upward movement of the upper body along the back of the seat, is reduced. This ramping movement may cause the head to move backwards over the head restraint, resulting in a reduction in the support of the head restraint to the head.

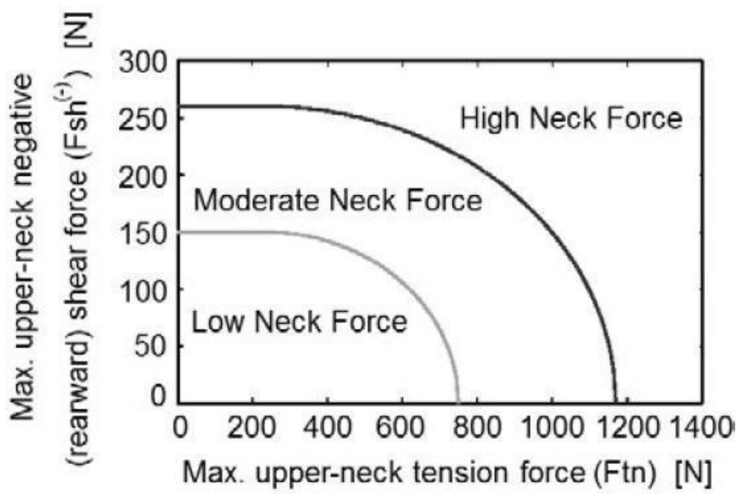

Figure 5.1. Classification of IIWPG neck force (Adapted from [39].).

Table 5.1. Shear force comparison after implementation of several crash pulses.

Crash pulse	Maximum shear force (N)		% shear force reduction
	Without mechanism	With mechanism	
SN 9.4	80.418	61.668	23.3
SN 13	107.29	76.39	28.8
TR 16	122.49	81.182	33.7
IIWPG	113.72	82.165	27.7
SN 20.4	162.15	90.927	43.9
TR 24	167.17	109.15	34.7
FMVSSHS	237.18	166.72	29.7

Table 5.2. Tensile force comparison after implementation of several crash pulses.

Crash pulse	Maximum tensile force (N)		% tensile force reduction
	Without mechanism	With mechanism	
SN 9.4	164.95	33.65	79.5
SN 13	167.32	42.248	74.7
TR 16	110.33	120.82	-9.5
IIWPG	207.51	101.21	51.2
SN 20.4	151.48	103.79	31.5
TR 24	87.485	168.69	-92.8
FMVSSHS	573.13	190.81	66.7

The mechanism provided to return the seatback to a more upright position before a crash has been shown to significantly improve the performance of the seat. Thanks to this mechanism, the seat can absorb higher crash energies in more severe crashes. The initial forward rotation of the seatback increases the potential to absorb energy during the backward rotation of the seatback, which will be very useful in autonomous vehicle crashes.

As a result of turning the seat back forwards, the forces coming to the human body during the crash were absorbed by the large area of the seatback and the injury criteria were improved. Again, the forward movement of the seatback restricted the freedom of movement of the occupant model and reduced the injury criteria. The forward movement of the head restraint of the seat also prevented the head from being thrown back relative to the body and supported the restriction of movement. The fact that the seat acts on the human body at steeper angles thanks to the mechanism causes the forces acting from the seat to the body to be more horizontal than the ground. This ensures that the energy of the crash is absorbed more effectively.

In the following part of the thesis, real crash test scenarios were verified in computer environment to study the how horizontal, vertical and angular acceleration affect occupant during severe crashes and to design protective systems that will eliminate the negative effects of these accelerations in current accident moments. Subaru Impreza and Toyota Yaris model vehicles were used in the verification studies of real crash scenarios. In real crash test scenarios, especially angular acceleration data are not provided. By utilizing the angular acceleration data obtained in the verification simulation, a preliminary study of the development of a system that will protect people from such high intensity collisions is carried out in this section. Horizontal and vertical displacement, velocity and acceleration data taken from the simulations are checked whether similar to the data from actual crash to validate the simulations.

The design parameters needed during the modelling of the vehicles used in the validation simulations were taken from the NCAP-CAL-14-013 report prepared on 15 April 2014 for the Subaru Impreza model vehicle and from the NCAP-MGA-2006-011 report prepared on 21 June 2006 for the Toyota Yaris model vehicle. Subsequently, simulation environments were completed by calculating the positions of the vehicles' centers of gravity, tire sizes and moments of inertia. After the completion of the simulation environment, the relationship between the forces that the vehicles are exposed to from the impact surfaces and their actual deformations were also defined in the simulation environment. Finally, accelerometers were added on the vehicles to obtain the data needed on the vehicles based on real crash scenarios. The data obtained from these accelerometers added in the simulation environment are as follows;

- X direction vehicle acceleration
- Z direction vehicle acceleration
- X direction vehicle velocity
- Z direction vehicle velocity
- X direction vehicle displacement
- Z direction vehicle displacement
- Vehicle angular acceleration about y axis
- Vehicle angular displacement about the y axis

The data listed above are plotted on the same graph with the data in the real crash scenario as a function of time. When these graphs of simulation and real data sets are analyzed, it can be seen that the real crash scenarios are verified in the simulation environment. In addition to this verification study, the ride comfort of the vehicles modelled in the simulation environment was also examined with a few parameters and it was seen that the values examined were close to the values determined for ride comfort.

Analyzing the section of the thesis where torso plates are proposed, it can be seen that the injury risk of the rear-facing seat that was proposed in this thesis study is low. The N_{km} and rebound velocity values of head are below the injury threshold values considered for low velocity rear impacts. The neck compression forces are also below the threshold values given for high velocity impacts. The maximum value of the 3 ms clip thorax acceleration was 32 g, which is well below the critical threshold value of 60 g. The thorax torso plate did not generate any lumbar tension force at the highest impact intensity, while the lumbar compression force was around 55 per cent of the threshold value. Tensile and compression forces in the neck were also obtained well below the limit values. Spine joint rotations are also within the range of motion of the occupant model. The BrIC value obtained at the highest intensity is lower than the value in a similar study in the literature [9]. The risk of AIS2 type brain damage is almost non-existent. The risk of AIS1 type minor injury did not exceed 0.06. Head trauma criterion values are also very low compared to the 700-limit value.

The NIC values also do not exceed the respective threshold values. However, the NIC criterion was developed for rear impacts occurs at low-speed, which deals with the S-shape-like deformation during head retraction. Consequently, it is not a criterion for high-speed impacts. Fsh(+) values are low at all impact intensities. Looking at the volunteer test data, the head movement towards to back relative to the body is not at critical level since the NDI(+) values are below the critical level. It would be good to further investigate the NIC assessment for high velocity impacts. Neck intervertebral angle changes are within range of motion of human body model [31]. The head rest foam and seat back foam/suspension stiffness is much stiffer than the forward-facing seat. In addition, the head restraint and seatback work together to limit the internal movement of the neck.

The results for the highest upper and lower neck moment values (Myu and Myl) were below the limit values determined for low intensity crashes even at the highest crash intensity. The contact time between the head restraint and the head (HrCt) is also below the limit values at all crash intensities. The maximum lower neck shear force (FshL) exceeded the limit value only in the NCAP(64) crash simulation at low intensities (TR(24)). The highest acceleration value of the first thoracic vertebra (T1a) exceeded the threshold value for TR(24) crash severity at the NCAP(43) and NCAP(64) crash intensities. It should be noted that these values are not very high since the comparisons were made according to the low crash intensities in the EuroNCAP protocols. The head injury criterion (HIC15) value at the highest crash intensity is 12 per cent of the threshold value. It was also mentioned in the previous section that the seat was moved forward by 10 cm 2 seconds before impact. In this design, the seat only moves back a total of 17.9 cm when subjected to the highest crash severity of NCAP (64).

However, during high-speed frontal crashes, the large surface area of the seatback evenly compensates for the pressure on the rear part of the torso. Therefore, the chest deformation in frontal crashes is less than the deformation caused by seat belts [X. Jin et al. 2018]. The bio-accuracy of the human model should not be of much concern as the of the head movement, neck and torso is restricted and the motion range of the joints is not exceeded.

In real-life applications, the body plates can be manually adjusted according to the height of the occupants and can consist of several parts depending on the height of the occupants. It is important for the occupants to be willing to make use of these additional restrictions. If the occupant moves out of the protected seating position in the event of an impending collision, an audible signal can be activated to warn the occupant to remain in the protected position.

Protecting a rear-facing occupant from high severity frontal collisions is a challenging task. It can operate safely at crash intensities between 9.4 km/h and 64 km/h Delta-V.

The suggested rear-facing seat will be used to restrict the movement of the human head and body. Head movement will be restricted relative to the head restraint and body movement will be restricted relative to the seatback. If the movement restrictions specified for a sitting position other than the normal sitting position are not met, serious injuries are inevitable. For this reason, a design has been created that minimizes the space between the human body and the seat surfaces, except for the extremities. The design is also supported by an integrated seat belt. The design utilizes two rigid plates extending from the seatback to the back of the passenger's torso. These plates extending to the back and waist area of the passenger will provide the movement restriction mentioned above. These plates, which can be removed and adjusted according to the height of the passenger, will work more efficiently when the head restraint and the head clearance is minimized. In addition to the support provided by the head restraint, the seat belt and torso plates will eliminate the possibility of the passenger jumping upwards (Figure 5.2).

Figure 5.2. The motion sequence of the seat-occupant system subjected to the pulse NCAP(64).

Despite the torso plates used rear faced seat, it has been observed that when high intensity rear impact pulses were applied to the forward-facing seat, the seat rises into the air. This situation increased the forces in the neck, but also increased the compression forces, especially in the lumbar region. In order to reduce these compression forces, a torsion bar element was used to restrict the upward movement of the seat. This torsion bar will try to hold the seat in its position by applying a moment in the direction opposite to the direction of rotation of the seat during a high intensity impact. The results of the simulations using the torsion bar show that this torsion bar works effectively.

In NCAP(64) simulations with torso plates and torsion bar (forward facing seat-rear impact) the Nkm value obtained here (0.53) was below the threshold value obtained at low speeds (0.74). The head rebound velocity from the head restraint (1.38 m/s) was also one-fourth of the threshold value (5.6 m/s) obtained in low-speed collisions. The head injury criterion HIC15 had a thresshold value of 700 in high-speed collisions. At 56 kph impact intensity, this value was only 78.1 with the torso plates and torsion bar working together. The BrIC value obtained at the highest intensity was 0.005 for AIS2 type brain damage risk and 0.4 for AIS1 type minor injury risk. The highest value of the positive and negative neck shear forces is one tenth of the threshold value in high-speed collisions. Again, when the tensile and compressive forces acting on the upper neck were analyzed, forces around one ninth of the lowest threshold value were observed. The threshold value of the Ta3 criterion, which is the maximum clip thorax acceleration value of 3 ms, is 60 g in high-speed impacts. For the forward-facing seat, this value was 24.4 g for a 40 kph impact and 29.6 g for a 56 kph impact. This shows that even in the most severe collision, half of the threshold value cannot be reached. Finally, when the lumbar tensile and compressive forces are considered, it is seen that the values obtained from the simulation are well below the threshold values.

Note: Further details can be accessed at https://www.mdpi.com/2075-1702/11/12/1076

6. REFERENCES

[1] S. Himmetoğlu, An Adaptive Car-seat to Mitigate Whiplash in Rear Impacts, Proceedings of the 21st International Scientific Conference Transport Means, Juodkrante, Lithuania, 32-38, **2017**.

[2] F. Spitzhüttl, H. Liers, Calculation of the Point of No Return (PONR) from Real-world Accidents, Proceedings of the 26th ESV Conference, Eindhoven, The Netherlands, National Highway Traffic Safety Administration, paper 19-0141, **2019**.

[3] R.E. Trempel, D.S. Zuby, M.A. Edwards, IIHS head restraint ratings and insurance injury claim rates, Traffic Injury Prevention, Vol.17, No.6, 590-596, **2016**.

[4] D. Otte, T. Facius, H. Johannsen, T. Hüfner, Estimation of Injury Risk of the Cervical Spine of Car Occupants after Emergency Braking, SAE Technical Paper 2018-01-0541, **2018**.

[5] V. Eis, P. Fay, R, Sferco, A Detailed Analysis of the Characteristics of European Rear Impacts, Proceedings of 19th ESV Conference, Washington DC, USA, National Highway Traffic Safety Administration, paper 05-0385-O, **2005**.

[6] S. Himmetoğlu, L. O. Kılıç, Safety Issues in Fully Autonomous Cars: A Turkish Perspective, Proceedings of 23rd International Scientific Conference. Transport Means 2019, **2019**.

[7] X. Jin, H. Hou, M. Shen, H. Wu, K. H. Yang, Occupant kinematics and biomechanics with rotatable seat in autonomous vehicle collision: a preliminary concept and strategy, In 2018 IRCOBI Conference Proceedings, IRCOBI, **2018**.

[8] H. Zellmer, F. Manneck, Assessing Injury Risk of Car Occupants on Rearward Facing Seats in a Full Frontal Impact–Sled Tests in a Generic Test Environment, In Proceedings of the 26th ESV Conference, Eindhoven, The Netherlands, **2019**.

[9] V. Hasija, R. Kelkar, E. G. Takhounts, SIMULATION ASSESSMENT OF INJURY TRENDS FOR 50TH PERCENTILE MALES USING POTENTIAL SEATING CONFIGURATIONS OF FUTURE AUTOMATED DRIVING SYSTEM (ADS) EQUIPPED VEHICLES.

[10] J. Östh, K. Bohman, L. Jakobsson, Evaluation of Kinematics and Restraint Interaction when Repositioning a Driver from a Reclined to an Upright Position Prior to Frontal Impact using Active Human Body Model Simulations, In Proceedings of the IRCOBI Conference, **2020**.

[11] J. Becker, G. A. D'Addetta, M. Wolkenstein, F. Bosma, R. Verhoeve, S. Schaub,

M. O .Hamacher, Occupant Safety in Highly Automated Vehicles Challenges of Rotating Seats in Future Crash Scenarios, In Proceedings of the IRCOBI Conference, **2020**.

[12] A. Soni, S. Schilling, J. Faust, B. Eickhoff, Responses of HIII, THOR and SAFER-HBM occupant models in rearward-facing seat configuration for high severity frontal impact, In Proceedings of the IRCOBI Conference, **2020**.

[13] P. Luttenberger, F. Feist, D. Kofler, W. Sinz, G. A. D'Addetta, H. Freienstein, M. Wolkenstein, Assessment of future occupant restraint principles in autonomous vehicles, In Proceedings of the IRCOBI Conference, **2020**.

[14] H. Wu, H. Hou, M. Shen, K. H. Yang, X. Jin, Occupant kinematics and biomechanics during frontal collision in autonomous vehicles—can rotatable seat provides additional protection?, Computer Methods in Biomechanics and Biomedical Engineering, 23(5), 191-200, **2020**.

[15] K. Rawska, B. Gepner, S. Kulkarni, K. Chastain, J. Zhu, R. Richardson, J. R. Kerrigan, Submarining sensitivity across varied anthropometry in an autonomous driving system environment, Traffic injury prevention, 20 (sup2), S123-S127, **2019**.

[16] T. L. McMurry, G. S. Poplin, G. Shaw, M. B. Panzer, Crash safety concerns for out-of-position occupant postures: A look toward safety in highly automated vehicles, Traffic injury prevention, 19(6), 582-587, **2018**.

[17] J. Moon, I. Bae, S. Kim, A pre-crash safety system for an occupant sitting on a backward facing seat for fully automated vehicles in frontal crashes, In 2017 IEEE International Conference on Vehicular Electronics and Safety (ICVES) (pp. 168-171), IEEE, **2017**.

[18] R. F. Chandler, C. E. Clauser, J. T. McConville, H. M. Reynolds, J. W. Young, Investigation of Inertial Properties of the Human Body, National Highway Traffic Safety Administration, Washington, DC, Report no. DOT HS-801 430, **1975**.

[19] S. Yavuz, S. Himmetoğlu, Development of a Restraint System for Rear-Facing Car Seats, Machines 2023, 11, 1076, **2023**.

[20] U.S. Department of Transportation National Highway Traffic Safety Administration Office of Crashworthiness Standards, Final Report of New Car Assessment Program Frontal Impact Testing of a 2014 Subaru Impreza five door station wagon NHTSA No.: M20145500, **2014**.

[21] U.S. Department of Transportation National Highway Traffic Safety Administration Rulemaking, Final Report of New Car Assessment Program Testing

of a 2007 Toyota Yaris NHTSA No.: M75102, **2006**.
[22] G. Heydinger, R. Bixel, W. Garrott, M. Pyne, J. G. Howe, D. A. Gunther, Measured Vehicle Inertial Parameters-NHTSA's Data Through November 1998, SAE Technical Paper 1999-01-1336, **1999**.
[23] http://www.tiresize.com/calculator (Last Access: **12 May 2024**).
[24] A. Patil, S. Sawant, Ride Comfort Analysis of Quarter Car Model Active Suspension System Subjected to different Road Excitations with Nonlinear Parameters, International Journal of Advance Research In Science And Engineering (IJARSE) 4 (2015), **2015**.
[25] Y. S. Unlusoy, AUTOMOTIVE ENGINEERING_Lecture Notes. 10.13140/RG.2.2.30673.66401, **2021**.
[26] G. Aydan, Ride comfort improvement by application of tuned mass dampers and lever type vibration isolators, MS thesis, Middle East Technical University, **2010**.
[27] H. Köylü, Improvement of dynamic wheel load oscillations by coupling pitch motion into bounce motion during pitching motion of passenger vehicle, Politeknik Dergisi: 1-1, **2021**.
[28] EuroNCAP, European New Car Assessment Programme–Assessment Protocol–Adult Occupant Protection; Version 9.1.3; EuroNCAP: Leuven, Belgium, 2021; 49p., **2021**.
[29] R.Eppinger, E. Sun, F Bandak, M. Haffner, N. Khaewpong, M. Maltese, S. Kuppa, T. Nguyen, E. Takhounts, R. Tannous, Development of Improved Injury Criteria for the Assessment of Advanced Automotive Restraint Systems—II; NHTSA: Washington DC, USA, **1999**.
[30] E. G. Takhounts, M. J. Craig, K. Moorhouse, J. McFadden, V. Hasija, Development of brain injury criteria (BrIC), Stapp Car Crash J., 57, 243–266., **2013**.
[31] S. Himmetoğlu, M. Acar, K. B. Marouf, A. J. Taylor, Reactive seat design for optimum whiplash mitigation at different crash severities, In International IRCOBI Conference 2009, York, United Kingdom, **2009**.
[32] K. U. Schmitt, P. F. Niederer, D. S. Cronin, B. Morrison, M. H. Muser, F. Walz, Trauma Biomechanics, 5th ed.; Springer Nature: Cham, Switzerland, **2019**.
[33] I. V. Lau, D. C. Viano, The Viscous Criterion—Bases and applications of an injury severity index for soft tissues, SAE Trans, 95, 672–691, **1986**.
[34] A. Bracq, R. Delille, C. Marechal, B. Bourel, S. Roth, O. Mauzac, Rib fractures prediction method for kinetic energy projectile impact: From blunt ballistic

experiments on SEBS gel to impact modeling on a human torso FE model, Forensic Sci. Int, 297, 177–183, **2019**.

[35] J. D. Rupp, C. A. C. Flannagan, A. M. Kuppa, Development of New Injury Risk Curves for the Knee/Distal Femur and the Hip for Use in Frontal Impact Testing; Report No. UMTRI-2009-08; The University of Michigan Transportation Research Institute: Ann Arbor, MI, USA, **2009**.

[36] S. Kuppa, J. Wang, M. Haffner, R. Eppinger, Lower Extremity Injuries and Associated Injury Criteria, In Proceedings of the 17th ESV Conference, Amsterdam, The Netherlands, **2001**.

[37] J. R. Funk, R. W. Rudd, J. R. Kerrigan, J. R. Crandall, Analysis of Tibial Curvature, Fibular Loading, and the Tibia Index, In Proceedings of the 2003 Ircobi Conference, Lisbon, Portugal, 25–26 September 2003; pp. 135–147, **2003**.

[38] D. C. Viano, Role of the Seat in Rear Crash Safety; Society of Automotive Engineers: Warrendale, PA, USA, **2002**.

[39] S. Yavuz, S. Himmetoğlu, Neck protection in autonomous car crashes, In 24th International Scientific Conference on Transport Means 2020, Kaunas, Lithuania, pp.147-152, **2020**.

APPENDIX

AP 1 - Publications Derived from the Thesis

S. Yavuz, S. Himmetoğlu, Development of a Restraint System for Rear-Facing Car Seats, Machines 11.12 (2023): 1076, **2023**.

AP 2 - Conference Papers Derived from the Thesis

S. Yavuz, S. Himmetoğlu, Neck protection in autonomous car crashes, 24th International Scientific Conference on Transport Means 2020, Kaunas, Lithuania, pp.147-152, **2020**.